Aalto University
School of Engineering

Mikko Niemi

Simulation and Safety features of NuScale Small Modular Reactor

Master's Thesis submitted in partial fulfilment of the requirements for the degree of Master of Science in Technology

Espoo 27.11.2017
Supervisor: Professor Sanna Syri
Advisors: M.Sc.Eng Timo Toppila
M.Sc.Eng Antti Rantakaulio

Aalto-yliopisto
Insinööritieteiden korkeakoulu

Aalto-yliopisto, PL 11000, 00076 AALTO
www.aalto.fi
Diplomityön tiivistelmä

Tekijä Mikko Niemi

Työn nimi NuScalen Pienen Modulaarisen Reaktorin simulointi ja turvallisuustoiminnot

Koulutusohjelma Energia- ja LVI-tekniikka

Pää-/sivuaine Teollisuuden energiatekniikka **Koodi** Ene-59

Työn valvoja Professori Sanna Syri

Työn ohjaajat Diplomi-insinööri Timo Toppila, Diplomi-insinööri Antti Rantakaulio

Päivämäärä 27.11.2017 **Sivumäärä** 75 **Kieli** Englanti

Tiivistelmä

Pienet modulaariset ydinreaktorit (SMR) ovat verrattain uusi konsepti ydinenergiateollisuudessa. Siinä missä tavalliset reaktorit kohtaavat huomattavia haasteita suuren kokonsa vuoksi, pienet modulaariset reaktorit pyrkivät kiertämään ne hyödyntämällä pienen kokonsa ja modulaarisuutensa mahdollistamia ominaisuuksia. Siirtyminen SMR:iin sisältää tosin myös avoimia kysymyksiä. Energiateollisuus ja ydinturvallisuusviranomaiset ovat tottuneet käsittelemään suuren kokoluokan laitoksia ja niihin liittyviä ilmiöitä, kun taas kokemukset SMR:istä ja niiden ilmiöistä ovat vähäisiä. Käytännössä tämä luo tarpeen SMR:iin kohdistuvalle tutkimukselle, jota tämäkin opinnäytetyö pyrkii tukemaan. NuScale SMR valittiin tämän työn tutkimuksen kohteeksi kyseisen konseptin kohtuullisen korkean valmiusasteen ja siinä hyödynnettävien mielenkiintoisten passiivisten ilmiöiden takia.

Työssä rakennetaan Apros-ohjelmalla simulointimalli NuScalen konseptin mukaisesta SMR -koelaitteistosta. Mallin avulla validoidaan Aprosin SMR:ien simuloimiseen tarvittavaa laskentaa. Työn toinen tavoite on esittää NuScalen konseptille suunniteltuja erityisesti nykyisistä ydinvoimalaitoksista eriäviä ominaisuuksia teknisestä näkökulmasta, ja verrata niitä Suomen ydinvoimalain ja ydinturvallisuusohjeiden (YVL-ohjeet) turvallisuusvaatimuksiin.

Ominaisuuksien projisointi paljastaa, että osa suunnitteluominaisuuksista sopii perustavanlaatuisella tasolla nykyisiin määräyksiin muutamin poikkeuksien. Työssä huomataan, että haasteita on muun muassa modulaaristen reaktoreiden massatuotannon ja passiivisten ominaisuuksien osalta.

Simulointitulokset osoittavat Aprosin nykytilassaan kykenevän SMR:ien ja passiivisten turvallisuustoimintojen mallinnukseen. Tulokset kuitenkin osoittavat, että passiivisten systeemien tarkka simulointi hyötyisi kyseisien alueiden koodien jatkokehityksestä. Työssä myös esitetään mallinnusperiaatteita, joita olisi hyvä noudattaa, kun Aprosilla mallinnetaan SMR:iä.

Avainsanat Apros-simulointiohjelmisto, dynaaminen mallintaminen, helikaalinen putkihöyrystin, NuScale, passiivinen turvajärjestelmä, pieni modulaarinen reaktori

Aalto University
School of Engineering

Aalto University, P.O. BOX 11000, 00076 AALTO
www.aalto.fi

Abstract of master's thesis

Author Mikko Niemi		
Title of thesis Simulation and Safety features of NuScale Small Modular Reactor		
Degree programme Energy and HVAC Technology		
Major/minor Industrial energy engineering		**Code** Ene-59
Thesis supervisor Professor Sanna Syri		
Thesis advisors M.Sc.Eng Timo Toppila, M.Sc.Eng Antti Rantakaulio		
Date 27.11.2017	**Number of pages** 75	**Language** English

Abstract

Small modular reactor (SMR) is a relatively recent concept in the nuclear power industry. Whereas the traditional large scale reactors are facing challenges due to their size, the small modular reactors intend to bypass the problems by utilizing aspects that their small size and modularity enables. However, the transition to SMRs includes many open questions. The energy industry and nuclear safety authorities are accustomed to large scale power plants, whereas experience with SMRs are shallow. This effectively creates a need for SMR studies, some of which this thesis aims to answer to. NuScale SMR was chosen as a focus of this thesis due to the concept's reasonable level of maturity and its interesting utilization of passive safety systems.

In the framework of this thesis, a NuScale SMR simulation model is built using the Apros program. The model is used to validate Apros calculation required for SMR simulation. The second objective of this thesis is to present the specific safety features of NuScale SMR that differ from current nuclear power plants. They are presented from a technical point of view and are briefly projected on Finnish regulatory guides.

Feature projection reveals that many of the design features are fundamentally compatible with current guides with a few exceptions. In this thesis we perceive that among others the modular reactor mass production and passive functions could face challenges.

The simulation results show that Apros code is capable of SMR and passive safety system modelling. However, the results also show that precise simulation of passive safety systems would benefit from further code development on those fields. The thesis also presents modelling guidelines that are beneficial when Apros is used for SMR modelling.

Keywords Apros simulation software, dynamic modelling, Helical Coil Steam Generator, NuScale, passive safety system, small modular reactor

Acknowledgements

The work of this thesis was carried out between September 2016 and May 2017. I wish to thank my employer Fortum Power and Heat Oy for the great opportunity to write this thesis and for providing me with a good working environment and tools to complete my studies. I also wish to thank IAEA for providing me access to experimental data. The data was used to enhance the preliminary validation and visual appearance of this work.

This thesis was done as a part of Fortum's research and development entity on Small Modular Reactors and Apros development. It is a continuation to Kristiina Söderholm's doctoral thesis on SMR licensing and Hannes Alarotu's master's thesis on SMR safety features. The goal of this thesis was to discuss Apros capabilities in advanced SMR simulation, study NuScale design features and to briefly project them to Finnish regulatory guides. This does not conclude the SMR research in Fortum, and I wish that my contribution would be useful in future projects.

Although the thesis was carried out as an individual project, I was never without support. I am eminently grateful to my advisors Timo Toppila and Antti Rantakaulio for their invaluable guidance throughout the project. Without their broad expertise in nuclear engineering, this work would have been impossible to write. I am also thankful to my acting supervisor professor Pekka Ahtila for his interest and contribution to the project. I also wish to thank my official supervisor professor Sanna Syri, who helped me to conclude my work. Special thanks to Mika Juntti who provided me with essential guidance and information concerning Apros modelling.

I also wish to thank my colleagues at Fortum for their advice and support. With your help, I was not only able to finish my thesis, but also to grow up to a Master of Science in Engineering.

Finally, I am especially grateful to my parents and my sister Kirsi for their unquestioned faith in my studies and me.

Espoo 27.11.2017

Mikko Niemi

Mikko Niemi

Contents

Symbols

c_p	J/kgK	specific heat at constant pressure
D	m	diameter of helix
d	m	inside diameter of pipe
d_h	m	hydraulic diameter
F	-	Reynolds number factor
F_{cont}	m	force that a certain control volume experiences
f_k	-	friction pressure loss coefficient of a certain phase
G	kgm/s	mass flux
H	m	height
$h_{g,sat}$	J/kg	enthalpy of gas
$h_{l,sat}$	J/kg	enthalpy of liquid
h_{lg}	(J/kg)	latent heat of vaporization
L	m	length
Nu	-	Nusselt number
Pr	-	Prandtl number
Δp_e	Pa	vapor pressure difference between saturated steam and steam in wall temperature
$\Delta p_{hydrostatic}$	Pa	hydrostatic pressure difference
$\Delta p_{friction}$	Pa	major pressure losses inflicted by duct friction
$\Delta p_{mechanical}$	Pa	pressure changes inflicted by mechanical components
$\Delta p_{single\ resistance}$	Pa	pressure losses inflicted by single component resistance (strangulation etc.)
Δp_{total}	Pa	total pressure change along the fluid's flow path
q_{cr}	W/m^2	critical heat flux
$q_{cr,Z-G}$	W/m^2	critical heat flux predicted by Zuber-Griffith correlation
$q_{cr,B}$	W/m^2	critical heat flux predicted by Biasi correlation
Re	-	Reynolds number
Re_k	-	Reynolds number of certain phase

R_{helix}	m	radius of helical coil helix
S	-	suppression factor
ΔT_e	K	temperature difference of a wall and saturated fluid
V_{cont}	m^3	control volume
w	m/s	flow velocity
w_{tan}	m/s	tangential velocity
X_{tt}	-	Lockart-Martinelli parameter
x	-	volume fraction of a phase
x_e	-	equilibrium steam quality

Greek symbols

α_t	W/m^2K	heat transfer coefficient of total heat flow
α_{nb}	W/m^2K	heat transfer coefficient of nucleate boiling
$\alpha_{sp,l}$	W/m^2K	convective heat transfer coefficient of liquid
ε	m	roughness
ζ	-	coefficient of single flow resistance
λ	-	relative roughness
λ_l	W/mK	thermal conductivity of liquid
μ_g	kg/ms	dynamic viscosity of gas
μ_l	kg/ms	dynamic viscosity of liquid
ν	m^2/s	kinematic viscosity
ρ	kg/m^3	density
ρ_g	kg/m^3	density of gas
ρ_l	kg/m^3	density of liquid
σ	N/m	surface tension

Abbreviations and Acronyms

ADS	Automatic Depressurization System
Apros	Dynamic Process Simulation Software, trademark owned by Fortum and VTT
BASS	Boric Acid Shut-down System
BWR	Boiling Water Reactor
CPV	Cooling Pool Vessel
DCA	Design Certification Application
DHRS	Decay Heat Removal System
ECCS	Emergency Core Cooling System
EIS	Emergency Injection Systems
Helicoil	Helically coiled
HCHE	Helical Coiled Heat Exchanger
HCSG	Helically Coiled Steam Generator
HPC	High Pressure Containment
HTP	Heat Transfer Plate
iSMR	Integrated Small Modular Reactor
LBLOCA	Large Break Loss Of Coolant Accident
LOCA	Loss Of Coolant Accident
LWR	Light Water Reactor
MASLWR	Multi-Application Small Light Water Reactor
NPM	Nuclear Power Module
NPP	Nuclear Power Plant
OSU	Oregon State University
PWR	Pressurized Water Reactor
RPV	Reactor
R&D	Research and Development
RRV	Reactor Recirculation Valve
RVV	Reactor Vent Valves
SG	Steam Generator
SMR	Small Modular Reactor
STUK	Radiation and Nuclear Safety Authority (Translated: Säteily Turvakeskus)
TECDOC	Technical Document
UHS	Ultimate Heat Sink
YVL	Regulatory Guides on Nuclear Safety (Translated: Ydinturvallisuusohjeet)

1 Introduction

Small Modular Reactor (SMR) represents a new perspective to nuclear industry. Until recently there has been a trend in energy industry towards larger reactor units. The increasing size and complexity leads to high initial capital requirements, involving high risks for investors. In contrast the SMR concept focuses on simplifying the design, mass production and standardization. Advanced SMRs could also be based on passive safety systems, which are considered more reliable but lack practical experience.

The NuScale SMR concept was chosen as the focus of this thesis, due to the concept's reasonable level of maturity: Design Certificate Application, DCA, is currently under Nuclear Regulatory Commission's reviewing process. Furthermore, the NuScale SMR contains many designs that are rare in typical large scale NPPs and could benefit from further discussion.

The first objective of this thesis is to create a dynamic NuScale SMR test facility model with Apros simulation software in order to evaluate the software's capabilities in SMR modelling. Alongside basic modelling a set of steam generator correlations are preliminarily validated. The second objective of the thesis is to describe NuScale technical aspects and to project them on to Finnish regulatory guides. This thesis also aims to answer the following questions: What are the main design features of a NuScale SMR? Second, how do the new design features project themselves on to the Finnish regulatory guides? Third, what are the specific modelling characteristics that need to be taken into account in SMR modelling?

This study is done in co-operation with Fortum Power and Heat Oy and Technical Research Centre of Finland Ltd (VTT). The first version of preliminary NuScale SMR test facility model was available from Fortum's earlier SMR project. Correlations considering Helical Coil Steam Generator (HCSG) are chosen and implemented by Fortum and VTT HCSG collaboration project and are discussed and preliminarily validated in this thesis.

The structure of this thesis is as follows: The second chapter, Small Modular Reactor concept, presents NuScale SMR in general. Some selected important features are gathered and discussed in chapter 3, Design features in NuScale SMR, from a technical standpoint. Then the design features are briefly projected on to the current Finnish regulatory guides in chapter 4, NuScale specific design features projected on Finnish regulatory guides. In chapter 5, SMR test facility modelling and preliminary validation, modelling work and preliminary validation are discussed. The theory and simulation of Helical Coil Steam Generator are discussed in chapter 6, Helical coil steam generator. The final chapter of this thesis, Summary, summarizes the main points and results.

2 Small Modular Reactor concept

This chapter gives a short description of the Small Modular Reactor (SMR) concept. The main focus is on the NuScale SMR, so other SMRs [1] or typical reactor concepts are not covered in this thesis. It should also be noted that NuScale Nuclear Power Plant (NPP) contains many conventional systems, but they are not included in the scope of this thesis.

The trend in nuclear power plant development has so far been towards larger units with better efficiency. This effectively makes nuclear industry a strongly capital intensive business. Larger and more complex reactors often tend to have very long commission times. Furthermore, no power is produced before the whole NPP is completely finished. This increases initially required capital investment and uncertainties on commissioning. The proportional initial investments could be decreased by modularization and simplifications [2].

Nuclear industry is a highly political business, which is considerably affected by public opinion. That opinion has worsened especially due to the major catastrophes in nuclear industry (for example: Three Mile Island 1979, Tshernobyl 1986, Fukushima 2011 etc.). One way to increase public acceptance and undermine the political nature of the issue is an international, open and standardized licensing process. The internationalization is difficult to carry out with large and complex NPPs due to great variations in safety requirements in different countries. Internationalization could be hastened by simplifying NPP designs to accommodate most national regulations [3].

A considerable amount of NPP related workload deals with safety design. Active safety systems are never completely fault tolerant and thus require backup systems. Furthermore, extended and complex systems could be troublesome to analyze and somewhat prone to common mode failures. One of the governing ideas with SMRs is to simplify safety related systems by introducing passive safety systems [3]. Some of the passive safety systems are troublesome to implement with large scale NPPs due to their massive load of decay heat production. However, it should be pointed out that many passive phenomena could be utilized also in large scale units like AP1000 etc. [4]. The above pros and cons are generalized and summarized in Table 1 below.

Table 1. A generalized comparison between typical large scale NPPs and SMR-type NPPs

Typical large scale NPPs	SMR NPPs
+ High efficiency	+ Relatively small initial investment
+ Experience from previous NPPs	+ Gradual implementation
+ Supported by present regulatory guides	+ Capable for mass production
	+ Simplified safety measures
- Complex	- Little previous experience
- Capital intensive	- Difficult to fit into present regulatory guides
- Single-shot implementation	
- Case specific	

NuScale Power Modular and Scalable Reactor has been developed since 2007 by NuScale Power Inc. NuScale was founded as a kick-off company to commercialize the preliminary design project of advanced Small Modular Reactor developed by Oregon State University in collaboration with Nexant-Betchel and Idaho National Engineering Laboratory. The

preliminary work is known as Multi-Application Small Light Water Reactor (MASLWR), but during the commercialization it was later renamed to NuScale [5].

The NuScale SMR is a light-water reactor (LWR). Each NuScale Power Module is a self-contained unit that operates independently within a multi-module configuration [6]. NuScale SMR is part of advanced SMR and integrated SMR (iSMR) categories, but in the scope of this thesis it is simply referred to as SMR.

A single NuScale Power Module is a relatively small unit with 150 MW of thermal power, whereas the same attribute in a large unit could be over 4000 MW. NuScale's small decay heat production and conventional stable reactor design enables several new designs. The small decay heat production enables a continuous passive heat transfer chain to an Ultimate Heat Sink (UHS) even in the event of Loss of Coolant Accident (LOCA). Primary flow inside a NuScale Power Module is a natural circulation flow driven by temperature difference between a riser and a downcomer. Passive core coolant circulation is discussed more in section 3.1. A natural circulation flow does not need pumps to effectively decrease the size of the primary circuit. The use of compact Helical Coil Steam Generators (HCSG) provides a relatively high heat transferring capability in a small volume with a low pressure drop. By combining passive coolant circulation with HCSGs, the whole primary circuit could be fitted into a relatively small Reactor Pressure Vessel (RPV) [7]. The NuScale power module is presented in Figure 2 below.

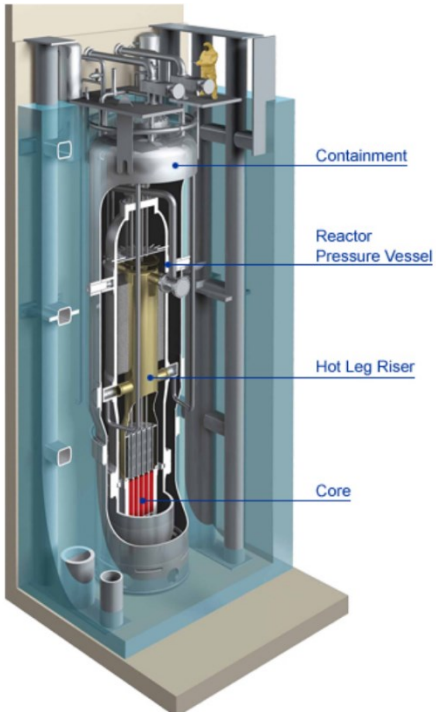

Figure 2. NuScale power module cross-section [8]

Since the primary systems are completely inside the RPV, the containment (surrounding primary systems) could also be downsized significantly. These dimensions among other significant features are presented in Table 2 [9]. All values presented in Table 2 are nominal and are provided for comparison only. Small containment is designed to withstand high pressure loads and is hence referred to as High Pressure Containment (HPC). The HPC functions as a radiation barrier like typical containments, but also works as an emergency heat exchanger and pressure controller. Normally a Loss of Coolant Accident (LOCA) leads to a depressurization of the core, but a small HPC pre-emptively prevents

critical depressurization. Also, the overpressure inside RPV could be blown into the HPC like in some BWR types [10].

Table 2 Typical pressurized water reactor compared to NuScale [9] (Edited)

Plant Feature	Typical PWR	NuScale
Nominal gross electrical output (MWe)	1200	45/50
Core thermal output (MWt)	3400	160
Electrical efficiency (%)	35	28/31
Core		
Effective fuel length (m)	3.7	2
Average linear heat rate (kW/m)	17.7	8.2
Reactor coolant system		
Number of heat transfer loops	4	0
Operating pressure (bar)	155	127
Hot leg temperature (°C)	325	310
RPV		
Vessel inner diameter (m)	4.4	2.7
Containment		
Vessel inner diameter (m)	42.6	4.3
Vessel inner height (m)	60	23

The HPC, and therefore the whole power module, is located inside a cooling pool. The cooling pool is designed to be large enough to provide decay heat cooling for all power modules, simultaneously acting as a secondary Ultimate Heat Sink (UHS) if the primary UHS is not available. The HPC's direct access to a UHS effectively enables long-term passive emergency cooling through the HPC walls. This system is called Emergency Core Cooling System (ECCS) and is further discussed in section 3.4.2. Furthermore, the cooling pool serves as a UHS for a redundant passive cooling system called Decay Heat Removal System (DHRS). The DHRS directs secondary side steam into the heat exchangers in the cooling pool when the normal feed water is not available. Again, pressure difference between HCSG and DHRS heat exchangers serves as a driving force for the fluid flow, thus making the DHRS a passive system. The DHRS is further discussed in section 3.4.1. The integrated power module design and the passive emergency cooling options promote the isolability of the power module. The possibility to completely isolate individual power modules is an important design feature in NuScale design and it is further discussed in sections 3.3 and 3.4.

A NuScale power plant is planned to include 1-12 independent reactor units, although plants with 6 or 12 units are commercially preferred. Each power module is independent from the other modules: Each module has its own steam cycle, including turbine and condenser [9], and in some concepts even cooling towers. However, a few design features are shared with all power modules: all power modules are located in the same reactor hall, and more importantly, in the same cooling pool; all of the modules are also monitored and operated from a single control room.

The maintenance of the NuScale power modules is executed in an innovative way. The entire power module is lifted from an operational section of power modules to the refueling section of the reactor hall. There the HPC is opened and the RPV is lifted out. The RPV is in turn opened and refueling operations commence. Possible revisions to the power modules could also be made during this phase. Unfortunately there is a lack of detailed information on NuScale SMR maintenance, so further research is required for in-depth analysis.

The construction and some phases of the maintenance of the NuScale SMRs have to be performed in a centralized manufactory. The main principle of mass production is cost reduction: a standardized process is relatively simple to replicate while maintaining high production standards compared to case specific processes. It is also apparent that replicating standardized processes requires far less monitoring, thus further cutting down production costs. On the other hand, standardized processes have large difficulties fulfilling present day country specific licensing processes [2]. Licensing characteristics are only briefly discussed in the scope of this thesis.

One interesting aspect in the NuScale SMR concept is the possibility for mass maintenance. In other words, the in-depth maintenance of power modules could also be executed in manufactories. This could be a difficult procedure from the regulatory point of view, because most regulatory guides do not address power module transportation after it has been commissioned.

3 Design features in NuScale SMR

This chapter presents the characteristics of the passive and inherent safety features in NuScale SMRs. Design features that are common to typical NPPs are not discussed in this thesis.

3.1 Passive core coolant circulation concept

Primary side coolant circulation is completely passive in the NuScale SMR. The design of most NPPs takes advantage of a passive circulation as an intensifying effect, but in the case of NuScale SMRs there are no primary side coolant pumps, not even as an extra safety measure.

All flow loop systems that are in balance do complete the total pressure equivalence criteria [11] (Edited):

$$\Delta p_{total} = \Delta p_{hydrostatic} + \Delta p_{friction} + \Delta p_{single\ resistance} + \Delta p_{mechanical}, \quad (1)$$

where Δp_{total} is the total pressure change along the path (Pa), $\Delta p_{hydrostatic}$ the hydrostatic pressure difference (Pa), $\Delta p_{frinction}$ the pressure losses inflicted by duct friction (Pa), $\Delta p_{single\ resistance}$ the pressure losses inflicted by contractions (Pa), bends etc., $\Delta p_{mechanical}$ the mechanical pressure changes inflicted by components (e.g. turbines and pumps) (Pa).

There are no pumps in the primary circuit, so the driving force is hydrostatic pressure, and the other terms are losses. The working principle of a natural circulation is to have a closed loop between the heat sink(s) and heat source i.e. the reactor core. The hydrostatic pressure at any point in the loop can be calculated with the following equation [11]:

$$p_{hydrostatic} = \rho g H, \quad (2)$$

where ρ is density (kg/m^3), g gravitational acceleration constant (m/s^2) and H the height of the fluid above (m). The following assumption is valid for water with good accuracy in normal NPP conditions:

$$\rho = \rho(T, p) \approx \rho(T), \quad (3)$$

where T is the average temperature of the water above (K) and p the pressure (Pa). From Equations 2 and 3 can be derived that the hydrostatic pressure of the coolant water depends practically only on the temperature and the hydrostatic height:

$$p_{hydrostatic} \propto TH \quad (4)$$

Calculation of minor pressure losses can be represented in the following basic form [11] (Edited):

$$\Delta p_{single\ resistance} = \zeta \frac{1}{2} \rho w^2, \quad (5)$$

where ζ is the coefficient of single resistance representing flow resisting characteristics and w the flow velocity (m/s). The major pressure losses inflicted by the pipes roughness could be calculated by the following formula:

$$\Delta p_{friction} = \lambda \frac{L}{d_h} \frac{1}{2} \rho w^2, \quad (6)$$

where λ is the coefficient of resistance dependent on the pipes roughness, L the length of the pipe (m) and d_h the hydraulic diameter of the pipe (m). Natural circuit design principles are all based on the formulas above. Basically the hydrostatic pressure difference related factors are maximized and the loss factors minimized.

The first design principle is to increase the driving hydrostatic pressure difference. Like Equation 4 states, the hydrostatic pressure difference could be increased by increasing the height that the rising water travels upwards and the descending water moves downwards. In practice, this is done by placing the core on the bottom section of the RPV and the HCSG on top. Also the height of the primary circuit is kept as long as possible.

The second design principle is to minimize pressure losses. In practice, this is done by minimizing the length, which working fluid must flow through horizontally and avoiding large changes in the flow area etc.

A third good principle considering the primary loop architecture is to avoid any unstabilizing effects. For example, the heat source(s) and sink(s) should never be designed along a horizontal path because stratification could inflict backward secondary flows. A cross-section of the RPV is presented in Figure 3, in which the previously presented general design principles could be seen in use.

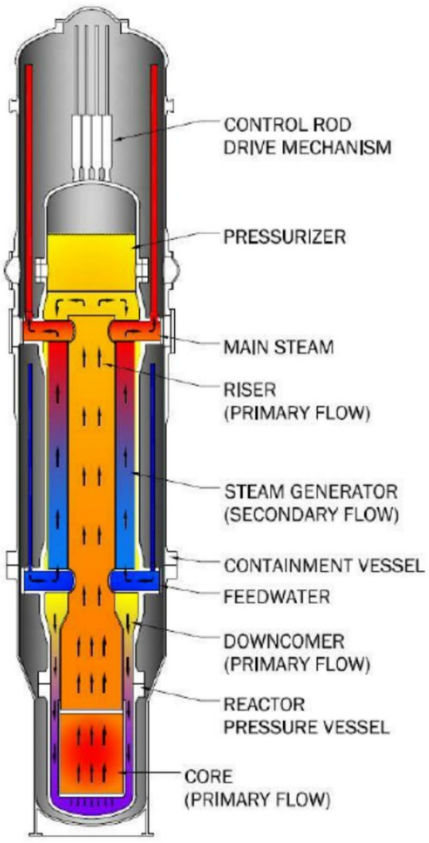

Figure 3. Cross-section of NuScale SMR with flow and heat patterns [12]

3.2 Helical coil steam generator

One new design feature in the NuScale SMR is the use of a Helical Coil Steam Generator (HCSG). A helical coil heat exchanger is not a recent concept. The subject attained academic attention in the 1950s, but the original draft of a coiled pipe heat exchanger originates from the 1910s. Although the idea of a coiled heat exchanger is quite old, the concept was rarely used. One of the main reasons behind the unpopularity is the complex phenomena occurring inside the flow - especially in the case of multiple phases or fluids [13]. This chapter gives a general understanding of the helical coil steam generators characteristics. A more theoretical and in-depth approach is taken in section 6, where HCSG modelling is covered.

The NuScale HCSG basic structure is as follows: a helically coiled counter current heat exchanger wrapped around the reactor chimney in order to save RPV volume. The HCSG is designed to be a once through steam generator to cut down the need for multiple heat exchangers. The secondary flow inside the tubes is driven by pumps in normal operation. However, the HCSG is also capable of supporting natural circulation in the event of emergency. A NuScale HCSG bundle design is illustrated in Figure 4. The basic design of a counter-current helical coil steam generator is illustrated in Figure 5.

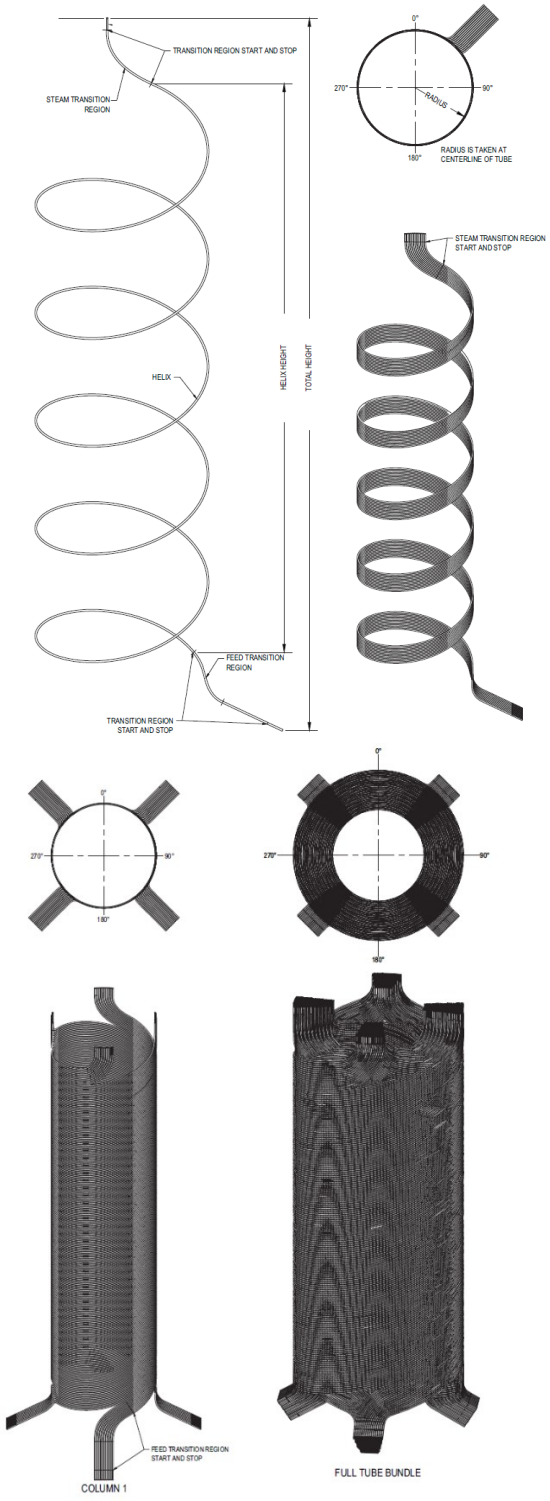

Figure 4. NuScale steam generator [14]

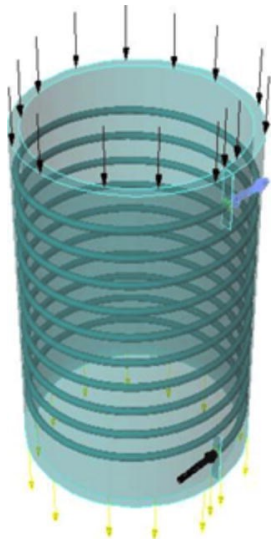

Figure 5. A counter-current helical heat exchanger [15]

From a primary circuit's perspective, the HCSG has several advantages [13]. First, the helical design geometry allows for longer pipes to be fitted in the RPV, which decreases the need for multiple parallel pipes and reduces the size of the RPV. It should be noted that the HCSG arrangement does not include any primary pipes outside the RPV, which in turn decreases the probability of LOCA and further enhances the isolability of the RPV. Second, the relatively high heat transfer efficiency means that the overall pipe length can be reduced. Another benefit of the helical design is a better resistance to both thermal and pressure related stresses. The circular shape of the coil limits its axial expansion so that it endures high temperature changes better. The enhanced pressure resistance of the HCSG relates indirectly to its design, but also directly to the arrangements that it enables. Typically the highly pressurized primary side flows inside the SG tubes, inflicting expanding pressure strain on the tubes, but in this case secondary side flows inside the SG pipes inflict squeezing pressure strain that the circular pipes endure much better [16]. One more benefit of the helical geometry from a primary perspective is the countercurrent flow direction, enabling maximal temperature difference for a high heat transfer rate. For example, horizontal straight tube heat exchangers have higher temperatures inside the other end of the pipe, which is not necessarily surrounded by a higher temperature fluid.

Some of the advantages of a helical design are seen in inside heat transfer. Inner heat transfer is notably more efficient with helical than with straight pipes. The high efficiency can be explained with the helical form as it causes the flowing fluid to experience a centrifugal effect, which increases the mixing of the fluids especially on, or near, the pipe walls [17]. This mixing effect is notably stronger with two-phase flows, thus increasing steam drying. The dry and superheated steam does not require moisture separators or separate super heaters, which cuts down equipment costs and the size of the primary circuit. NuScale HCSG is therefore designed to be once-through [18]. The HCSG involves no U-bends and rises steadily inside the RPV, which further enhances utilization rates in natural circulation flow systems during an emergency. This possibility is utilized in the DHRS concept discussed in section 3.4.1.

The HCSGs are nowadays still relatively little used in NPP concepts. The HCSGs are though frequently used in refrigeration -, air-conditioning -, heat recovery systems and dairy and chemical processes [19]. The present helical coil correlations for heat transfer calculations have not been widely used for power plant calculations. Especially the two phase region, which is the most important section in SGs, has had only a few in-depth

publications [13]. The modelling of HCSGs and a power maneuvering simulation are discussed in section 6 and emergency transient simulation results are discussed in section 5.4.

3.3 Integrated reactor pressure vessel and high pressure containment

The combination of a passive primary coolant circulation and a helical coil steam generator reduces the volume the primary circuit and the RPV require. The small RPV enables a new design perspective for containment structures. Typically a containment structure is designed only for low pressure operations and resembles an isolatable reactor hall. Low pressure and large volume by design leaves the primary system somewhat prone to LOCA, thus requiring several backup systems for such events. The NuScale concept HPC is designed to withstand LOCA, diminishing the need for other LOCA related emergency systems. For comparison, a typical containment structure design and the HPC are represented in Figures 6 and 7. The HPC and its integration are examined from the RPVs point of view. The integration of the HPC and a cooling pool are discussed later in section of 3.4.

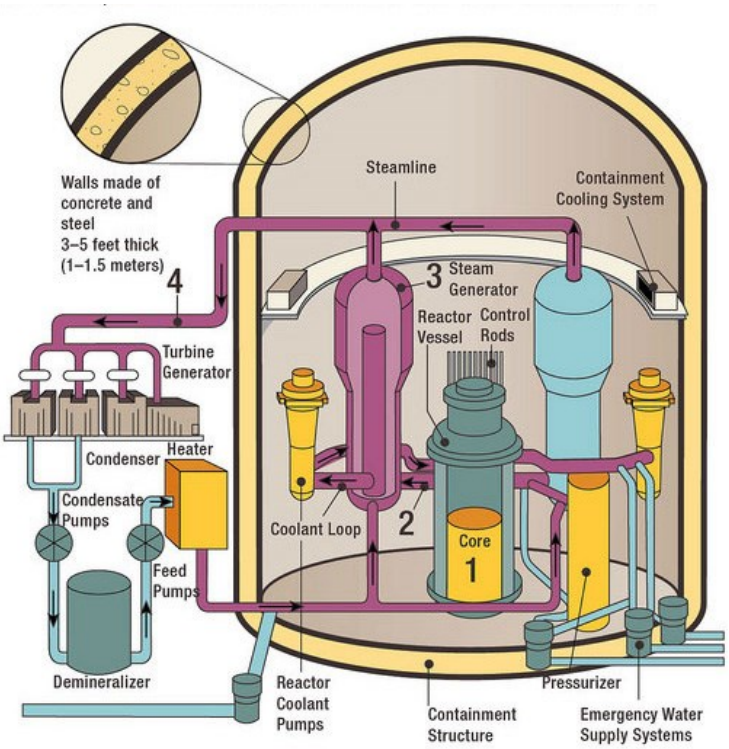

Figure 6. Typical PWR containment structure [20]

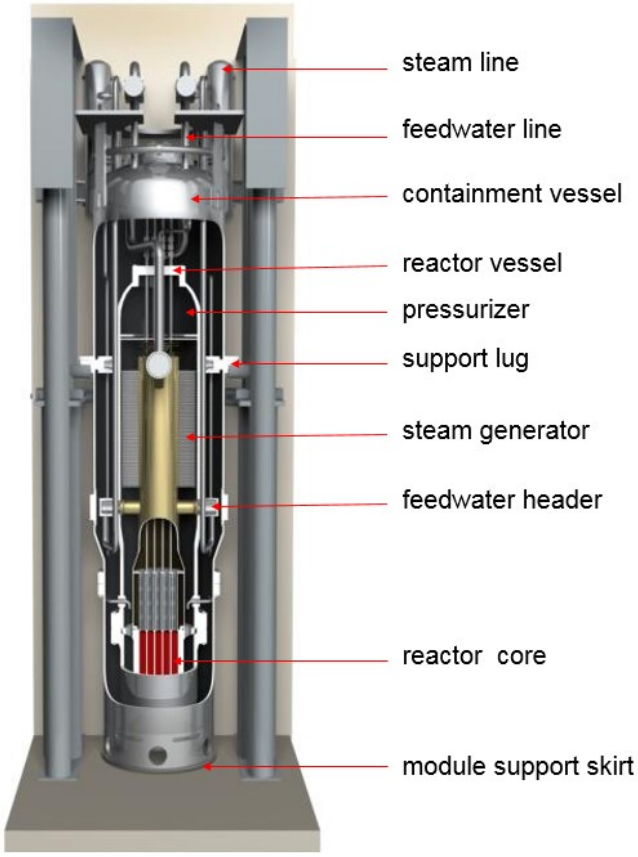

Figure 7. NuScale high pressure containment and power module [21]

The HPC is an evacuated pressure vessel fabricated of a combination of low alloy steel and austenitic stainless steel that houses, supports, and protects the RPV from external hazards and provides a barrier to the release of fission products. Exact design dimensions remain unpublished, but like shown in Figure 7, the HPC does not contain much free volume compared to a typical containment structure. It should also be noted that HPC does not contain other actuating devices than valves, which further enhances the isolability of the unit by reducing the number of required penetrations for cables or pumps etc. The HPC is partially filled with borated water to enable sump recirculation procedures during LOCA. Again, exact data remains unpublished, but the estimated filling percentage is about 50 %. The HPC is maintained partly immersed in a below grade, borated-water filled, stainless steel lined, reinforced concrete pool to facilitate heat removal [22]. Heat removal and its applications are further discussed in section 3.4

The HPC contains three distinctive differences compared to typical NPP containment structures that are high pressure tolerance, small free volume and limited reachability. The HPC is designed to endure large pressure differences well. For example, the design pressure of the HPC is 68.9 bar, whereas the average design pressure of a typical PWR containment is between 1.03- 4.5 bar. This is represented in Figure 8. It should be noted that the small size alone does not enable high pressure endurance. It is possible to construct typical large containment structures with equivalent pressure capabilities, but the high proportional cost makes it unprofitable. Furthermore, the typical containment structure has no need for high pressure endurance, because the safety is maintained by other means.

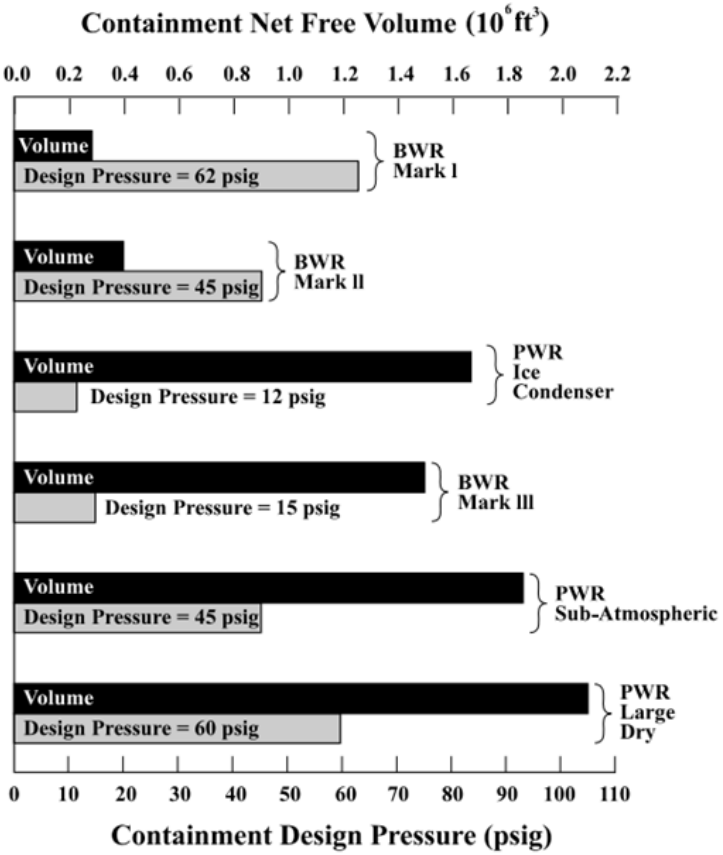

Figure 8. Typical containment design pressures and volumes [23]

A small free volume in the HPC reduces depressurization related crises on the primary side. The depressurization crisis originates typically from a Large Break Loss of Cooling Accident (LBLOCA), in which coolant discharges to the containment building. In a case of RPV breach, primary pressure drops from a normal operation pressure of 127 bar [7] to 63 bar [6], which is still substantially higher than the boiling pressure of the core inlet flow 46.17 bar [5]. The design temperature of a core inlet in normal operation is 258.3 °C [24]. With the HPC, the sudden pressure drop is tolerable keeping the void fraction in core low and thus keeping the fuel from being damaged.

Limited free volume and the partial filling of the HPC also reduces water level drops and core exposure. This is very important because the feature effectively makes large scale emergency injection systems unnecessary and these can be left out of the design [25]. The lack of emergency injection trains further enhances the isolability of the power module.

The new containment design does, however, have some disadvantages when compared to more common designs. Firstly, during operation or accident, the RPV is not reachable by plant personnel. This means that a HPC equipped plant is not as flexible to operate in unexpected events, which require manual maintenance. The possibility or even the existence of such events is not well researched and requires additional studies. Second, the lack of an emergency water injection system means that there are no emergency related boron injection systems available, which means that short term reactivity control is only enforced with control rods.

3.4 Integrated ultimate heat sink and passive heat removal systems

The objective of this section is to provide a short briefing on the integrated relation of the HPC and the cooling pool. The safety related systems Emergency Core Cooling System (ECCS) and Decay Heat Removal System (DHRS) utilize the cooling pool as UHS. These systems are described in separate sections of 3.4.1 and 3.4.2.

The NuScale NPP cooling pool is shared not only by power modules, but also by the refueling systems. The spent fuel pool is, however, separated from rest of the cooling pool with a weir. In order to support refueling procedures and sustain radiation leaks, the pool water is borated and is constantly circulated through a cooling pool clean-up circuit. The cooling pool is presented in Figures 9 and 10.

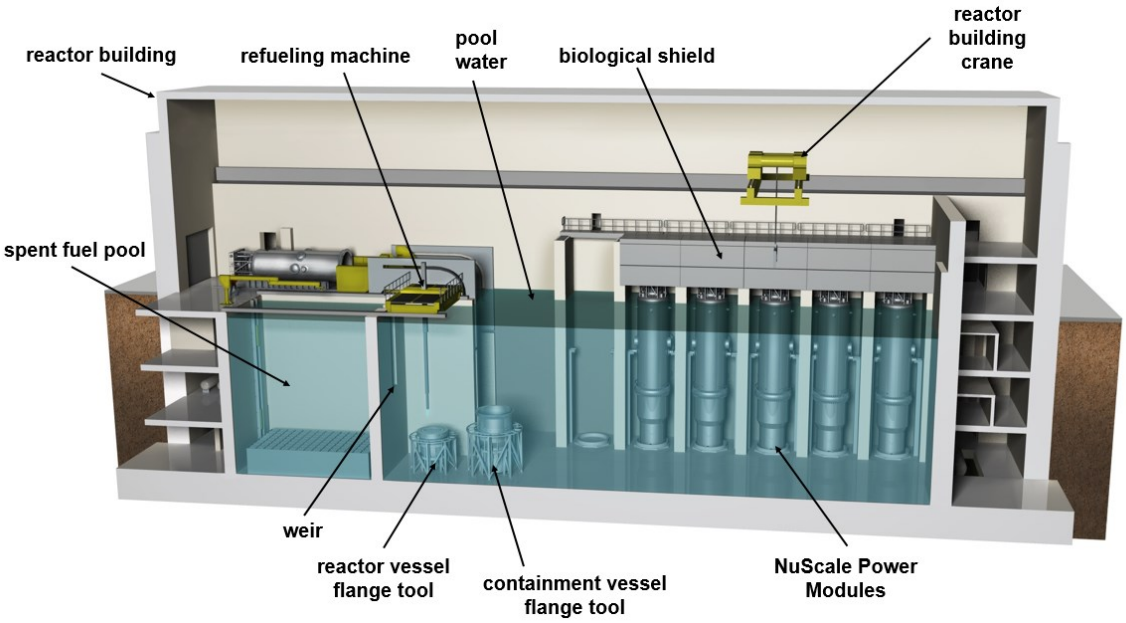

Figure 9. Cross profile of NuScale NPP reactor hall and cooling pool [26].

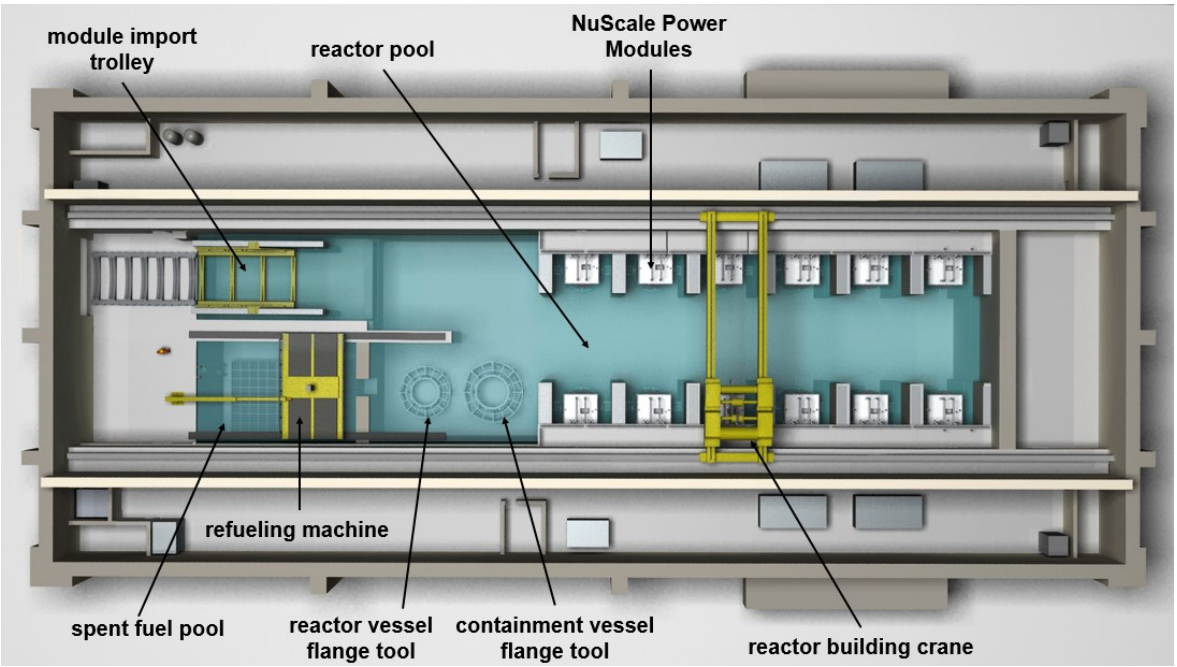

Figure 10. Cross profile of NuScale NPP reactor hall and cooling pool from above[26].

The reactor pool surrounds the HPC and is considered an Ultimate Heat Sink (UHS) during emergency procedures. The UHS serves several safety functions that include the following: providing a cooling medium for the decay heat removal systems, the containment vessels, and the spent fuel assemblies stored in the storage racks; providing borated water for reactivity control during refueling; providing radiation shielding for the spent fuel assemblies and nuclear power units; and providing input to the plant protection system [25]. Unlike a typical heat transfer chain from primary side to UHS, the NuScale concept heat transfer chain to cooling pool includes relatively few steps and after actuation, it is completely passive. The presented typical long term heat transfer chain requires AC power for water pumping and contains several steps which each are critical for long term heat transfer.

The cooling pool inventory is dimensioned to sustain a lone malfunction in one power module and the decay heat production of the rest [25]. The NuScale NPP is thus designed to sustain a site black-out and a malfunction in one power module and to manage the cooling without any extra cooling water or backup power production. In this case it should be noted that the cooling pool inventory alone is sufficient only, if the cooling pool water is boiled away. This is presented in Figure 11. Detailed analyses on emergency procedures and margins are not released yet, so in order to draw conclusions, a more in-depth research is needed.

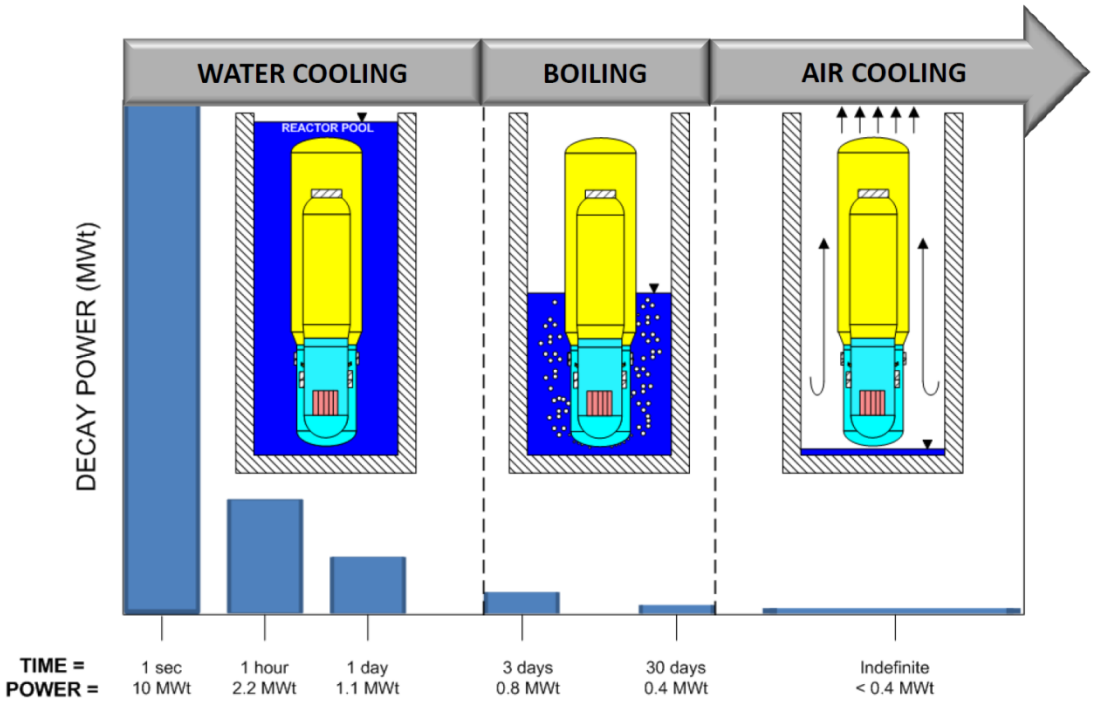

Figure 11. NuScale concept long term cooling using only cooling pool [27]

3.4.1 Passive Decay Heat Removal System

The Decay Heat Removal System (DHRS) provides secondary side reactor cooling for non-Loss of Coolant Accident events when normal feed water is not available. The system is a closed loop, two-phase natural circulation cooling system. Redundant trains of decay heat removal equipment are provided, one attached to each steam generator loop [25].

The working principle of the DHRS is presented in Figure 12. Automation system isolates SGs from the rest of the secondary loop and then redirects flow to DHRS trains. The procedure is performed using only a set of shut-off valves, thus enabling the operation in a case of a station blackout. After the connecting procedure is performed, the flow in the DHRS circuit is driven by the hydrostatic pressure difference between the SG heat exchangers located in the reactor pool. It should be noted that the DHRS is designed to operate in both two-phase - and one-phase flow cases [26].

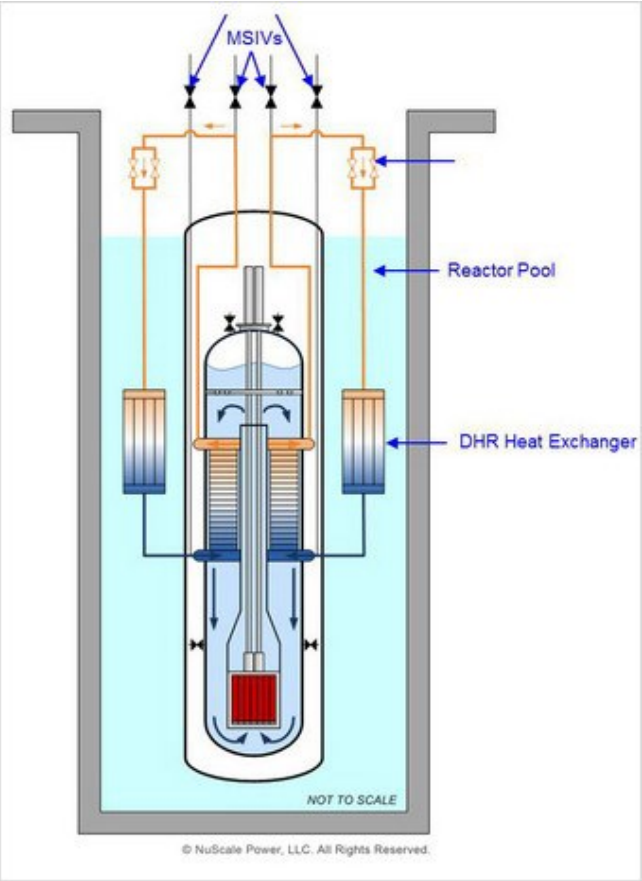

Figure 12. Decay Heat Removal System [26]

The DHRS is similar to a common secondary side reactor cooling system. The DHRS operates through SGs and it transfers heat towards an ultimate heat sink. However, there are a couple of differences. The common secondary side reactor cooling system usually transfers heat to a tertiary cooling circuit, whereas the DHRS transfers heat directly to the UHS. Secondly, the DHRS is independent from a secondary loop (excluding SGs), which means for example that the DHRS remains functional in an event of a large main condenser leak [28]. Third and foremost, the DHRS does not depend on a power supply to enable normal functioning in station blackouts. The DHRS valves are designed to open upon interruption of control power [14], [29] thus enabling the DHRS in a complete site blackout scenario.

The HCSG simulation is a relatively new subject. Furthermore, most of the HCSG cases cover only forced flow regimes, whereas the DHRS is designed to be used when both primary and secondary flow regimes are passive. Therefore also the DHRS needs extensive simulations. Lack of published data on DHRS experiments and its complexity leaves DHRS modelling and simulation out of the scope of this thesis. In future, models that are able to simulate decay heat removal from the core to the cooling pool using only the DHRS are needed.

3.4.2 Passive Emergency Core Cooling System

The primary function of the High Pressure Containment (HPC) is to house, support and protect the RPV from external hazards and provide a barrier to the release of fission products (same as with conventional NPP). The secondary function of the HPC is to enable a

passive Emergency Core Cooling System (ECCS) that could be utilized in core cooling and depressurization and can be utilized even in LOCA [22].

The ECCS consists of three reactor vent valves (RVVs) mounted on the upper head of the reactor pressure vessel (RPV), two reactor recirculation valves (RRVs) mounted on the side of the RPV, and associated actuators located on the upper part of the HPC as shown in Figure 13. All five valves are closed during normal plant operation and are opened to actuate the system during applicable accident conditions. The RVVs vent steam from the RPV into the HPC, where the steam condenses and a liquid condensate collects on the bottom of the containment. The RRVs allow the accumulated coolant to re-enter the RPV for recirculation and cooling of the reactor core. The elevation of the RRV penetrations on the side of the RPV is such that when the system is actuated, the coolant level in the RPV is maintained above the core and the fuel remains covered. The cooling function of the ECCS is entirely passive, with heat conducted through the HPC wall to the reactor pool [29].

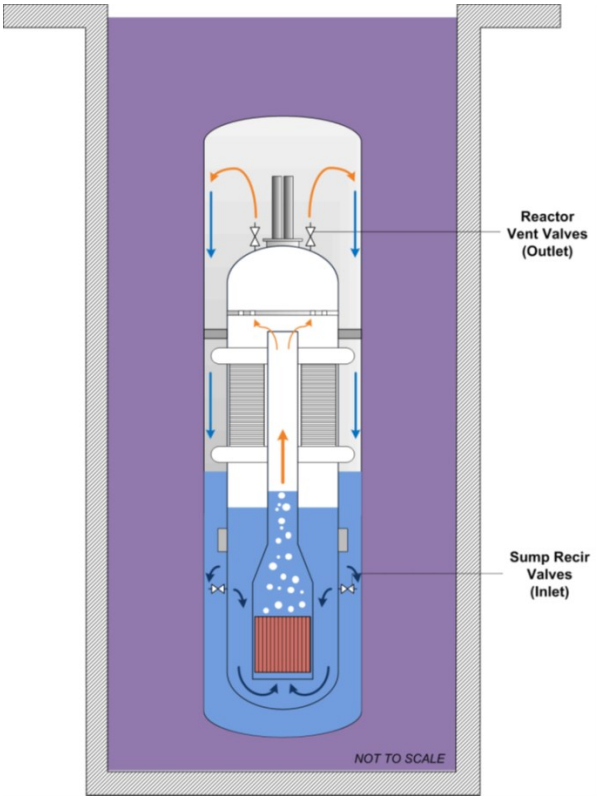

Figure 13. NuScale Emergency Core Cooling System (ECCS) [30]

The ECCS serves three fundamental purposes. The system is normally in a standby state in which the five valves are closed and function as a part of the reactor coolant pressure boundary (RCPB). The principal function of the ECCS is to cool the reactor core when it cannot be cooled by other means, such as during a LOCA inside the HPC. In addition, the ECCS provides low temperature overpressure protection (LTOP) for the RPV.

It should be noted that, like the DHRS discussed in the previous section, the ECCS system requires very few systems in order to actuate, and after actuation, it is completely passive. In order to work properly, the ECCS requires that one of the three RVVs opens, one of the two RRVs works and the integrity of the HPC is not lost. Furthermore, the ECCS remains operational even in a case of LBLOCA.

However, the ECCS inflicts the system with new possible malfunctions. For example, the malfunctioning RVV or RRV opening depressurizes the RPV and leads to a LOCA. This kind of accident leads to a notable pressure drop in the RPV and a large pressure increase in the HPC [31]. This kind of malfunction leads to the highest HPC pressure peak in the scope of the NuScale analysis [22]. This is a relatively major consequence from a single malfunctioning component, so further discussion is advised.

4 NuScale specific design features projected on Finnish regulatory guides

The specific NuScale design features are discussed from a technical point of view in the previous chapter. Nuclear industry is, however, a highly regulated field of engineering [2] and therefore the discussed design features should also be discussed from a regulatory perspective.

In this chapter, the new concepts and design features presented in chapter 3 are discussed from the Finnish legislative point of view. It should be noted that the Finnish legislation and Nuclear Regulatory Guidelines are constantly kept up to date. Therefore the design features are projected only on current edicts and old and upcoming guidelines are not discussed in this thesis.

4.1 Legislation

Radiation and Nuclear Safety Authority (STUK) supervises radiation and nuclear safety in Finland. The safety requirements and regulatory guides (YVL) that STUK formulates are based on the Finnish legislation. Nuclear legislation and guidelines are constantly updated and complemented. The nuclear regulatory pyramid of Finland is presented in Figure 14.

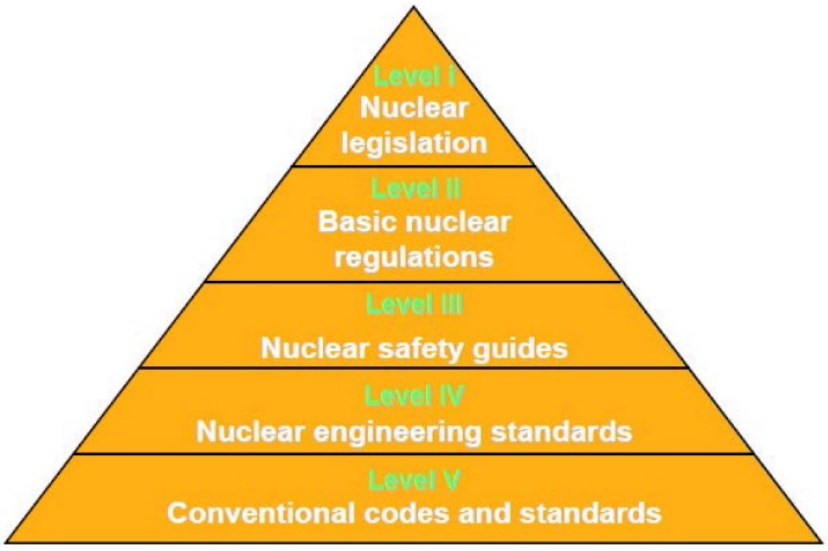

Figure 14. Finnish regulatory pyramid [32]

The foundation of the nuclear legislation in Finland is based on the Finnish constitution (731/1999) [33]. It provides for, among others, that a citizen has the right to safety, his belongings are secure, he has a responsibility for nature and the environment and the public authorities shall endeavor to safeguard the citizen's right to affect the decision-making concerning their living environment. The most important laws concerning the nuclear industry are the Nuclear Energy Act (990/1987), the Nuclear Energy Decree (161/1988) and the Radiation Act (592/1991) [32] (Levels I and II in the pyramid). The Finnish nuclear legislation is very general in nature, so the design feature study done in the scope of this thesis cannot reasonably be conducted on Levels I or II.

The nuclear legislation authorizes Radiation and Nuclear Safety Authority (STUK) to formulate safety requirements and regulatory guides (YVL) concerning the use of nuclear energy, and also to monitor their compliance [34]. From the nuclear licensee's point of view, these are the main requirements to be fulfilled and are briefly discussed in this thesis (Level III in the pyramid).

Many of the YVL guidelines demand that the safety features are projected on both the nuclear - and basic engineering standards with the nuclear standards on higher priority (Levels IV & V) [2]. Many of these standards are detailed or case specific and thus are not discussed in the scope of this thesis.

All in all, the following sections discuss the specific safety features on the nuclear regulatory guide level, because upper levels are too general and lower levels too specific for the current maturity of the NuScale concept. In future, more precise discussion is advised.

4.2 Modular production and maintenance of NuScale nuclear power plants

The first interesting feature from a regulatory perspective is the supervisibility criterion. It should be noted that YVL guidelines are designed for current, single-case, non-modular and stationary NPPs. YVLs state that not only do the construction and operation phases have to be well supervised, but so does the design phase. The design phase can be supervised in a typical case-specific NPP projects, but in a NuScale design project it cannot be supervised, because most of the design is already done. Additionally, the supervision executed by some other authority may not fulfill all of the requirements. Guidelines regarding construction and location would also require some new interpretations: NuScale power modules are manufactured in centralized factories, whereas current nuclear power plants are assembled individually on the NPP site. The YVLs considering supervision [35] require a lot of interpretation, because the current on-site supervision standards may turn out to be impossible to fulfill. It should be noted that the manufactory is not necessarily located in the same country or even on the same continent where the NPP site is located, thus further complicating observability.

The second aspect is the concept of mass production [2], [5]. At the moment there is not much information released regarding the NPM production characteristics, but a few points could be drawn: current NPP construction related subcontract chains are maintained individually in each NPP project and thus can be altered, if some subcontract requirements are not approved. In the case of mass-produced NPPs, the case- or country-specific alterations in subcontractor chains are no longer possible.

The third aspect is the possible concept of modular maintenance. In order to fully utilize the advantages of SMR concept, not only the production, but also the maintenance could be issued in series. For example, one SMR module could be in maintenance or refueling, while other modules are still on power production or are temporary shutdown. This kind of operation is common in traditional multi-reactor NPPs. However, the reactors and heavy lifts done during in the process are usually located in different reactor halls or buildings, whereas the heavy lifts in NuScale SMR concept are done in the same reactor hall. This aspect is not further discussed in the scope of this thesis due to the current lack of published information on maintenance procedures. However, a future in-depth analysis on the subject is advised.

On the other hand, modularity has potential for new licensing approaches [2]. The NuScale NPMs and their subcomponents are essentially identical among themselves. This reduces the need for individual design examination. However, supervision during construction and assembly is still required. Furthermore, it is arguably possible to standardize a NPP design in order to use the same license also on other sites [2]. The other module specific licenses could also be spread into sections. For example, the licensing of the second module could be timed to occur during the construction phase of the first module.

4.3 Passive design features

The Finnish regulatory guides handle passive safety functions only briefly due to their relatively rare use in the current Finnish NPPs. Most of the passive aspects used in the Finnish NPPs, and thus discussed in the YVLs, are basically more like passively triggered functions, e.g. check valves, whereas passive processes like natural circulation are not mentioned.

Arguably the most important aspects are the ones that are replaced by passive safety systems [28]. For example, the YVLs contain many requirements considering active components, which are lacking or not necessarily needed in the NuScale concept. The missing passive system requirements could reduce the licensing related workload, or on the other hand increase it. In other words, there are no certain guidelines to be followed, but the demonstration of safety without clear safety definition methods could be troublesome.

The Defense-in-Depth (DiD) strategy refers to several redundant safety systems that shelter the reactor core on multiple levels [28] in a functional perspective. If one level fails, there are still multiple independent levels remaining. DiD is one of the most fundamental rules in NPP design [36], and it is one of the governing principles in NuScale design [8], [37]. Levels that are maintained with passive safety features are considered more reliable, thus strengthening the given level. The possible problems arise from the required structure of the DiD strategy. The structure of the DiD levels is defined by Western European Nuclear Regulators' Association (WENRA) and is represented in Figure 15. Although the new passive systems could arguably be strong, it would be problematic to fit some of the new systems onto current DiD levels. One reason for this is that some of the specific safety features could be placed in many levels [28]. In order to fulfill the independency criteria, a division may have to be put in place. This could lead to a situation where some levels contain only relatively few safety systems [28]. Another possibly problematic characteristic is the fundamental structure of WENRA DiD levels; whereas NuScale SMR is designed to fit into DiD levels utilized by NRC [8]. The two DiD systems are mostly the same except that WENRA has the Level 3 separated into Level 3a and 3b [2]. This division certainly requires a new interpretation of the guidelines.

Levels of defence in depth	Objective	Essential means	Radiological consequences	Associated plant condition categories
Level 1	Prevention of abnormal operation and failures	Conservative design and high quality in construction and operation, control of main plant parameters inside defined limits	No off-site radiological impact (bounded by regulatory operating limits for discharge)	Normal operation
Level 2	Control of abnormal operation and failures	Control and limiting systems and other surveillance features		Anticipated operational occurrences
Level 3 (1) 3.a	Control of accident to limit radiological releases and prevent escalation to core melt conditions (2)	Reactor protection system, safety systems, accident procedures	No off-site radiological impact or only minor radiological impact (4)	Postulated single initiating events
3.b		Additional safety features(3), accident procedures		Postulated multiple failure events
Level 4	Control of accidents with core melt to limit off-site releases	Complementary safety features(3) to mitigate core melt, Management of accidents with core melt (severe accidents)	Off-site radiological impact may imply limited protective measures in area and time	Postulated core melt accidents (short and long term)
Level 5	Mitigation of radiological consequences of significant releases of radioactive material	Off-site emergency response Intervention levels	Off site radiological impact necessitating protective measures(5)	-

Figure 15. Defense in Depth levels [38]

In the end, the most interesting adaptations are related to the technical differences between the current NPPs and the new features. First and foremost, the passive systems are not directly controllable. For example, primary coolant flow depends on the temperature differences between riser and down comer and could not be directly controlled by e.g. adjusting the speed or rotation of the primary pumps. Second, the passive systems (after possible activation) are constantly on and turning them off may require some active functions. The previous characteristics do not necessarily contain obstacles for licensing, but they do require a new interpretation.

4.4 Integrated design and high pressure containment

Although the integrated design and the new concept of the High Pressure Containment enable many new safety features, they also require a lot of interpretation of the regulatory guidelines. Problems arise from the very nature of the HPC; it is partially both a containment structure and a pressure vessel, which are discussed in specific YVL guides of B.6 [39] and E.3 [40]. In general, it could be troublesome for a system to fulfill two separate guides concerning two different systems. Fitting the two separate guides for HPC is not further discussed in this thesis, due to the required workload, but a few separate interesting guidelines are picked and discussed.

First, the submersion and small containment restricts the accessibility of the RPV and the HPC. During operation and until the complete shutdown, the RPV and the HPC to a lesser extent are inaccessible for the plant personnel by design. The YVLs require that some

accessibility is maintained [40], [41], but again those guides are issued only for current NPPs. In this case new interpretations should be drawn.

Second, there are no filtering structures in the ECCS recirculation, which the YVLs do require for sump recirculation [35]. On the other hand, the amount of insulation and coating materials in the HPC is negligible, in which case the need for sump filtering is also negligible.

Third, although the HPC can withstand pressure better than most of the conventional containment structures used in current NPPs, it has some issues in fulfilling the current YVL guides. For example, it is stated that containment should withstand the highest pressure load in the worst postulated accident scenario with a 10 % safety margin [39], whereas the HPC's margin is only 8 % [22]. Again the absolute pressure margins are completely on a different scale: HPC: 3.4 bar and conventional containment: ~ 0.2 bar, thus increasing the need for new interpretations and discussions.

4.5 Safety related features that require further studies

The NuScale SMR concept includes plenty of new and modified safety features. The full scope of these alterations is not discussed in this thesis, but the most important ones are presented.

The NuScale concept involves no Boric Acid Shut-down System (BASS). Second, Emergency Injection Systems (EIS) are also left out. It is arguable that the extra water injection systems are not needed, because there are no primary circuit pipes and the LOCAs are handled by the HPC. The YVLs still require the mentioned systems all the same [34]. The same cannot be said of the missing BASS. It is one of the governing principles in the regulatory guides that essential safety functions, including reactivity control, are maintained with at least two independent systems that implement the diversity principle [42]. The NuScale SMR includes a maintenance circuit for boron concentration adjustment, but it is used primarily for the fuel burnup compensation throughout the fuel cycle [7]. It is noted that the boron adjustment could be exploited during postulated accidents, but it is not required, nor designed so. In practice, the short-term emergency reactivity control in NuScale SMR is enforced only with control rods, thus leaving the YVL requirements seemingly unfulfilled. However, the discussion done in the scope of this thesis is superficial, so in order to draw conclusions, a deeper analysis is required.

The NuScale concept could arguably benefit from uncommon site locations. It is discussed on general level that, in addition to power production, SMRs could be utilized to some other secondary processes [1], [28]. Some of the secondary processes could possibly be heat production for district heating or industrial processes, or steam generation for food industry, for example. All of the previously mentioned example process systems would benefit significantly, if SMRs and the end user are sited close to each other. For example, the pressure losses of district heating network are notably lower, if the power plant is located near a population center. The NPPs are normally sited relatively far from population centers and industrial towns for safety reasons [35]. The unconventional site locations would require a deeper survey, but due to the current maturity of SMRs and the hypothesis of their secondary utilization, the speculations are left out of the thesis. However, future analyses on the matter are advised.

5 Simulation of SMR test facility

One of the main objectives of this thesis is to model an indicative Apros simulation model of the OSU-MASLWR test facility. It is mainly based on the information published in IAEA TECDOC 1733 [43]. The conducted simulations are described in sections 5.4 and 6.2.

5.1 Apros simulation software

Apros® is multifunctional software intended for modelling and dynamic simulation of processes and power plants. Apros is developed and owned by Fortum Power and Heat Oy (Fortum Oyj) and VTT. The development of the software was started in 1986 as a joint effort to create an Advanced Process Simulation (APROS) environment for the simulation of conventional and nuclear power plant processes. Presently Apros contains extensive models not only for thermal hydraulics, but also for automation and electrical systems. With the includable program packages for containment, burning reactions and flue gas flow modelling, it is nowadays possible to simulate whole power plants (nuclear or combustion) using only Apros [43].

In Apros, all of the flow models are one dimensional. This common simplification for the so called lumped parameter codes is used in order to increase simulation speed and thus enable the modelling of entire power plants. Multidimensional phenomena are taken into account through analytical or empirical correlations or by modelling a pseudo two or three dimensional model consisting of one dimensional components [45].

The Apros thermal hydraulics model library contains three different sophistication levels for one dimensional two-phase fluid flows. These are the 3-equation homogenous model and the 5- and 6-equation two-phase models. The aforementioned models are used to solve the one dimensional conservation laws of mass, momentum and energy [46]. The three equations are applied collectively and separately to liquid and gas phases resulting in three to six equations. All of the models manage to solve two-phase flows with the following simplifications: 3-equation model assumes both phases have the same temperature and velocity and are perfectly mixed, the 5-equation model assumes same they have the temperature and mixing. Although the 6-equation model is very computationally intensive compared to the 3- and 5-equation models, it is preferred because of high simulation accuracy [47]. All models in the scope of this thesis are modelled with the 6-equation model.

The flow solution in Apros is based on a staggered grid discretization scheme. In this scheme, the static variables such as pressure and enthalpy are calculated in the middle of the mesh, i.e. in a node and the flow related variables are calculated at the border of two nodes, i.e. in a branch. These nodes and branches form the calculation level of the thermal hydraulic solution [45] and most of the process components are based on them.

Apros is well validated and widely used simulation software [47]. Furthermore Apros is already being used to model many of the processes of the NuScale SMRs. Apros also contains models for reactor physics-, containment- and automation-components [48].

Therefore Apros is a good choice for modelling the MASLWR test facility, and depending on the findings, a possible choice for future SMR modelling. Alternative simulation software is not discussed in the scope of this thesis.

5.2 Test facility description

This chapter provides a brief overview of the Oregon State University (OSU) Multi-Application Small Light Water Reactor (MASLWR) test facility.

Oregon State University (OSU) has constructed a system-level test facility to examine natural circulation phenomena, which are of importance to integral reactors. A series of three tests was conducted from 2002 to 2003 at the OSU MASLWR test facility in order to assess the behavior of this reactor concept in both normal and transient operation. After the completion of this preliminary test series, an IAEA International Collaborative Standard Problem (ICSP) test series was conducted. A major part of the data acquired during the ICSP tests was published in 2014. The test cases presented and the test model built in this thesis are based on that data.

NuScale has also built a new NIST-1 (NuScale Integral System Test) facility to depict an actual NuScale SMR more accurately. NIST-1 includes the power module and a cooling pool, thus improving the range and accuracy of the produced data [48]. However, there is still very little publicized data of this facility and thus its predecessor MASLWR was chosen for this thesis instead. In the future, when the required information is made public, it would be beneficial to also model the NIST-1.

The conceptual design of the MASLWR test facility is same as the NuScale SMR, which is presented in chapter 3. The test equipment is presented in Figure 16.

Figure 16. Oregon State University Multi-Application Small Light Water Reactor test equipment [42]

It should be noted that some changes and simplifications had to be made to the MASLWR design [49]: the test facility is scaled down to 1:3 length, 1:254 volume and 1:375 thermal power. This was done in order to reduce the cost of the facility and to simplify the test arrangements. It's notable that in spite of the extensive scaling analysis, scaling distortions are still possible and therefore the data accumulated from the MASLWR experiments is not directly comparable to a full-scale unit [50].

In this model the CPV, HPC and RPV are all separated, whereas in the case of an actual unit, the vessels would be within one another. This schematic arrangement can be seen in Figure 17. The separation eliminates the need to take conduction heat flow from the RPV to the HPC into account, which further simplifies testing conditions. Heat flow through the RPV walls is dependent only on the temperature of the primary side and thus static. The convection in the actual unit depends on the conditions of the HPC. In normal operation the HPC is depressurized diminishing the convection above the water level. Furthermore the heat flow through the RPV wall changes significantly during ECCS operation. In order to represent heat flow from the HPC to CPV correctly, heaters have been installed on the HPC walls, thus making sure that condensation happens only on the heat transfer plate.

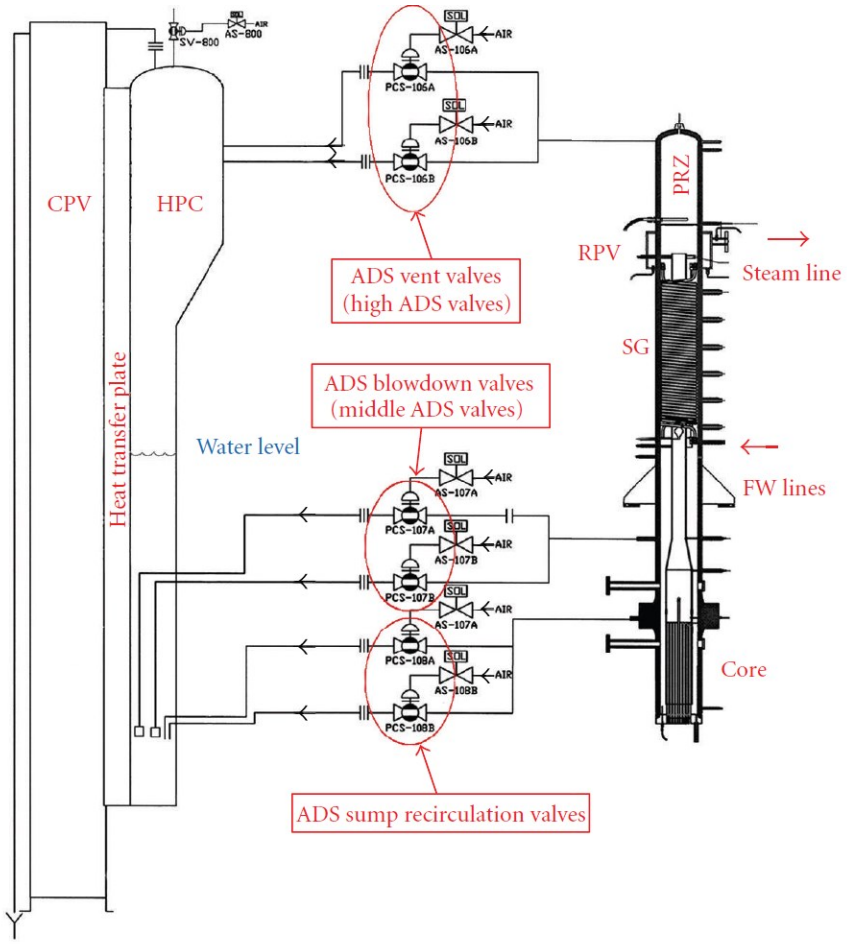

Figure 17. Schematic picture of test facility arrangement [50]

The core is modelled by cylindrical electric heater rods, which rules out the reactivity feedback present in the core during transients.

The CPV is quite limited in size compared to the actual cooling pool. During the ECCS test, the temperature of the cooling pool increases significantly, whereas the increase would be much smaller in the actual pool.

5.3 Apros simulation model

One of the main objectives of this thesis is to construct an Apros simulation model based on the OSU-MASLWR test facility and run ICSP benchmarking simulations on it. This modelling work was done as an extension of a previous model of the OSU-MASLWR test facility [52].

The data used for the model is based fully on the *Evaluation of Advanced Thermohydraulic System Codes for Design and Safety Analysis of Integral Type Reactors,* which is a technical documentation released by IAEA in 2014 [43]. It documents an evaluation run of different thermohydraulic system codes as compared to two ICSP test runs with MASLWR equipment.

The modeled facility is composed of a Reactor Pressure Vessel (RPV), a High Pressure Containment (HPC) and a Cooling Pool Vessel (CPV). All of the vessels are modelled

with the Apros six-equation nodes in order to make dynamic simulation possible in different test conditions. Apros also contains specific containment nodes, which could possibly calculate the regular containment structure more accurately [50], but the six-equation nodes were used here due to them being universally accepted as valid in high pressure and high fluid velocity scenarios. Because of this, in order to simulate multidimensional objects that are not already in the component library, some creative modeling must be used. One approach is to connect one-dimensional components in three directions, thus making a pseudo 3D model. Another way is to make simplifications and to exploit symmetry. The latter option was chosen for this thesis because of its simplicity and the fact that most MASLWR systems are rotationally symmetrical. This kind of 'low level' modelling (modelling that uses only the very basic of calculation components) was used only on the three aforementioned vessels, because all the other process components are already available in the Apros component library.

The reactor core is modelled with a standard 1D-reactor component without neutronics, making it essentially an electrical heater. The primary circuit is modelled mostly as a 1D circuit using six-equation nodes and branches to model flow volumes, and heat transfer structures to model the reactor chimney and RPV walls. For simplicity, the electrical heater of the pressurizer is also modelled with heat structures and power can be adjusted automatically during simulation. All of the possible heat flows and trains connecting from outside to the primary side are marked as external flags on the RPV diagram. The external flag does not affect the Apros calculations at all, because it only transfers the signal to another diagram. This separation is made purely for visual purposes. The RPV model diagram is presented in Figure 18. Red lines have been drawn on the Figure 18 in order to clarify the RPV geometry.

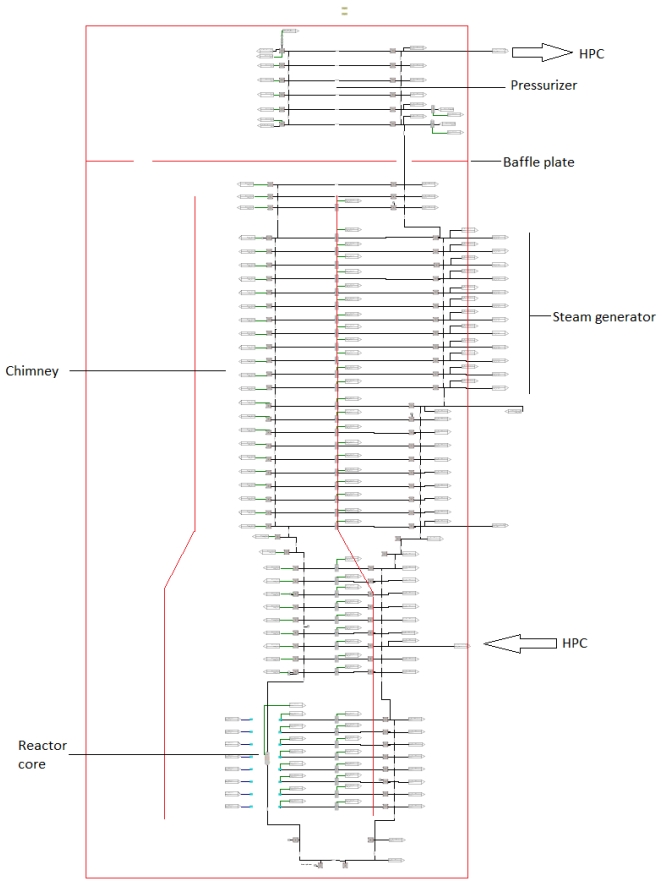

Figure 18. Apros Reactor Pressure Vessel model

During RPV modelling a few physical simplifications and approximations had to be made. A rotationally symmetric flow pattern was assumed: it is known that the angle of the helix of the HCSG induces small radial flows in the downcomer, but due to the small angle of ascent in the HCSG, the flows are assumed negligible.

1D approximation (i.e. no parallel calculation nodes) is possible because the primary circuit is approximately rotationally symmetric and it is assumed that there are no major temperature differences between the two sides of the node. 1D approximation assumes that every individual flow of elements has the same direction and speed in a certain cross-section. In other words, the 1D approach restricts the liquid on one side of the pipe to backward movement, while the other side moves forward. The nature of the six equation model, however, allows for two different phases to travel with different velocities and directions, so the possible two-phase conditions are taken into account.

Many of the smaller approximations have to do with heat flow modelling. The bottom and the top of the RPV are considered adiabatic due to the lack of insulation details and as such the top and bottom of the RPV are modelled without heat losses. The separate heat transfer components on the riser chimney and the RPV walls are not connected to each other, because heat transfer along the walls is assumed to be negligible.

The HCSG is modelled with basic heat pipe components and it is connected to the primary side via heat transferring structures, this is presented in Figure 19. Apros recognizes the modelled structure as a straight ascending pipe with heat transferring capabilities and as such the HCSG geometry and physics are implemented with a specific set of correlations. This is further discussed in chapter 6.

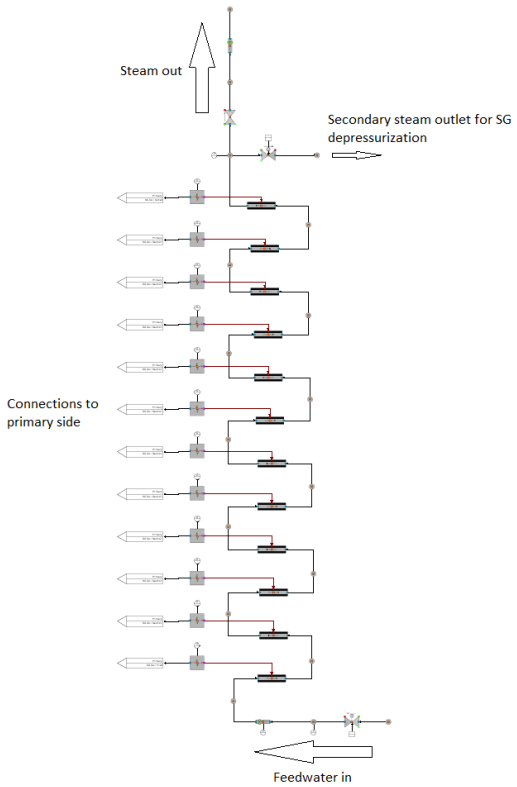

Figure 19. Apros Steam Generator model

The HPC diagram presented in Figure 20 consists of two sections: Automated Depressurization System (ADS) trains and the HPC vessel. The ADS trains are modelled with normal pipe and point components and the HPC vessel is modelled in pseudo 2D form with six equation nodes and branches. The left column in the HPC vessel is completely insulated and ADS connected, whereas the right column partly transfers heat to the heat transfer plate. The blue and white animations on the six equation nodes represent the water level in the given node.

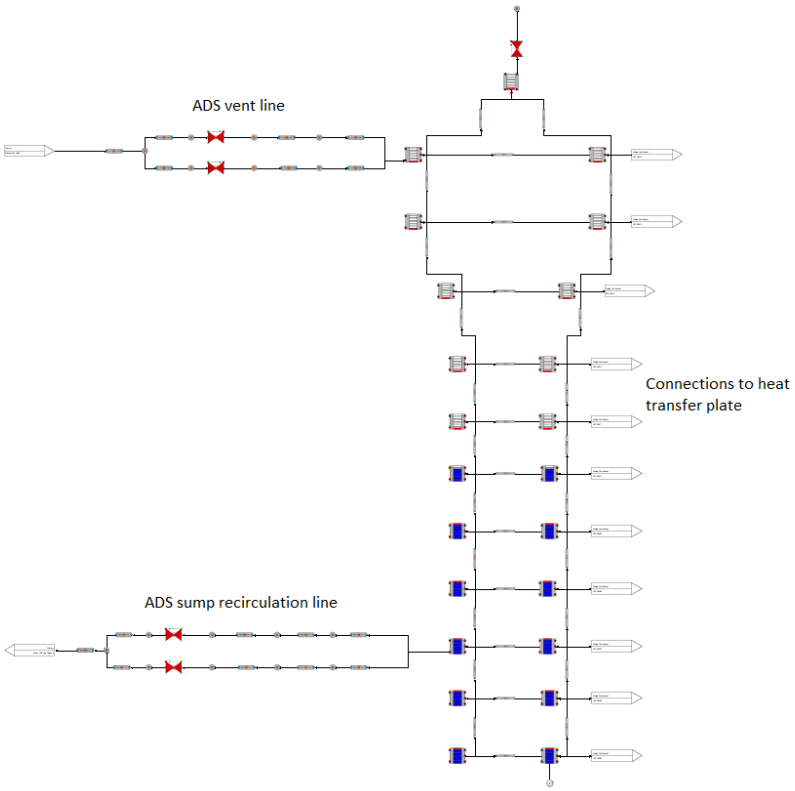

Figure 20. Apros High Pressure Containment model

Due to the lack of information in the technical documentation, the vessel's elevation in relation to the RPV Vessel and the CPV had to be estimated. The effects of any possible estimation errors are negligible during normal operation and the short term cooling phases (in which only the topmost ADS vents are operated). However, when the lower ADS vents are open, at the beginning of the long term cooling phase, the water level difference in the RPV and the HPC balance out. The balancing affects water temperatures of the vessels and, more importantly, the water level inside the HPC. This water level determines the heat transfer rate to the HTP, because the exposed part of the HPC wall transfers heat better than the submerged part. This is due to the fact that water in the HPC is notably colder at the beginning of the test and warms relatively slowly, whereas the condensing steam is always at the saturation temperature.

The CPV, like the HPC, is also modelled in pseudo 2D format with two columns of six equation nodes and branches. The Heat Transfer Plate (HTP) is modelled with basic heat transfer structures including both HPC and CPV walls. Heat Connector components are included along the HPC wall because, in the analytical preliminary calculation, it was found that the heat transfer along the HPC wall is not negligible. The Heat Connector components have no other effect than the heat transfer from one structure to another.

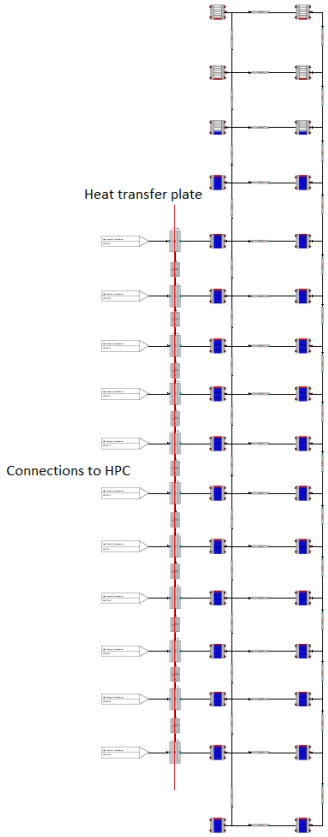

Figure 21. Apros Cooling Pool Vessel model

The automation systems were modelled to have the correct functionality, but not fully in detail. This was done because of the lack of published information considering automation architecture or characteristics. In other words, control obstructions could be present in the simulation model. Note that the automation features that are not relevant to any given test are turned offline. With the maximum time step of 0.01 seconds and the average number of sequential automation components 5, the automation response time is practically instantaneous and should not inflict major deviations to simulations.

The ADS automation diagram, in table 3 below, contains the control logic of the Automated Depressurization System (ADS), which resembles the ECCS from the emergency shutdown tests. This diagram contains the control automation logic for the ADS valves presented in Figure 20. The two ADS vent valves (PCS-106A and PCS-106B) are located near the top of the HPC and they are responsible for venting steam from the RPV to the HPC. The lower ADS recirculation valves (PCS-108A and PCS-108B) are used for recirculating the HPC sump water back to the RPV during long term cooling periods. The ADS has two main functions: Primary pressure reduction after the reactor trip signal is detected, and long term cooling once the pressure on the primary side of the HPC is low enough.

Table 3. Automatic Depressurization System valve control logic [43] (Edited)

RPV pressure (MPa)	HPC pressure (MPa)	PCS-106A	PCS-106B	PCS-108A	PCS-108B
>9.406	-	OPEN	SHUT	SHUT	SHUT
-	>1.825	SHUT	SHUT	SHUT	SHUT
≈ HPC pressure	≈RPV pressure	OPEN	OPEN	OPEN	OPEN

Valve 106A, one of the two ADS vent line valves, participates in the primary side pressure reduction by releasing steam into the containment vessel. Valve 106A opens if the primary pressure reaches 9.409 MPa. Containment vessel pressure must be maintained below the safety limit, so 106A is shut if the containment pressure reaches 1.825 MPa. Valve 106A will reopen once the containment pressure is reduced to below 1.48 MPa, via the cooling provided by the CPV. This cycle will continue until the pressure difference between the primary side and the containment is below 0.034 MPa and all four valves are opened for long term cooling.

During an emergency shutdown test, the HCSG is slowly drained until the pressure reaches atmospheric levels. This operation was not mentioned in the technical documentation, but one of the benchmark participants referenced to the procedure and preliminary analytical calculations also suggested such an operation. The characteristics of the emptying process are completely unknown, so in this model it is assumed that the emptying process is independent i.e. a boundary condition from the simulation perspective. The emptying rate is determined by the target pressure taken from one of the participant's simulation results.

There are a few other automation and supporting process diagrams such as the feed water flow control and heat loss diagrams, but they are not relevant for this thesis and are thus left out.

5.4 Simulation of loss of feed water transient

This section presents the emergency reactor shutdown procedure in an event of feed water loss. This simulation is intended to test Apros' capabilities to simulate natural flow conditions during a feed water loss event and a reactor trip.

An SP-2 test run has three distinctive evaluation objectives. First: to evaluate the ability of the code to simulate passive flow characteristics in a high pressure environment and for the given geometry. Although Apros supports the modelling of natural circulation, it has little to no testing in the SMR geometry or conditions. Second: to test the ability of the code to predict passive high pressurized steam condensation under the influence of non-condensable gases. Although the HPC is kept free of air, some of the accident scenarios include it. Third: to test the accuracy and robustness of the code in a reactor trip scenario.

5.4.1 Test procedures

An SP-2 test was conducted to simulate a loss of feed water event and the following actuation of safety systems, and the following long term cooling. The test was conducted in three phases: pre-test (designed boundary conditions), blind (experimental boundary conditions) and open simulation (experimental results also available) [43]. This thesis utilizes the blind calculation results as comparison material. The material is publicly available, so it is not presented in this thesis. It should be noted that the work done in the scope of this thesis has access to the experimental results, so it is not reasonable to compare this work directly to the blind work of other participants.

The test will be performed as follows: Initially the test facility is brought to a stable state at 75% capacity with the primary pressure at 8.62 MPa and the main feed water pump running on the secondary side. Once the initial conditions are reached, the test is initiated by stopping the main feed pump and thus cutting off flow to the steam generator. With the subsequent loss of the reactor heatsink, the primary pressure will begin to rise. When the pressurizer pressure reaches 9.06 MPa, the MASLWR core heaters will be set to decay power mode (core heater input is given as a table function), and Reactor Vent Valve (RVV) PCS-106A will be placed in "Auto" mode to allow ADS-106A to open on high pressure (9.41 MPa) venting into the high-pressure containment. PCS-106A is operated in automatic mode to vent the primary system to the high-pressure containment. Automatic mode prevents the HPC from exceeding its maximum operating pressure of 2.17 MPa by closing PCS-106A when pressure exceeds 1.83 MPa. After the HPC pressure decreases to below 1.47 MPa, the PCS-106A is opened again. This procedure of opening and closing the RVV is continued until the pressure difference between RPV and HPC is less than 0.034 MPa. At that point both RVVs (PCS-106A, PCS-106B) and both Reactor Recirculation Valves (RRVs) PCS-108A, PCS-108B are opened. This procedure is marked as a transition to the long term cooling phase. Long term cooling phase continues until the pressurizer pressure drops below 0.618 MPa after which the test is ended.

5.4.2 Simulation results

The feed water flow was stopped at 0 seconds, resulting in an immediate pressure increase on the primary side. The decay power mode was activated at 26 s, which is shown in Figure 22. The initial reactor power drop was rapid, but it could not compensate for the reduced heat flow to the SG. The pressurizer pressure reached 9.41 MPA at the 40 s mark and the ADS system was activated by opening the PCS-106A. The HCSG depressurization system was also activated resulting in a steady pressure drop in the secondary side, as shown in Figure 23. The pressure of the secondary side reached 0.11 MPa at 2000 s and the secondary side was effectively cut out of the system.

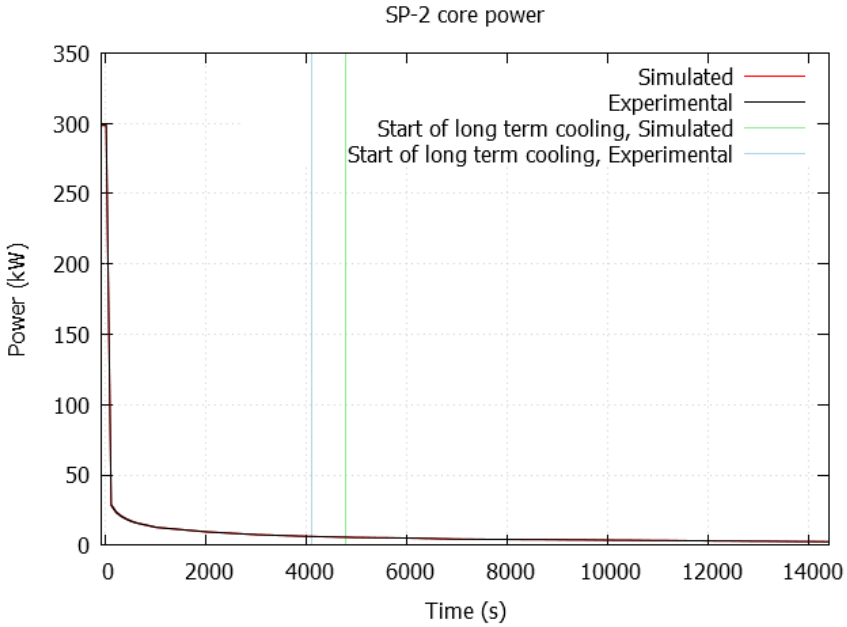

Figure 22. Reactor power during feed water loss test

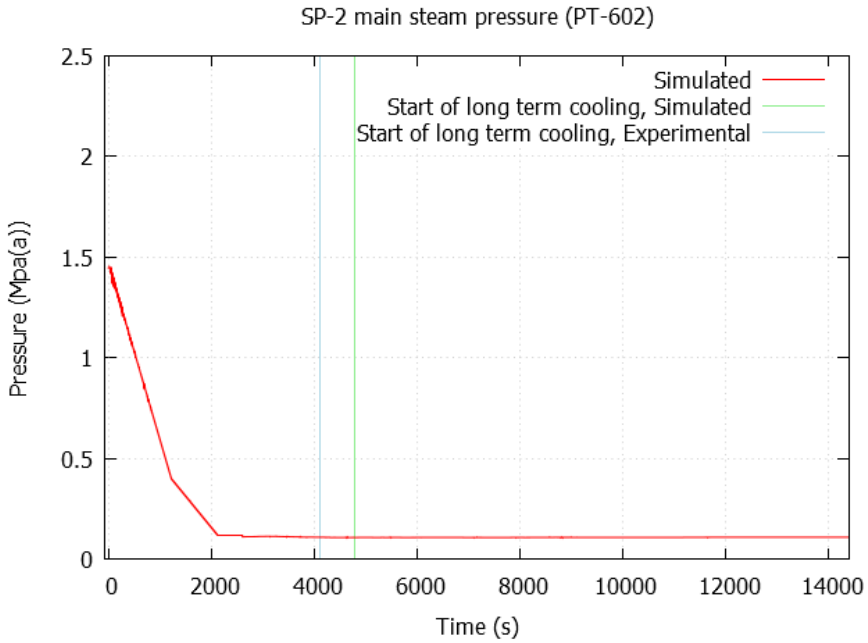

Figure 23. Main steam pressure during feed water loss test

The ADS system released steam from the pressurizer to the HPC resulting in a rapid pressure drop in the primary circuit. Steam was blown until the HPC pressure reached 1.83 MPa at 84 s and the PCS-106A was closed. At that point the primary pressure had dropped to 3.60 MPa. The ADS valve was opened again at 92 s, when the HPC pressure had dropped under 1.49 MPa. This cycle of periodic steam blowdown was continued until at 4782 s, when the primary pressure reached 1.85 MPa, and the long term cooling process started. The long term cooling was initialized by opening the remaining RVV and the two RRV valves, which caused the RPV water level to rise 0.20 meters.

The long term cooling phase continued until the pressurizer pressure reached 6.18 MPa at 13 600 s, and the test was ended. The most important events of the SP-2 test run are summed up in Table 4.

Table 4. Important events during feed water loss test

Event	Experi-mental (s)	Simula-tion (s)	Differ-ence (s)	Comparative difference (%)
Start of simulation – steady state (start of data collection)	0	-60	-	-
Stop feed water flow	0	0	-	-
PZR pressure (PT-301) ≥ 9.064 MPa Enter decay power mode	30	26	4	-13.3
PZR pressure (PT-301) ≥ 9.409 MPa Open ADS vent valve (PCS-106A)	48	40	8	-16.7
Start long-term cooling Pressure difference between RPV and HPC (PT-301 - PT-801) ≤ 0.034 MPa Open and remain open of RVVs Open and remain open of RRVs	4117	4782	-665	16.2
PZR pressure (PT-301) ≤ 0.618 MPa End of test	15822	13600	2222	-14.0

As a conclusion, the SP-2 test run shows relatively good results. The simulated timing of the most important events differs less than 16 % from the experimental values.

The simulation results considering passive phenomena in the primary circuit were quite promising. Primary pressure (shown in Figure 24) is the most important attribute from the depressurization test's perspective. The pressure behaves like in the experiments but with the following differences: The pressure oscillates with a variable amplitude. The varying amplitude and frequency can be explained with the different RRV, RVV driving times and HPC characteristics. It should be noted that steam blowdown to the HPC affects the characteristics of later blowdown periods. The free volume in the HPC decreases as more steam is vented, which is visible in Figure 25 as increasing water level. The remaining space in the HPC affects the amount the RPV could be depressurized in a single depressurization period. This phenomenon is visible in simulated results, but for some reason could not be distinguished from experimental results.

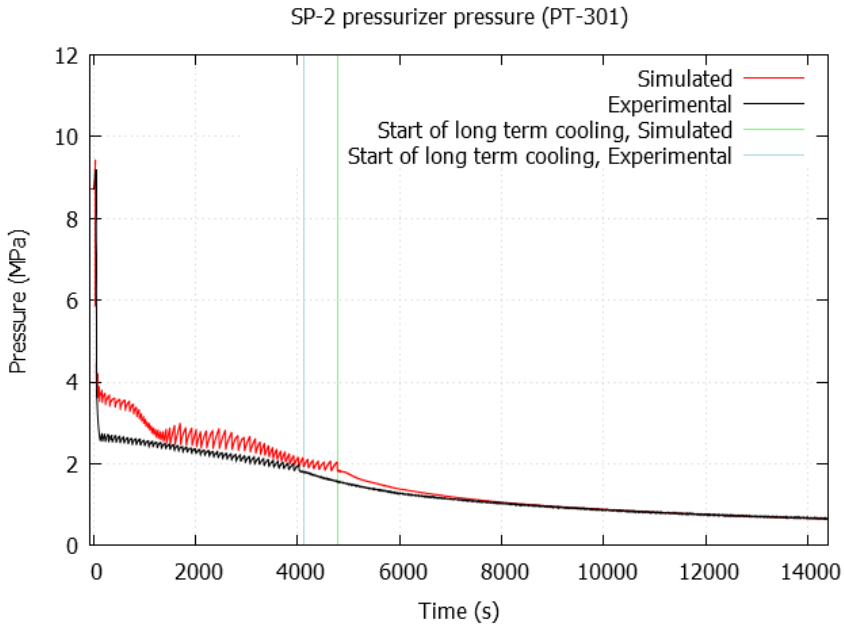

Figure 24. Pressurizer pressure during feed water loss test

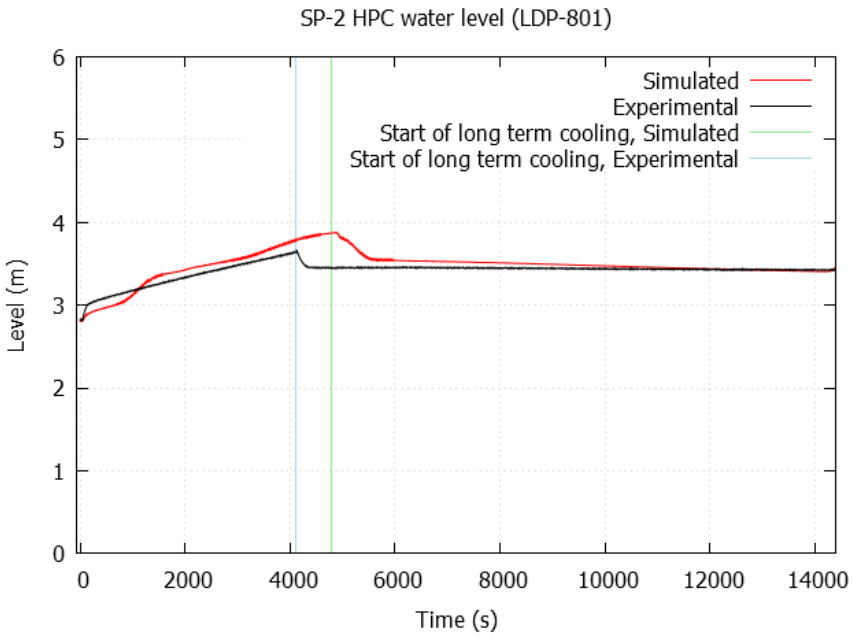

Figure 25. High Pressure Containment water level during feed water loss test

Decreasing reactor power, depressurization of the HCSG and primary heat losses to the reactor hall air all affect the primary side's heat balance. Reactor power, after the initial drop, decreases linearly from 25 kW at 200 s to 5.8 kW at 4700 s. The depressurization of the steam generator contributes with 3 kW at 200 s, 6kW at 1600s and <0.5 kW from 2000 s onwards. These phenomena are easy to distinguish in the pressurizer pressure chart in Figure 24. For example, the HCSG depressurization intensifies significantly at 1200 s, but is significantly slowed at 1800 s, thus explaining the strange behavior between 1200 s and 2000 s. It is not known why neither of these phenomena are visible in experimental data.

The primary chimney mass flow rate responds to the reactor trip as expected. However, no experimental data was published considering the primary mass flow, so the quantitative comparison was made between the Apros simulation and the blind simulations ran by the benchmark participants [43].

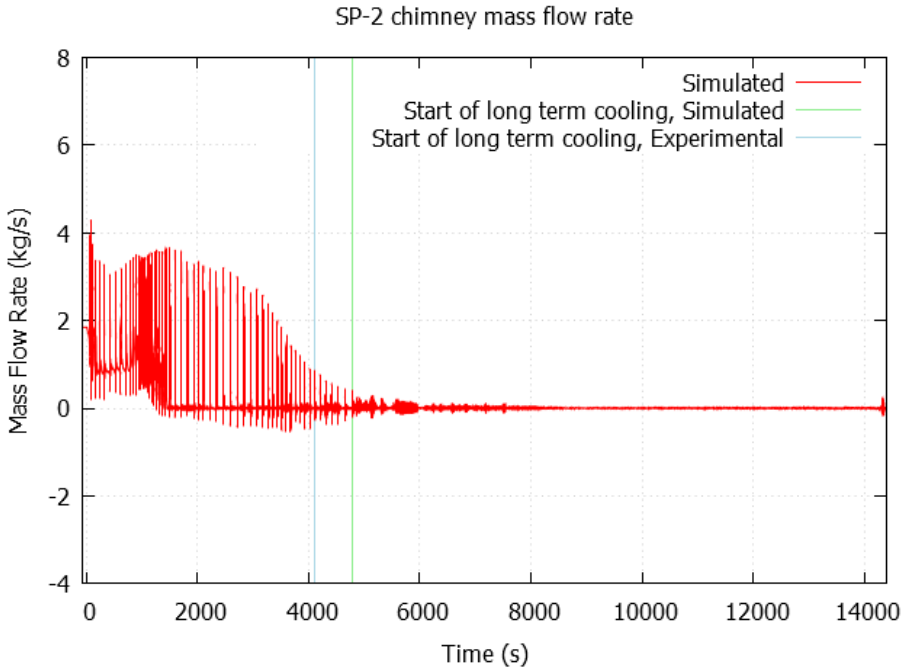

Figure 26. Chimney mass flow rate during feed water loss test

Comparisons of the RPV water levels in Figure 27 revealed several differences in the simulated and the experimental levels measured. The simulated water levels are computed by summing up the level of liquid in each node, whereas the experimental values calculate the water level by the pressure difference between the top and the bottom sections. The brief but large oscillations present in the simulated water levels are caused by flash boiling during the opening of the ADS valve. The saturated primary water starts to boil due to the sudden pressure drop, resulting in a considerable vapor fraction in the submerged nodes, which gives the impression of a suddenly diminished water level.

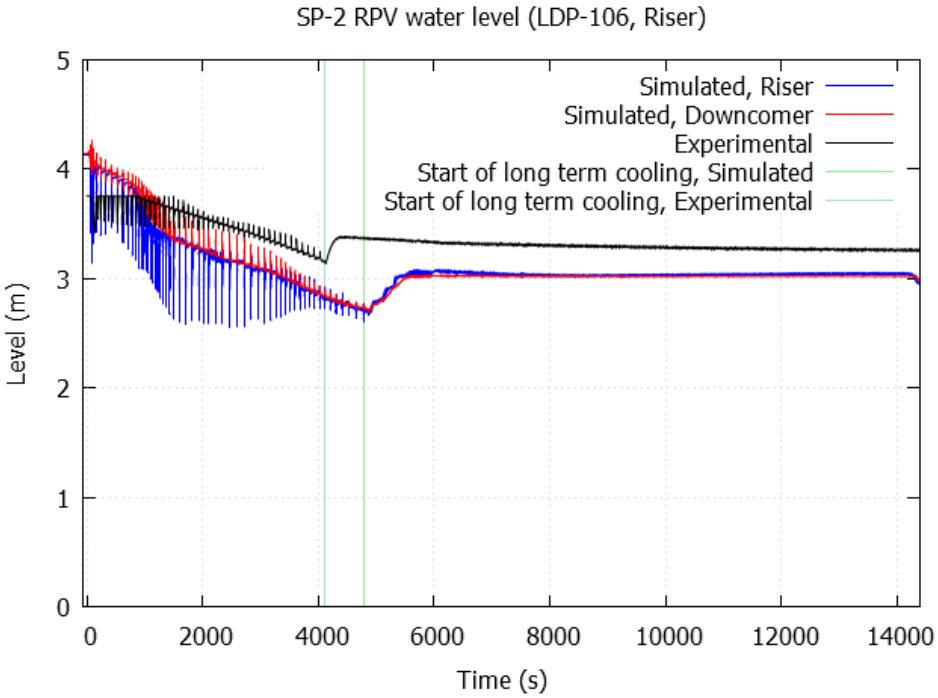

Figure 27. Reactor Pressure Vessel water level during feed water loss test

Void fractions were not measured during the experiment run, but blind simulation results were published. Simulation results presented in Figure 28 reproduce the phenomena present in the blind results [43]. This indicates that Apros 6-equation calculation is capable of modelling passive water evaporation and steam-water separation in the primary systems.

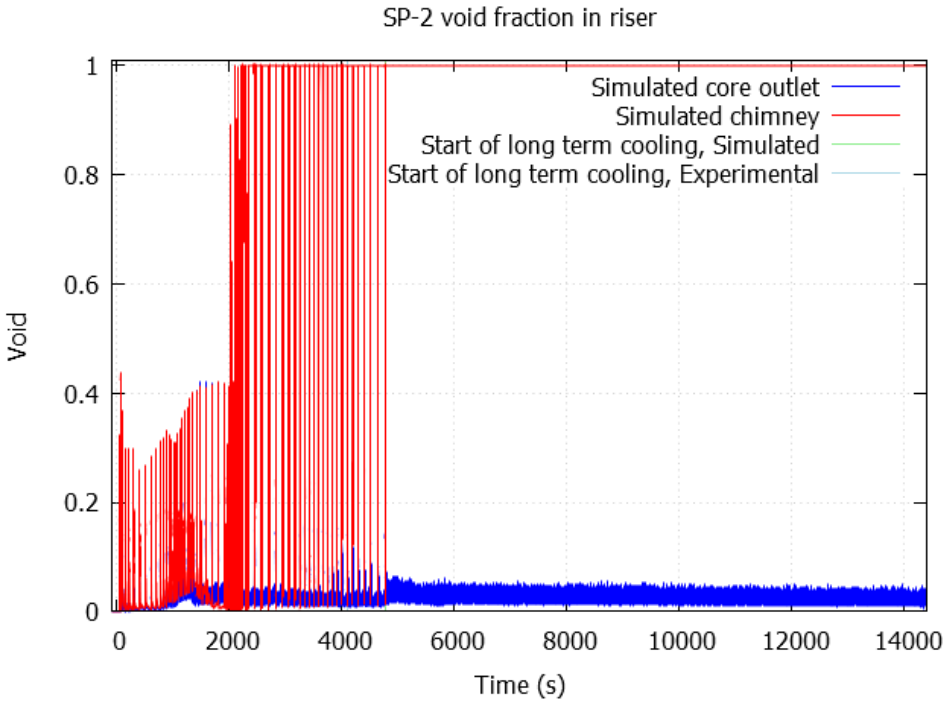

Figure 28. Void fraction in riser during feed water loss test

The most considerable deviations present in the RPV have to do with stratification and temperature measurements. The temperature measurements in the simulation are taken directly at the middle of the given node without a sample time, whereas the experiment equipment were connected to the RPV walls and effectively measured the temperature of the boundary layer, thus measuring a considerably lower temperature. These deviations are visible in Figure 29. The exact location of the temperature measurement is not published, so small prediction errors are possible also for that reason. It is also important to note that the experimental outlet temperature in the reactor outlet is too close to the inlet temperature in the beginning of the simulation. The temperature difference is so small that it could not maintain the primary natural circulation. It is possible that wrong temperatures were accidentally published so analysis based on the core outlet temperature is not reasonable.

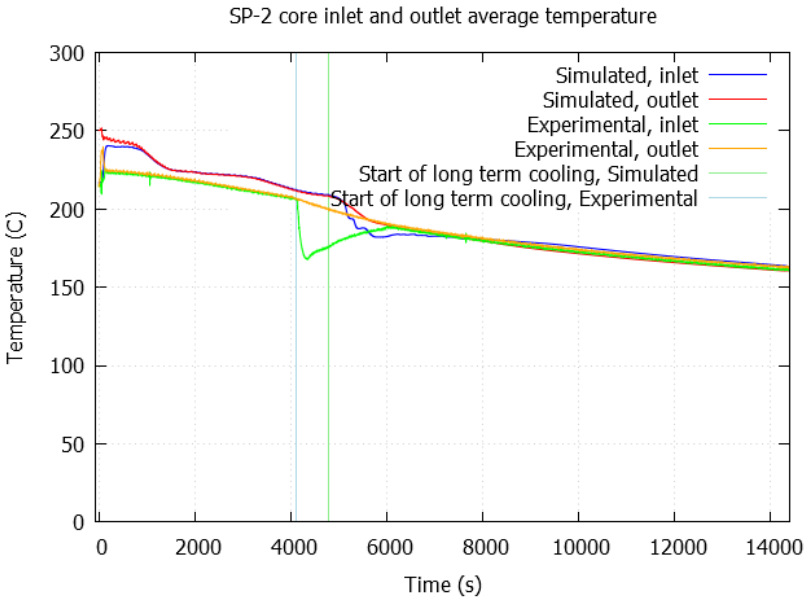

Figure 29. Core inlet and outlet temperatures during feed water loss test

The most notable drawback in the current Apros simulation relates to the stratification in the downcomer. During modelling it was assumed that the natural circulation in the RPV would always mix the primary water efficiently enough. However, the natural flow induced mixing is not enough when the RRVs are opened. After the initial surge of recirculation water, visible in Figure 29 as a drop in the core inlet temperature, the later mixing is too slow, leading to unnatural stratification. Unnatural stratification means that the colder and denser fluid floats above the warmer and lighter fluid. This problem originates in the 1D-approximation choice discussed at the start of the modelling. It is known that in order to form a density difference driven flow and mixing, the duct needs to be modelled using more than one adjacent flow channel. This is because upwards and downwards flow need to be calculated separately in order to let the streams pass each other [53].

Despite the stratification induced differences, the simulation of steam blowdown and later recirculation into the HPC (presented in Figure 30) imitate the blind simulation results [43] well. The cumulative mass flows through the ADS vents were not measured, so a quantitative comparison is not possible.

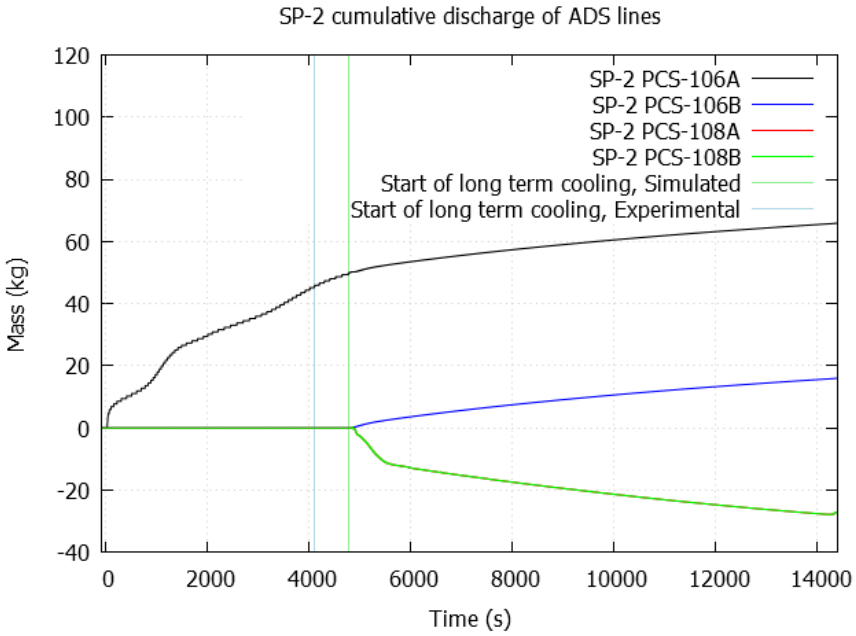

Figure 30. Cumulative flows through individual Automatic Depressurization System valves during feed water loss test

Although the simulated ADS flows do not seemingly differ much from the experimental values, there are a few deviations present in the HPC and CPV values. The periodic high end pressure of each blowdown event changes during the short term cooling period. This can be seen in Figure 31 as higher end pressure levels in the beginning of the simulation. This can be explained, if the predicted driving time of the RVV is said to be overestimated. The implemented driving time is 10 s, which is quite a common driving time for small valves. The driving time is critical, because the closing signal is given at a fixed HPC pressure of 1.825 MPa. The overshoot depends on the pressure difference between the RPV and the HPC, thus explaining relatively high overshoots at the beginning of the short term cooling. It is not known why this phenomenon is not distinguishable in the experimental results. Either the valve driving time in the experiments could be lower than in the simulations, or the valve is not opened as often as in the simulations.

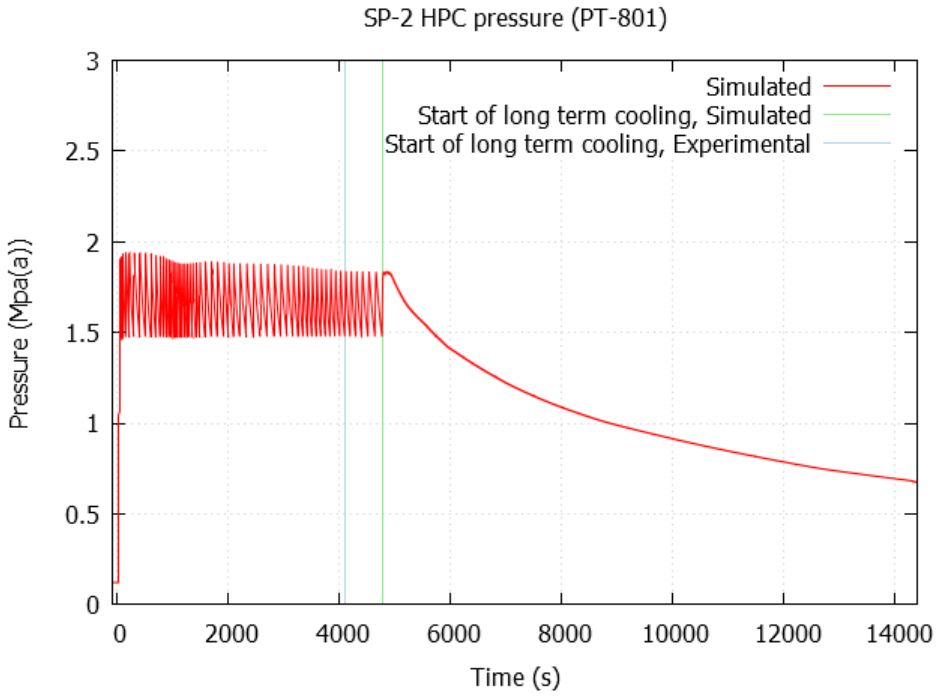

Figure 31. High Pressure Containment pressure during feed water loss test

The simulated temperatures of the HPC and the CPV also differ from the experimental results. Let's first consider a measured area at the height of 416.88 cm, because it is relatively free from the presence of cold HPC water. The simulated results are presented in Figure 32 and the experimental results in Figure 33. As it can be seen from Figure 29, the primary water temperature is well over 200 °C during short term cooling, thus the blown steam should also be at that temperature and this is equal to the simulated fluid temperature in the HPC nodes. In the experiment, the fluid temperature is measured from the wall so the temperature measured is actually the saturation temperature in a given partial pressure. The partial pressure of steam in the HPC is approximately 1.7 MPa with the saturation temperature of 204 °C. Neither the simulated nor the measured boundary layer or wall temperature is near the theoretical value. One possible reason for the difference is the unevenly distributed non-condensable gases in the HPC. It is a well known fact that non-condensable gases accumulate on the heat transferring walls during condensation and thus add a layer of heat transfer resistance [54]. This layer effectively lowers the wall temperature [55], and is not present in the simulated results. Apros simulates the effects with a Vierow-Schrock correction factor to correct the local heat transfer coefficient based on the Nusselt theory [56]. The correlation used for the Vierow-Schrock correction factor is designed for in-tube condensation and for notably lower temperatures (72-146°C) [57]. That is probably the reason why the simulated heat transfer through the HTP is faster, resulting in a quicker pressure drop in the HPC and the RPV.

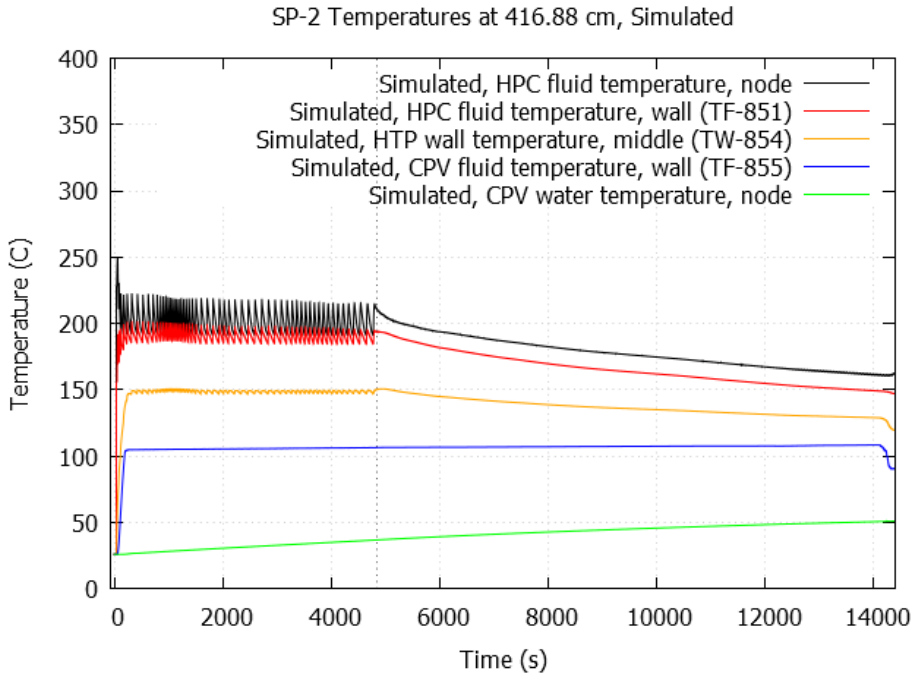

Figure 32. Simulated temperature distribution from High Pressure Containment free volume to the Cooling Pool Vessel free volume on height of 416.88 cm from reference level during feed water loss test

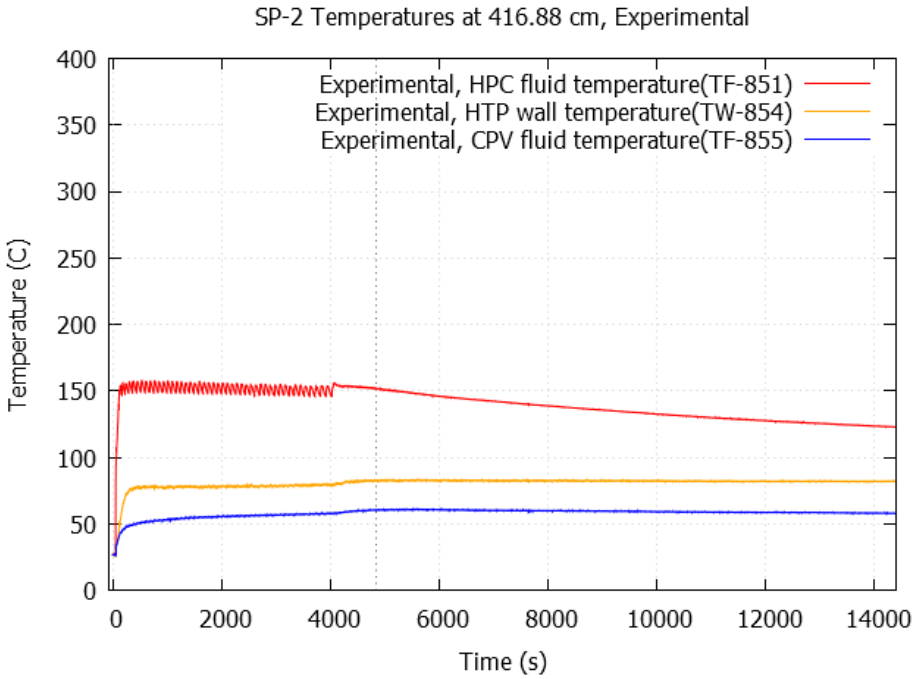

Figure 33. Experimental temperature distribution from High Pressure Containment free volume to the Cooling Pool Vessel free volume on height of 416.88 cm from reference level during feed water loss test

In order to evaluate Apros performance, the required iterations per step and the length of the time step variables are also examined. The most notable increases in required iterations per step (presented in Figure 34) are encountered during the short term cooling process. Seven iterations per step are considered acceptable, but exceeding 10 iterations per step is a signal indicating difficulties in the normal calculation [51]. It should be noted that the high iteration spikes do not last long, because with the increase of the number of iterations Apros shortens the current time step. The time step variation is presented in

Figure 35. Most of the time step decreases occur between 0 - 2000 s, during which the HCSG is emptied.

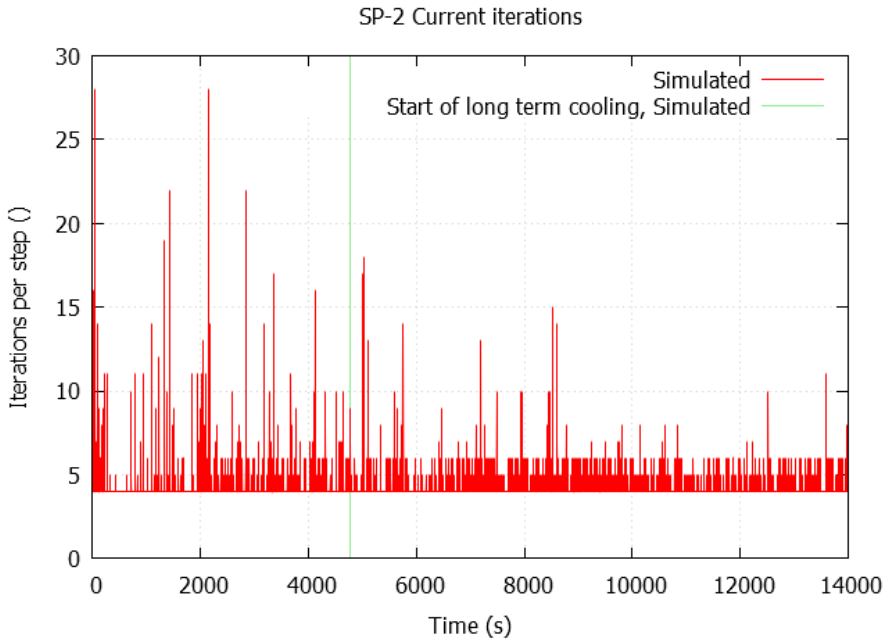

Figure 34. Current iterations during feed water loss test

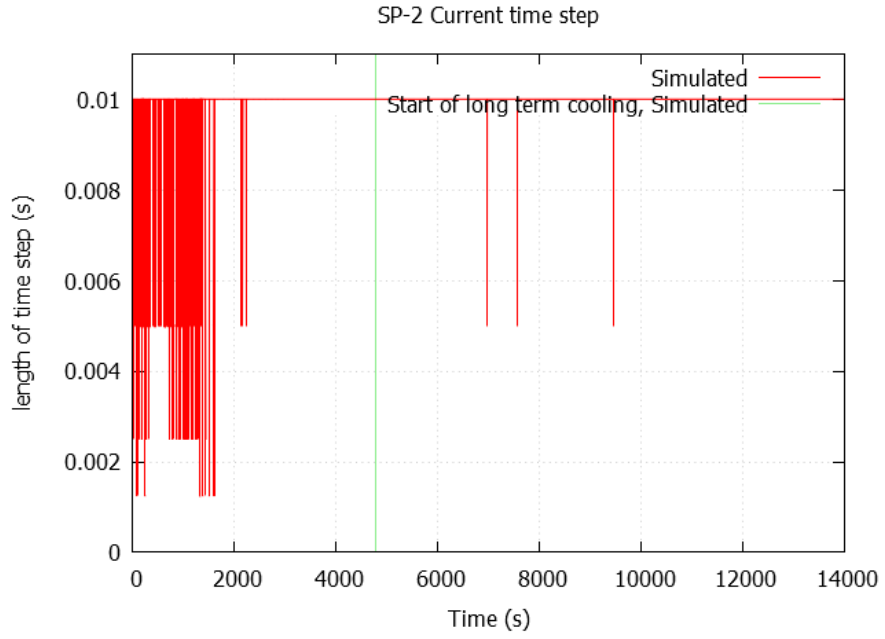

Figure 35. Current time step during feed water loss test

Apros console log reveals that a few simulation back steps are taken between 200- 4000 s. These back steps are taken inside the HCSG tubes and in the top most primary nodes connected to the HCSG. These are caused by the high heat transfer rates during the ADS blowdowns. Although the heat transfer spikes associated with the blowdown are relatively short (less than 1 s), the induced back step effect in the HCSG lasts for 30 s on average. The heat transfer spikes could be dealt with by assigning a maximum heat transfer value to the heat transfer components. The error made this way is negligibly small due to the small energy content transferred. The back steps taken on the primary side are quite

different. The blowdown induced back steps in the primary side are manageable, because most of the primary side's back steps are taken between the blowdown periods. A reason for the back steps in the given nodes could be the unstable heat transfer conditions. The downcomer primary nodes that are connected to the HCSG are revealed due to the diminished water level during the short term cooling. The top most nodes are under rapidly varying conditions: The nodes are never completely dry, because the heat transfer to the HCSG and the primary side heat loss both condensate steam. Furthermore, condensate water from upper parts of the RPV drips down to the given nodes. In addition the node receives heat through the RPV chimney, which induces evaporation. All the mentioned conditions are more or less independent in respect of timing. The fluctuating conditions induce great instability to simulation and in order to continue, the two topmost nodes have to be separated from the HCSG for the rest of the short term cooling. The nodes are attached back to the HCSG in the beginning of the long term cooling. The cut off inflicts a small drop in the secondary steam temperature, so the missing heat transfer is compensated by the heat transfer in the submerged nodes.

5.5 Sensitivity analysis

During modelling and the preliminary validation it was discovered that the simulation results are sensitive in respect to certain parameters. The primary flow is driven by a relatively small pressure difference, thus even slight changes in the pressure drop or a coarse nodalization affects results significantly. The Nodalization of the preliminary model was thus tripled compared to the initial model. The primary side's volume, that does not directly affect the pressure drop, is also susceptible for passive simulation. For example, the preliminary nodalization had a 30 liter error (approximately 16 % of the primary volume) on the primary side. This kind of error affects directly the dynamics of the primary side: the primary flow reacts slowly to changes in the secondary heat transfer; the ADS has more inventory to cool down, thus increasing the SP-2 test length; Different water inventory also affects the water level balancing after the RRV opening, thus inflicting more deviation when compared to experimental results. Quantitative simulation comparison between the inaccurate and accurate primary side volume turned out to be troublesome. One of the governing reasons was the location and its significance to the result. For example, when the volume of the flow paths (especially the narrow chokes) was increased, it seemingly affected the flow conditions of the RPV, in which case a different steady state at the beginning of the test affected the results. When the volume above the chimney was increased, the top of the chimney was not exposed in the beginning of the blowdown procedures. This allowed the primary circulation to continue, which further affected the results. Furthermore, if the extra volume was modelled to the downcomer it had effects on the results of the RRV opening. Due to the complexity of the previously mentioned factors, quantitative inspection on the possible RPV errors is not issued in the scope of this thesis.

Signs of the effect that are typical to the coarse nodalization, were examined visually, i.e. large quantitative deviations in simulated properties (temperature, pressure, mass flow etc.) between the adjacent components were sought during test runs. Most of the differences found were relatively small. For example, the temperature differences between adjacent nodes were generally under 2 °C. The largest exceptions could be found in the HPC nodalization. Near the water surface the temperature differences between adjacent nodes could be as high as 20 °C. This is due to natural stratification and arguably has some

effect on the HPC's natural circulation. The nodalization density was increased for one test run, but no significant changes could be found.

The importance of the secondary side was also tested. During the SP-2 test run, water in the HCSG first evaporates thus cooling down the primary side. Due to the HCSG depressurizing, the steam is vented out of the HCSG. In case of a HCSG isolation without depressurization, the evaporated HCSG steam begins to condensate as the primary temperature decreases, thus decelerating the primary cool down. To test the significance of a HCSG depressurization a modified SP-2 simulation test run was conducted. In this simulation run, the secondary side was completely isolated i.e. there was no emergency depressurization. The modified SP-2 test run is compared to the normal SP-2 simulation test run in Table 5. It can be seen that the depressurization of the HCSG affects heavily the short term cool down. The HCSG isolation inflicts over a 2200 second or 47 % delay for the start of the long term cool down. This result indirectly indicates that the HCSG depressurization has significant effect on the simulation results. The strange behavior during the HCSG depressurization could be thus explained by varying depressurization characteristics.

Table 5. Simulated feed water loss test cases with and without Helical Coil Steam Generator depressurization

Event	Simulation (s)	Simulation HCSG isolated (s)	Difference (s)	Relative difference (%)
Start of simulation – steady state (start of data collection)	-60	-60	-	-
Stop feed water flow	0	0	-	-
PZR pressure (PT-301) ≥ 9.064 MPa Enter decay power mode	26	26	0	0.0
PZR pressure (PT-301) ≥ 9.409 MPa Open ADS vent valve (PCS-106A)	40	41	1	2.5
Start long-term cooling Pressure difference between RPV and HPC (PT-301 - PT-801) ≤ 0.034 MPa Open and remain open of RVVs Open and remain open of RRVs	4782	7020	2238	46.8
PZR pressure (PT-301) ≤ 0.618 MPa End of test	13600	14820	1220	9.0

5.6 Validation status

The developed model simulates the experiment with the MASLWR facility fairly well, with approximately a 14 % difference in the test end times and a 16 % difference of the long term cooling starting point. The SP-2 test simulation preparatively validated Apros in the modelling of a small scale passive primary circulation during transiency. The presented validation is preparative so supplementary simulations would be beneficial.

Apros simulation stability was also tested for periodic steam blowdowns in the LWR reactors. It was found out that simulations, if the current HCSG correlations are used, are

somewhat instable in the low flow velocities. This was predicted because the current correlations are valid for highly-turbulent flow regions. Furthermore, the current HCSG code is not yet prepared for a large heat transfer rate fluctuation.

In the future simulation precision could be improved with a number of modifications. The downcomer side could be modelled in pseudo 2D. As it was noted in section 5.4.2, the unnatural stratification won't mix without handling rising and descending streams separately. Furthermore, the instability effects in the exposed downcomer nodes that are attached to the HCSG could be decreased with 2D nodalization. Also the HCSG instabilities could be decreased by code development. As it is stated in section 6.1, the current HCSG correlations are only valid for a turbulent flow regime and they are not yet fine-tuned. Another way to stabilize the HCSG side is to impose an upper limit for the momentary heat transfer rate. In addition, the condensation calculation in the HPC could be developed for an SMR specific application with new correlations. The current Apros condensation correlations are not validated for the given conditions, thus future research would be beneficial.

6 Helical coil steam generator

The modelling and validation of the Apros SMR model described in chapter 5 creates the option of running preliminary simulation tests for a helical coil steam generator. The objective of this chapter is to briefly introduce the theory behind the HCSG, and then present the results of the power maneuvering test simulation with included HCSG correlations.

6.1 Helical coil steam generator theory

This section gives a short introduction to the theory behind the helical coil heat exchanger. Previous work on HCSG theory is briefly covered, and some interesting phenomena are also discussed.

6.1.1 Previous work on helical coil heat transfer

The first studies describing curved pipe exchangers are relatively old. The first recorded experiments on curved tubes were performed by D. Jeschke in 1925 and the first theoretical analysis was done by W.R. Dean in 1927. In his papers, Dean described the secondary flow inherent to curved tubes and its effect on heat transfer and pressure drop for laminar flows by solving the Navier-Stokes equations [13].

Regardless of its heat transfer properties, interest in the helicoil research declined rapidly, thus postponing any new studies and experiments until as late as the early 1960s. This could be explained by plenty of technical difficulties. Most of the in-depth helicoil research was done on one-phased fluid flow, whereas the most beneficial phenomena occur in the two-phased flow. At the time, there was no need for compact heat exchangers. The heat exchanger was seen as an external component in the terms of the primary process. This sets very few requirements on efficiency or size of the heat exchangers, so there was little industrial pressure for compactness. Also, the straight tube heat exchangers are a lot simpler both analytically and in practice. The maturity of the straight tube applications was already achieved, whereas the research on curved tubes was limited.

In the 1960s, new interest in helicoils emerged for their application in biochemical processes. Dean's analytical work was expanded by Ito [57], attaching friction factors at extreme (very small and large) Dean numbers. Ito covered friction factors accurately, both analytically and empirically, and therefore many later authors refer to his work when handling heat transfer in helicoils.

Before 1960's no significant effort was made to characterize heat transfer in helicoils. It wasn’t until 1962 when Seban and McLaughlin began their work [58] on one-phase helicoil heat transfer. They were able to find an accurate correlation for one-phase turbulent heat transfer, and identify a thermal entry effect in the laminar flow. In 1966 the heat transfer study was carried further by Mori and Nakayama. Their extensive flow field analysis resulted in heat transfer correlations that cover a large field of fluid properties [59]. The correlations found have been widely used and still serve as benchmarks for future heat transfer calculation in helicoils.

Owhadi et. al. presented one of the first extensive two-phase heat transfer studies in 1968 [60]. They deduced that describing nucleate boiling from a theoretical base would have been troublesome, so extensive experiments were conducted. They discovered through data analysis that a highly turbulent helicoil boiling didn't differ substantially from a turbulent straight pipe boiling, due to turbulence's dominance in mixing. As a result, Owhadi and his fellow scientists found that in wetted wall areas helicoil boiling followed Chen's straight pipe boiling correlation within 15 % accuracy over the range of the experiments.

Academic interest has primarily been focused on the heat transfer inside tube coils. The first detailed experiments that discussed heat transfer on tube banks with varying geometrical parameters were conducted in the 1920's [61],[62]. The results concluded that heat transfer of a tube in a bank is significantly higher than that of a single tube. It was also discovered that the intensifying effect of a tube bank depended heavily on the bank's geometrical parameters such as arrangement, tube shape and intersecting angle.

The attention in 1960's focused primarily on the phenomena inside the tube and thus produced only few studies on the outer side heat transfer. One of the most notable experimental analysis on the outer heat transfer of the tube banks was conducted by Zhukauskas et. al in 1968 and continued in 1972 [63], [64]. The resulting turbulent forced convection correlations were quite general in form and covered the straight tube bank heat exchange fairly well. The work of Zhukauskas was expanded by researchers Kanevets and Politykina in 1989. Their goal was to project Zhukauskas' correlations to the helicoil heat exchangers with the use of empirical correction factors. They found that Zhukauskas' correlation already predicted turbulent heat transfer quite accurately and with the newly found correction factors they were able to improve correlation accuracy significantly [65]. Unfortunately the data range of their experiments was rather narrow and thus of little practical use.

After Kanevets and Politykina's work, there was no significant progress on helicoil heat exchange or on forced turbulent flow. However, there has been some research on natural convection in helicoils recently [66]. In the 1990's Ali [67], [68] and Xin & Ebadian [69], [70] conducted two different approaches to predict natural convection in helicoils. Both researchers approached the problem using a power law equation, but they based their correlations on different helicoil dimensions. Ali based his correlations on 'macro scale dimensions' such as the height of the helical coil bundle or the length of the helicoil tube [69], whereas Xin & Ebadian based their correlations on 'micro scale dimension' such as the tube's outer diameter. In 2004 Prabhanjan et. al. confirmed that both approaches produced relatively strong correlations, but also stated that the number of studies and studied data ranges discussing natural convection in helicoils was not sufficient and further experiments were needed [71], [72].

6.1.2 Physical phenomena of helical coil heat exchanger

A Helical coil heat exchanger is substantially different from a traditional straight pipe heat exchanger. The objective of this section is to offer an introductory understanding of the phenomena within the HCHEs.

One specific aspect of the HCHEs is the formation of a secondary flow field in the helical tubes. A fully developed laminar fluid flow field in a circular straight pipe is axially symmetric and there is practically no axial or radial thermal mixing present. This is illustrated in Figure 36 below.

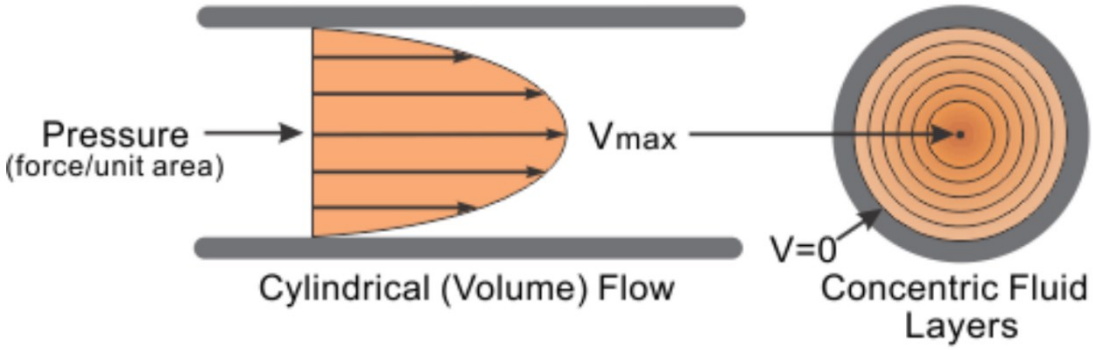

Figure 36. Laminar flow profile in cylindrical pipe [73]

If the velocity of the fluid flow is increased sufficiently, the flow undergoes a transition and becomes turbulent, applying axial and radial turbulent mixing. In order to illustrate a turbulent flow profile, a illustrative cross-section was plotted with ANSYS Fluent 17.2. This is presented in Figure 37 and is qualitatively comparable to the Figure 36.

Figure 37. Turbulent profile in cylindrical pipe visualized with ANSYS Fluent 17.2. [74]

A dimensionless number often used to predict the transition from a laminar flow to a turbulent flow is the Reynolds number [75]:

$$Re = \frac{wd_h}{\nu}, \tag{7}$$

where Re is Reynolds number, d_h hydraulic diameter of the pipe (m) and ν the kinematic viscosity of the fluid (m^2/s). Other phenomena considering straight pipes are not further discussed in this thesis.

A curved shape of the tube causes the flowing fluid to experience a centrifugal force, which is illustrated in the following equation of uniform circular motion.

$$\frac{F_{cont}}{V_{cont}} = \frac{\rho_{cont} w_{tan}^2}{R_{helix}}, \tag{8}$$

where F_{cont} is the centrifugal force a certain control volume of fluid requires in order to maintain its radial position (N), V_{cont} the volume of the fluid in consideration (m^3), ρ_{cont} the density of the fluid, w_{tan} the tangential velocity of the fluid and R_{helix} the radius of the helix (m).

The extent of the centrifugal force experienced depends on the local axial velocity of the fluid particle and the curvature radius of the coil [72]. Visible in the above pictures, the fluid particles flowing at the core of the pipe have significantly higher velocities than those flowing near the pipe wall. This effect forces the fluid from the core region to be pushed towards the outer wall. The mixing is not, however, restricted to the outer half of the tube, because as it is visible in Equation 8 (radius acts as divider), the fluid near the innermost tube wall experiences greater centrifugal force than the fluid near the top or down the wall of the tube. Those phenomena create two radial traveling spirals [13] that are illustrated in Figure 38. In Figure 38 the axial flowing direction is through the paper and the pipe curves to the left.

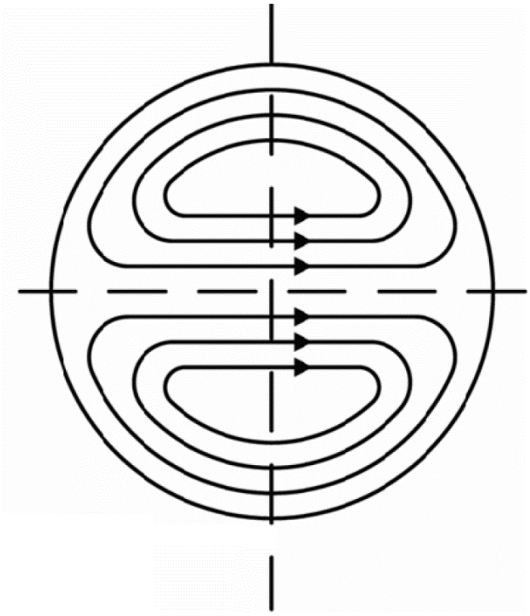

Figure 38. Secondary flows induced in helical coil [13]

All in all, there are two different phenomena that intensify mixing in helical coils; turbulence and centrifugal effect. It should be noted that according to experiments, the effect of the turbulence grows faster than the centrifugal effect [76], thus almost diminishing the effects of the curvature in large Reynolds numbers, $Re>2*10^5$ [77]. In other words, the straight pipe correlations cover helical coils more accurately in highly turbulent flows. Furthermore, the benefits of helical geometry are relatively smaller in highly turbulent flow regimes.

The evaporated fluid on the tube walls insulates the remaining liquid from further evaporation. That is one reason why mixing plays a key role in steam generators [78]. The centrifugal effect experienced by the fluid is also dependent on the density of the fluid as it can be seen in Equation 8. Denser, liquid, water experiences stronger centrifugal effect than gaseous steam, which intensifies liquid circulation on the tube walls [19].

6.1.3 Apros standard correlations

This section gives a short briefing on Apros equations that are later replaced with new helical coil correlations. The Apros library contains a large variety of correlation options, but none of them are designed specifically for helical coil geometry. The presented correlations are the ones used in the preliminary modelling and testing [52]. It should be noted that Apros contains alternative correlations for some of the presented equations. Backgrounds of why the presented correlations were selected and the characteristics of the alternative correlations are not discussed.

Provided that the default Apros friction correlations are used to calculate the friction factor for the tube bundle in laminar (Re<4000) and passive flows, Apros would use the maximum value of the friction factor for laminar flow and the friction factor obtained from the Blasius equation [71],[79]:

$$f_k = max\left(\frac{64}{Re_k}, \frac{0.316}{Re_k^{0.25}}\right) \tag{9}$$

where $f_k$is the friction pressure loss coefficient of the certain phase and Re_k Reynolds number of the certain phase. Equation 9 is also used inside the helical pipes, when the flow regime is laminar. If the flow regime is turbulent, the following equation is used for the friction coefficient [79]:

$$\frac{1}{\sqrt{f_k}} = 1.74 - 2log\left[\frac{1}{\sqrt{f_k}}\frac{18.7}{Re_k} + 2\frac{\varepsilon}{d_h}\right], \tag{10}$$

where ε is the roughness of the surface (m). It should be noted that the equations above represent the smooth flow regimes inside a circular pipe. The appropriate correlations are used inside the cross flow heat exchanger component etc., but are not applied for the six-equation nodes and branches. Thus it should be noted that Apros is capable of more accurate calculations, but the choices made in the current model do not allow for it.

The standard Apros heat transfer solver selects the heat transfer zone according to the wall temperature, fluid temperature, saturation temperature and the void fraction. The three heat transfer zones are: heat transfer to the wetted wall, transition zone and heat transfer to the dry wall. According to the Apros six-equation model data sheet the zones are selected with the following criteria [79] (Edited):

"If the void fraction is over 0.99999, it is assumed that dry out occurs and the dry wall is selected. Otherwise the wetted zone is always selected if the wall temperature is less than the saturation temperature. If the wall temperature is more than the saturation temperature, the calculated heat flux is compared with the critical heat flux. When the critical heat flux is exceeded, the heat transfer zone changes to transition or dry wall. If the wall temperature is less than the minimum film boiling temperature, the transition is selected. When the wall temperature exceeds the minimum film boiling temperature, the dry wall heat transfer zone. After the boiling crisis has happened (heat transfer zone is transition or dry wall), the heat transfer changes back to wetted wall only when the wall temperature goes below the saturation temperature."

When the heat transfer node is connected to a six-equation node and both the temperatures of the fluid and the tube walls are under the saturation temperature (wetted wall

zone), Apros chooses to use the Dittus-Boelter equation with the minimum value constraint [79],[80]:

$$Nu = max(0.023Re^{0.8}Pr^{n};\ 3.66) \tag{11}$$

where Nu is the Nusselt number, Pr the Prandtl number n=0.4 for heating and n=0.3 for cooling. The equation is valid when Re >10 000 and (L/D) > 50. The minimum value of 3.66 represents the laminar heat transfer coefficient. The Dittus-Boelter correlation is used for the turbulent flow regime inside a single straight tube and it is experimentally confirmed for completely different flow conditions. In practice, the Dittus-Boelter correlation is valid only on the inside surfaces of straight tubes, thus it could be beneficial to use some other correlation. On the other hand, Dittus-Boelter could predict some flow regions inside the helical coil tubes accurately. As it is stated earlier, the correlation predicts highly turbulent one-phase flow regimes fairly well [77], so the utilization during the high flow velocities on the dry region of the HCSG is reasonable. Dittus-Boelter is also used in the one-phased entry of the HCSG with relatively small significance for operation simulation.

When the heat transfer zone is between the wetted and the dry wall conditions in boiling, the heat flux is interpolated between the critical heat flux and the heat flux of the one-phase dry zone given by the Dittus-Boelter correlation. The critical heat flux has several alternative correlations: According to the Apros feature manual [56] the Zuber-Griffith correlation [81] and the Biasi correlation [82] combination is used. The combined heat flux is calculated as follows [79]:

$$q_{cr} = \left[C_i q_{cr,B} + (1 - C_i) q_{cr,Z-G}\right] min(10 - 10x_e\ , 1), \tag{12}$$

where q_{cr} is the critical heat flux (W/m^2), $q_{cr,Z-G}$ the heat flux predicted by Zuber-Griffith correlation (W/m^2), $q_{cr,B}$ the heat flux predicted by the Biasi correlation (W/m^2), G the mass flux (kgm/s) and x_e the equilibrium steam quality. C_i the interpolation coefficient and it is calculated with the following formula [69]:

$$C_i = max(min(0.01G - 1.1), 0) \tag{13}$$

As it can be seen from the interpolation, the Zuber-Griffith correlation is used alone if the mass flux is below 100 kg/m^{2}s. The Zuber-Griffith correlation is the following equation [81], (Edited):

$$q_{cr,Z-G} = 0.131[1 - min(x, 0.8)]\sqrt{\rho_g}\left(h_{g,sat} - h_{l,sat}\right)\left[\sigma g\left(\rho_l - \rho_g\right)\right]^{0.25}, \tag{14}$$

where $q_{cr,Z-G}$ is the heat flux predicted by the Zuber-Griffith correlation (W/m^2), x the volume fraction of a phase. If the mass flux is above 200 kg/m^{2}s the Biasi correlation is used [82] (Edited):

$$q_{cr,B} = max\left\{\frac{1.883 * 10^7}{(100d_h)^n (0.1G)^{0.1667}}\left[\frac{x}{(0.1G)^{0.1667}} - x_e\right], \frac{3.78 * 10^7 f_{p2}(1 - x_e)}{(100d_h)^n (0.1G)^{0.6}}\right\}, \tag{15}$$

In addition, Apros contains a heat transfer efficiency coefficient that multiplies the computational heat transfer. This coefficient is used to tune the heat transfer module calculation for the given conditions [69].

To sum up, Equations 9-14 are preliminarily used in the HCSG simulations with varying accuracy. Quantitative accuracy predictions are not included in the scope of this thesis, but certain conclusions can be drawn. All of the previous correlations are for in-tube flows. Calculations on the outer surface of the tubes are thus inaccurate in all the flow regions. Also, all of the correlations are for straight pipes with no centrifugal effects. The centrifugal effects are stronger in highly curved helixes and especially in two-phase flow regions (see section 6.1.2). Turbulent effects also become increasingly dominant in high flow velocities diminishing the effects of the curvature. In other words, the standard correlations could be fairly accurate in highly turbulent flows and in large helixes, but lack physical accuracy in the laminar flow fields.

6.1.4 Helical coil correlations

Helical coil correlations implemented in the MASLWR simulation model were all chosen and preliminarily tested before and outside the work of this thesis by personnel not involved in this thesis [83]. One of the objectives of this thesis is to validate the new calculations with the MASLWR simulation model.

Most of the implemented correlations are based on traditional straight pipe correlations and include some mainly empirical corrections in order to fit them into the helical geometry. The most notable addition to the traditional correlations is the presence of the D/d term, where D is the diameter of the helix (m) and d is the inside diameter of the pipe (m). The term follows the effects proportionally to the helical curvature.

The added friction correlations are presented next Ito presented the following correlations for friction factor calculations inside helical coils for laminar flow regions [84]:

$$f_c = \frac{344(D/d)^{-0.5}}{[1.56 + log_{10}(Re(D/d)^{-0.5})]^{5.73}} \tag{16}$$

valid for:

$$13.5\left(\frac{D}{d}\right)^{0.5} < Re < 2000\left[1 + 13.2\left(\frac{D}{d}\right)^{0.6}\right]$$

Ito presented the following correlation for a turbulent region [57]:

$$f_c = 0.076Re^{0.25} + 0{,}0075\left(\frac{D}{d}\right)^{-0.5} \tag{17}$$

valid for:

$$Re > 15\,000$$

The previous correlations only calculate wall friction and do not take interfacial friction into account. In order to predict the interfacial friction between the gas and liquid phases, a correlation predicting two-phase coefficient is needed. This implementation is still in progress and is thus left out this thesis. Some rough estimates predict that the im-

plementation of the two-phase coefficient calculation increases the heat transfer significantly and should thus be taken into account when the simulation results are evaluated [83].

The heat transfer correlations for inside tube heat transfer only cover turbulent flow regimes. During the preliminary work, the correlations were prepared only for the power operations where the flow regime is highly turbulent. It is therefore possible that notable deviations and instabilities are present during low-power operation.

Heat transfer correlation for subcooled water is calculated by the Mori-Nakayama correlation [84]:

$$Nu = 0.02439 * Re^{0.8} Pr^{0.4} \left(\frac{d_i}{D_c}\right)^{1/12} \left[1 + \frac{0.061}{[Re(d_i/D_c)^{2.5}]^{1/6}}\right] \quad (18)$$

valid for:

$$Pr > 1,$$
$$Re\left(\frac{d}{D}\right)^{2.5} > 0.4$$

Heat transfer correlation for superheated steam is calculated by another Mori-Nakayama correlation [59]:

$$Nu = \frac{1}{26.2} \frac{Pr}{Pr^{2/3} - 0.074} Re^{4/5} \left(\frac{d}{D}\right)^{0.1} \left[1 + \frac{1}{[Re(d/D)^2]^{0.2}}\right] \quad (19)$$

Heat transfer over the boiling region inside the HCSG is calculated in a relatively interesting way. It is known that the original Chen correlation predicts heat transfer quite accurately in a highly turbulent region. The original Chen correlation is following [84]:

$$\alpha_t = S * \alpha_{nb} + F * \alpha_{sp,l}, \quad (20)$$

where α_t is the heat transfer coefficient of the total heat transfer coefficient (W/m^{2}K), α_{nb} the heat transfer coefficient of nucleate boiling (W/m^{2}K), $\alpha_{sp,l}$ the convective heat transfer coefficient of a single phase liquid (W/m^{2}K), S is the suppression factor and F is the Reynolds number factor. Chen gave descriptions for both of the factors, but did not solve them analytically. The original Chen correlation used the previously presented Dittus-Boelter equation (Equation 11) to predict the convective heat transfer coefficient and the Forster-Zuber correlation (Equation 19) for the pool boiling heat transfer [85]:

$$\alpha_{nb} = 0.00122 \left(\frac{\lambda_l^{0.79} c_{p,l}^{0.45} \rho_l^{0.49}}{\sigma^{0.5} \mu_l^{0.29} h_{lg}^{0.24} \rho_g^{0.24}}\right) \Delta T_e^{0.24} \Delta p_e^{0.75}, \quad (21)$$

where λ_l is thermal conductivity of the liquid (W/mK), c_p the specific heat at a constant pressure (J/kgK), μ_l the dynamic viscosity of the liquid kg/ms, h_{lg} the latent heat vaporization (J/kg), ΔT_e the temperature difference of the wall and the saturated fluid (K), Δp_e the vapor pressure difference between the saturated steam and the steam at the wall temperature (Pa).

As it was previously stated, the original Chen correlation would utilize the Dittus-Boelter equation to calculate convective heat flow. That would not take the different HCSG dimensions into account, so a modified version of it is preferred [13]:

$$\alpha_{sp,l} = 0.023 \frac{\lambda}{d_i}(1-x)^{0.8} Re_l^{0.8} Pr_l^{0.4} \left(\frac{d}{D}\right)^{0.1} \tag{22}$$

$$F = 2.235(X_{TT}^{-1} + 0.213)^{0.736}, \tag{23}$$

where X_{tt} is the Lockart-Martinelli parameter, which is used in determining the two-phase pressure drop across a system, where both cases are turbulent [86] (Edited):

$$X_{tt} = \left(\frac{1-x}{x}\right)^{0.9} \left(\frac{\rho_g}{\rho_l}\right)^{0.5} \left(\frac{\mu_g}{\mu_l}\right)^{0.1}, \tag{24}$$

where μ_g is the dynamic viscosity of gas kg/ms. The suppression factor can be calculated in following way:

$$S = \begin{cases} \frac{1}{(1+0.12Re_{TP})}^{1.14}, & for \quad Re_{TP} < 32.5 \\ \frac{1}{(1+0.42Re_{TP}^{0.78})}, & for \quad 32.5 < Re_{TP} < 70 \\ 0.797, & for \quad Re_{TP} > 70 \end{cases} \tag{25}$$

Outside heat transfer is presumed to be one-phased, so the Zhukauskas method is valid for calculating the outside heat transfer [61]:

$$Nu = C * Re_{D,max}^m * Pr^{0.36} \left(\frac{Pr}{Pr_s}\right)^{0.25} \tag{26}$$

valid for:

$$0{,}8 \leq Pr \leq 5000, \quad Re_{D,max}^m < 20\,000$$

A few conclusions can be drawn from the previously presented substituting equations (14-26). The equations are tuned for helical coil geometry and as such their accuracy in differently dimensioned HCSGs is questionable. Most of the previously presented sources state that the correlations are tested with dozens of flow regimes, but only with a few geometries. Also some correlations have not gone through an extensive third party validation. As it was stated in section 6.1.1, the most extensively covered equations are the friction correlations due to their long history of research. The Chen correlation and its subparts are all relatively well validated [87], but the latest tuning without a deep third party validation [13], [83] brings uncertainties to the calculations. However, the largest uncertainties lie in the Zhukauskas correlation. It covers the whole primary side for the entire length and thus affects all of the areas of heat transfer. The Zhukauskas correlation has had some corrections [65] before. It is also stated that the correlation overestimates the heat transfer significantly especially in low flow velocity environments [13]. Furthermore, the Zhukauskas correlation could not be tested in the preliminary HCSG calculation project. The data used for the validation was attained with test equipment, of which the primary side was substituted with electrical heating [83].

6.2 Simulation of stepwise power maneuvering

6.2.1 Test procedures

The SP-3 test was conducted to characterize the steady-state natural circulation in the primary side during the various core power inputs at the MASLWR test facility. According to the original procedure, this was accomplished by configuring the MASLWR facility in a natural circulation state and varying the power inputs of the core heaters. The power inputs of the core heaters were increased step by step from 10 % of full power to 80 % of full power, with 10 % increments at each step. For each power input, the primary side flow rate, the hot leg and the cold leg temperatures were monitored to determine whether the flow stabilization was achieved. The primary side and the steam generator pressures were maintained at approximately 8.6 MPa and 1.4 MPa, respectively, for all power inputs. The timing of each of the events is displayed in Table 6 below:

Table 6. Important events during power maneuvering test

Event	Experiment time (s)
Start of simulation – steady state	-60
Initiate core power increase to 80 kW	0
Initiate core power increase to 120 kW	870
Initiate core power increase to 160 kW	1642
Initiate core power increase to 200 kW	2177
Start of injection[1]	2634[1]
Initiate core power increase to 240 kW	4004
Initiate core power increase to 280 kW	4498
Initiate core power increase to 320 kW	5096
End of test	6158

[1]Exact experimental timing remains unpublished. Presented timing is an estimate that is used in simulation.

According to the test report, several procedural problems were encountered by the staff personnel during the performance of the SP-3 [43]. First, by procedure, the MASLWR test facility should be allowed to reach a steady state prior to increasing the core power and moving on to the next step. Three parameters were used to determine whether the MASLWR test facility had reached the steady state conditions: The hot and cold leg temperatures in the RPV and the primary mass flow rate.

Following the completion of the test, during the data analysis phase, it became clear that although these three parameters may have been steady within the bounds of the procedure, many other parameters within the test facility might not have been so. Thus, the steady state conditions were not fully reached between steps during the completion of the SP-3 as required by the test procedure. For example, according to the simulations done in the scope of this thesis the hot leg temperature could seem to be steady as the temperature change is merely a 0.2 °C/min but yet it may change even 7 °C before settling to the real steady state temperature.

The second procedural problem was the result of inadequate adherence to the procedures by the test operators. Between each step, the test procedure calls for the operators

to adjust the feed water flow to achieve saturated conditions at the secondary side outlet. This action was not completed between each step.

The third deviation from the original procedure was an extra water injection to the RPV during the experiment. OSU provided detailed information to the ICSP participants, but the information remains unpublished. Due to the lack of information regarding the injection, it is not reasonable to compare the test runs during injection period.

The technical document states that the procedural problems were negligible from the simulation's point of view, because most of the procedural errors could be replicated within the simulation [43]. However, the second operational deviation is problematic, even from the simulation's perspective. If the temperature in the secondary steam outlet approaches the temperatures of the primary side, the quality analysis between the experiments and the simulations could be troublesome. For example, if the correlation used in the simulation predicts the heat transfer coefficients as remarkably too high, the temperatures of the outlet streams would not change due to the lack of a temperature difference. Furthermore, the primary purpose of a steam generator is to produce steam, thus highlighting the importance of the two-phase heat transfer. In the case of a notably superheated steam the examination of the relatively short two-phase region could become troublesome.

Despite the previously presented concerns, the accumulated data is accurate enough for the scope of the thesis. The data could also be used for future validation, but it would be beneficial to validate the code with a new data set.

6.2.2 Approximations implemented into simulation

The simulation was conducted as described above. The reactor power and the feed water temperature are given as boundary conditions. In order to enable quantitative comparison with the experimental results, the blind control of the feed water mass flow is not reasonable. The feed water flow should be controlled so that the generated steam is always a little over the saturation temperature. If the saturation temperature is not exceeded, dry out correlations are not tested. Furthermore, the saturation region is relatively instable due to the lack of a change in temperature and thermal feedback [19]. Direct comparison between the wet, saturated and superheated steam is not meaningful when the used comparison parameter is the temperature.

There is no published information considering the extra water injection and as such notable approximations were taken. The injection was commenced in order to avoid pressurizer heater exposure. It is assumed that the purpose of the water injection was to refill the pressurizer to the initial level. Required mass of the water injection was thus 10 kg in the modelled equipment. This amount is in good accordance with the participants' blind calculation values [43].

Preliminary test runs show that steady state prediction is relatively hard with only the primary temperature and the mass flow constraints. Following other critical process values as pressurizer heater work load (in order to maintain desired pressure level) gives notably better results, but increases the amount of traced variables significantly. It was thus decided that the steady state is determined by five factors: three of them are the same ones the test facility personnel used and two are purely calculative. The first calculated

parameter is the Energy equilibrium on primary side. It is done by distracting the outgoing heat flows from the incoming. The system is definitely not in a steady state if the heat balance notably differs from zero. The second parameter to observe is the heat losses on the primary side. Heat flow through the RPV wall should always stabilize before the next step. Otherwise the temperature of the RPV wall and the insulation material is still changing, affecting also to the primary side.

Preliminary tests also show that if correct feed water flow is set after each power level increase, the model could not reach a steady state before the next step. There are several reasons for the long stabilization time, but the most notable is that the primary flow rate is determined by the temperature difference between the riser and downcomer. The temperature difference is then determined by the primary side heat balance that depends on the primary flow rate. In other words, even if the steady state is correctly predicted, the time to reach it in certain intervals is too long to be fitted into the simulation. It should be noted that, from the simulations point of view, reaching the steady state is not crucial as long as the distance from it is accurately predicted. Since the MASLWR model is only preliminarily tested, the steady states attained with it are not necessarily identical. Comparing relative deviations of the reached states and the correct steady states between the experimental and the simulated results is not possible, because correct steady states were not examined in the test program and thus remain unpublished.

It is thus reasonable to implement an overshoot to the feed water control in order to attain the steady state faster. The preliminary runs confirmed that the temperature in the reactor is relatively stable. Although the stepwise increases in the reactor power and the feed water flow are issued simultaneously, their effects have different delays. The reactor power increase affects the heat balance almost immediately, whereas it takes over a minute for the feed water flow to affect the balance. By that time, the primary water has warmed and it takes too long for the system to stabilize. The instability in heat balance is located at the beginning of each step, so it is also logical to implement the overshoot right after each step and the overshoot should steadily, but swiftly, diminish. Thus the initial overshoot is decreased linearly and reaches the steady state set value after 80 seconds of increase in the power level. In order to approach the steady state quickly, the preliminary test simulations show that the feed water control should be made to artificially overshoot with a 10 % margin to the steady state set value. Although the optimal overshoot varies a bit, the previous values are used in the following simulations as good estimates.

With all the adjustments and approximations mentioned before, there are still a few challenges in the validation. In order to validate the simulation model to the experimental system, the number of deviating values needs to be decreased. For example, if the system is controlled so that the target feed water flow is adjusted precisely to the fluctuating experimental values the secondary heat transfer is not necessarily close to the reactor power due to the different heat transfer characteristics of the experimental and the modelled HCSG. In that case, the balancing happens purely on the primary side, which is a very slow process and the reached steady state could be difficult to compare to the experimental values.

It was thus decided that the primary side variations from the experimental values should be minimized. Furthermore, it was previously rationalized that large changes in the feed water mass flow could also be troublesome to compare due to high heat of evaporation. It was also previously argued that the notable differences in the outlet steam temperature are comparable only if the margin to the primary inlet temperature is high enough. Thus

the steam outlet temperature was also limited to the experimental values. With the previous elimination method it was decided that all the adjustable values were related to the HCSG heat transfer efficiency. This method is not without its problems, because the overall heat transfer efficiency from the primary circuit to the secondary circuit cannot be changed in the current implementation of the HCSG correlations. Thus only the outside heat transfer efficiency is adjusted with the coefficient that is iteratively determined in the preliminary simulation runs. Altogether, the simulation procedures are summed up in the following Table 7.

Table 7. Boundary conditions controlled by simulator during power maneuvering test

Value	Set value determination method	Adjustments
Transition to next power level	Timing attained from experiments	-
Reactor power	Amount attained from experiments	Immediate increase to predetermined value
Feed water mass flow	Set value attained from experiments	Immediate change in feed water control valve set point with 10 % overshoot, which linearly decreases to desired value
Heat transfer efficiency of outer HCSG surface	Set value attained from preliminary simulations	Set value is attained by analytically determining outlet temperature of steam in order to meet reactor input. Small manual adjustments are made in order to minimize large changes to primary side

Constraints confirming final values and stability are listed in Table 8 below:

Table 8. Constraints for acceptable steady states during power maneuvering test

Variables confirming stable steady state	Stability constraints	Acceptable final values
Core inlet and outlet temperature	± 1 °C oscillation acceptable	± 5 °C compared to experiments
Primary mass flow	± 2 % oscillation acceptable	± 10 % compared to experiments
Steam outlet temperature	± 1 °C oscillation acceptable	-
Primary heat loss	± 1 kW oscillation acceptable	0.5-1.5 kW absolute value
Primary heat flow equilibrium	± 4 kW oscillation acceptable	± 1 kW absolute value

6.2.3 Simulation results

The simulation results matched the experimental results relatively well. The reason for the good accuracy is that the simulation was constructed in an open manner. In other words, the implementation of the heat transfer efficiency coefficient diminished the majority of the HCSG related deviations. Like it was stated earlier, the characteristics of the extra water injection was unknown, thus the injection and the temperature adjustment in the middle of the simulation is marked with a blue box. Possible deviations in that area are only a sign of a different injection method.

The system state is defined by two parameters: The reactor core power and the feed water mass flow, which are presented in Figures 39 and 40. Slight deviations in the feed water

mass flow rates are present in the beginning of the test run, but their effect on the steady state conditions are small because they take place long before the next step.

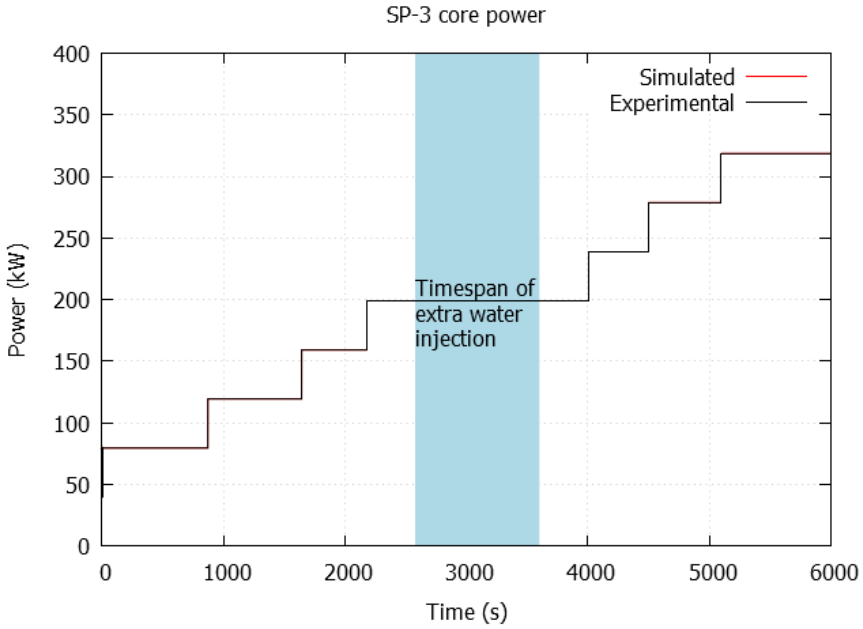

Figure 39. Core power during power maneuvering test

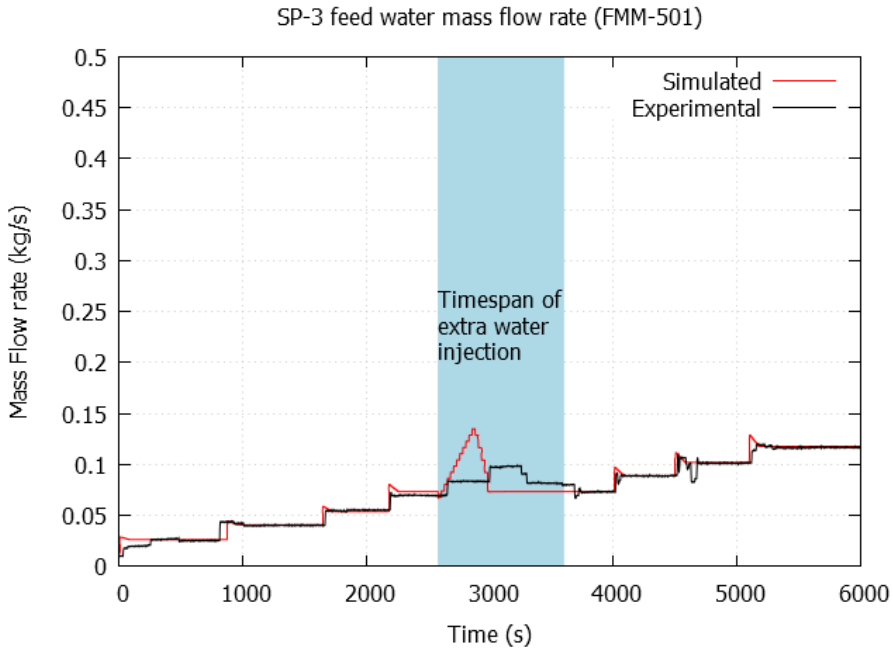

Figure 40. Feed water mass flow rate during power maneuvering test

The first thing to observe is whether the stability is reached or not before each rise in power level. The stability constraints used in the experiment were the core inlet and outlet temperatures and the primary mass flow in the chimney. These are presented in Figures 41 and 42. During the experiment it was noticed that the preset constraints were inadequate. As it can be seen in the following figures, it is fairly troublesome to predict system stability with only the primary values, especially from the oscillating primary mass flow rate measurements. Temperature levels in the chimney are also plotted in Figure 41, because it seems that a false outlet temperature measurement is plotted in the source material

[43]. This claim is reasonable, because the current experimental temperature difference over the core is too low to support the natural circulation. Furthermore, the experimental temperature measurements are notably higher and near the simulated values. It should also be noted that the simulated chimney and outlet temperatures do not differ much, due to the small heat loss throughout the chimney. It is thus advised that the experimental outlet temperatures are ignored and that the experimental chimney temperatures are used instead.

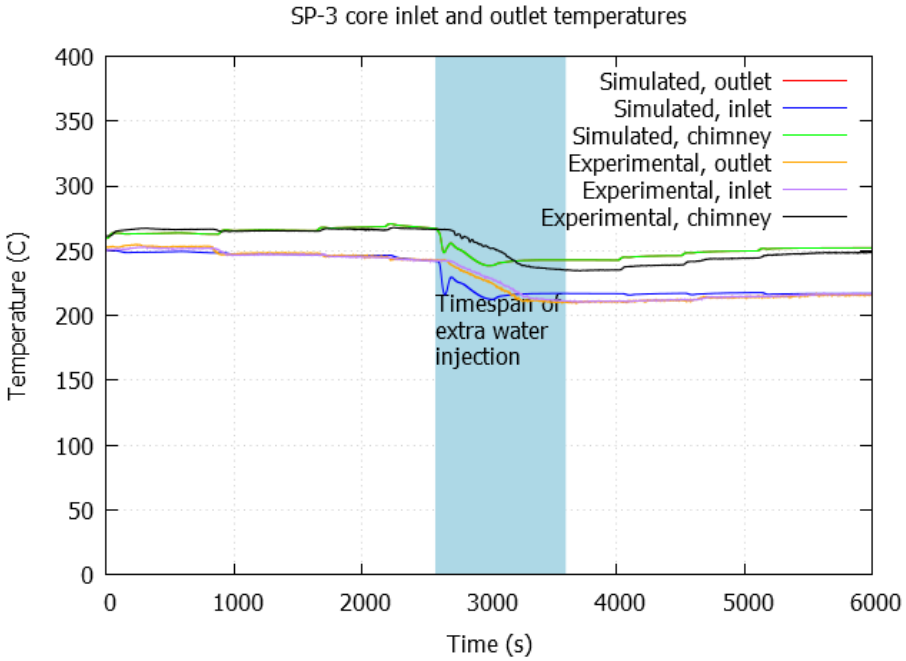

Figure 41. Core inlet and outlet temperatures during power maneuvering test

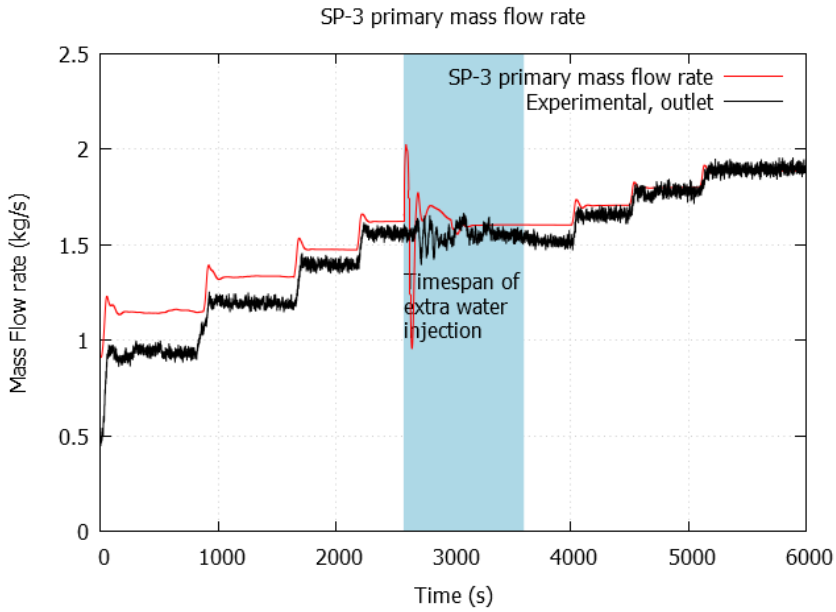

Figure 42. Primary mass flow rate during power maneuvering test

The computational stability prediction is more straightforward. In the simulation the primary side heat flow equilibrium is computed by summing up all the incoming and outgoing heat flows on the primary side. This is plotted in Figure 43 and it can be seen that stability (by the definition presented in section 6.2.2) is reached before each step. However, a few notable instabilities can be found in the Figure 43. The system is rather instable at the beginning of the simulation run. The instabilities could arguably derive from two separate phenomena. The lack of the laminar correlations for the HCSG heat transfer could inflict oscillations to the heat transfer, especially during the first two steps of the simulation, which can be seen in Figure 44. However, in order to confirm the previous prediction further studies are required. Furthermore, like it is predicted in the section 6.2.1, the on-off pressurizer heater control logic inflicts a 1.3 kW oscillation to the equilibrium in any case.

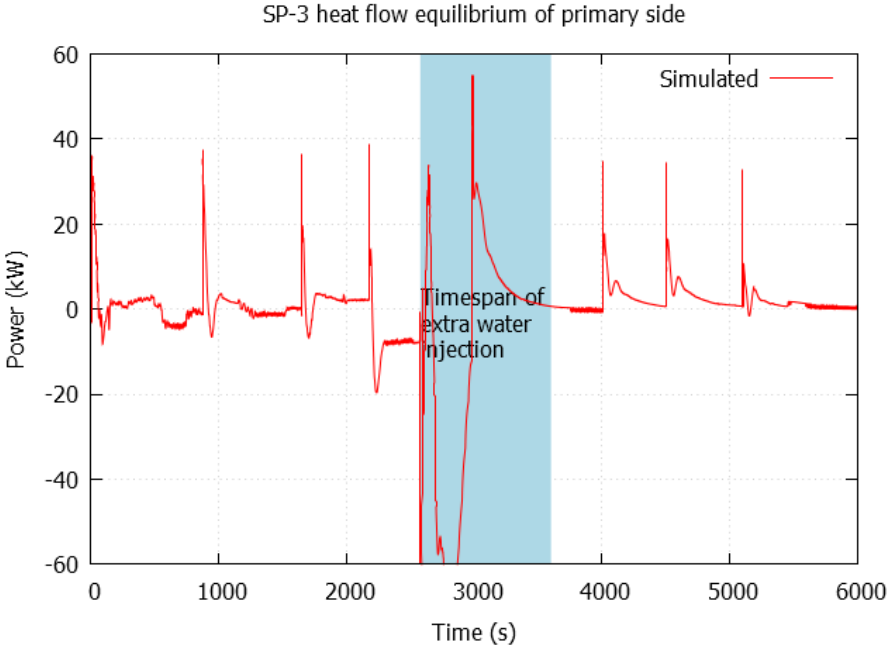

Figure 43. Heat flow equilibrium of primary side during power maneuvering test

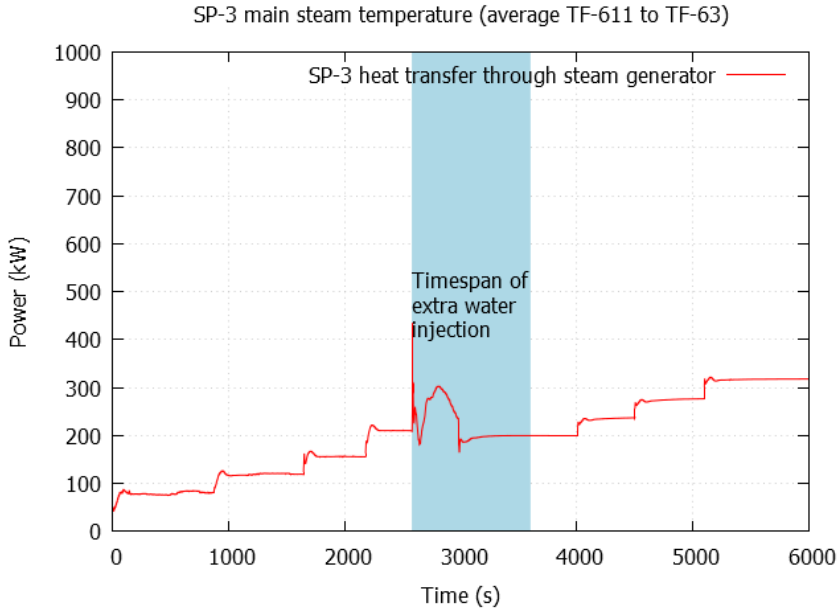

Figure 44. Heat transfer through steam generator during power maneuvering test

With the stability discussion already presented before, it was possible to do a steady state quality analysis. In the following analysis the primary and secondary parameters are compared separately and it is assumed that the only way they affect each other is through the total heat flow through the HCSG walls. This approximation does not take effects from the temperature distribution etc. into account.

Like it can be seen in Figure 40, the feed water mass flow in the steady state is roughly the same in the simulation and in the experimental results. Thus the possible steady state differences should be visible in the main steam temperature presented in Figure 45. As it can be noticed, differences in the experimental and simulated temperatures of the outgoing steam are relatively high: 10 °C at the maximum. Deviations this large cannot be explained simply by temperature measuring errors. Especially now, when the experimental steam outlet temperature is determined as an average of 13 separate measurement devices [42]. In principle the deviation could derive from an imbalance in the state, but in this case it is unlikely, due to the computational confirmation of the steady state. The origins of this difference can be traced to the primary side temperatures presented in Figure 41, where it can be seen that the simulated temperatures are higher than the experimental values. The first thing to be pointed out is that the deviations do not derive from the HCSG's heat transfer efficiency. If the efficiency is too low, the primary temperatures would be higher and the steam temperatures lower and vice versa. Also, after each step the steam temperature momentarily drops and later rebalances. Thus, even if the steady state is not reached, the steady state temperature is too high. By summing up the previous arguments, the reason for the deviations is likely an insufficient feed water flow. This is plausible, because even slight change in the feed water mass flow could inflict major changes to the outlet temperature. For example, in the experimental conditions, heating and evaporation of the feed water requires approximately 2660 kJ/kg energy, when the specific heat for steam is 2.85 kJ/kgK. In the case of 800 g/s feed water flow (the step after water injection), an error of 1 g/s inflicts a 1.15 °C change to the steam outlet temperature.

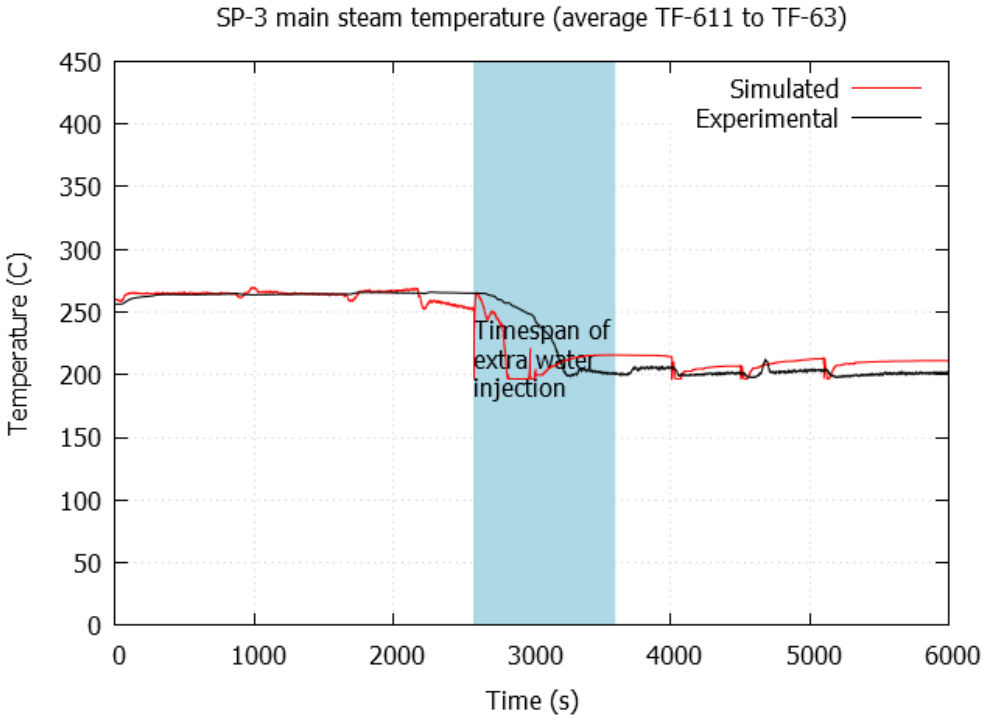

Figure 45. Main steam temperature at Helical Coil Steam Generator outlet during power maneuvering test

Apros simulation characteristics were also evaluated based on the simulation run. The number of current iterations and the length of the current time step are plotted in Figure 46 and Figure 47. Possible simulation back steps were also monitored through the Apros console. The brief evaluation shows that the Apros code had some difficulties during small flow velocities. This can be seen in Figure 45 as high and continuous iteration spikes before injection. The implemented HCSG codes were not designed for low flow velocities so these results were expected. On the other hand, if the spikes are derived only from the low flow velocities, the high number of iterations would have continued after the injection. It seems that the high number of iterations could also be explained by large temperature differences and a high HCSG heat transfer rate. After the primary side temperatures are lowered during the injection period, most of the instabilities disappear.

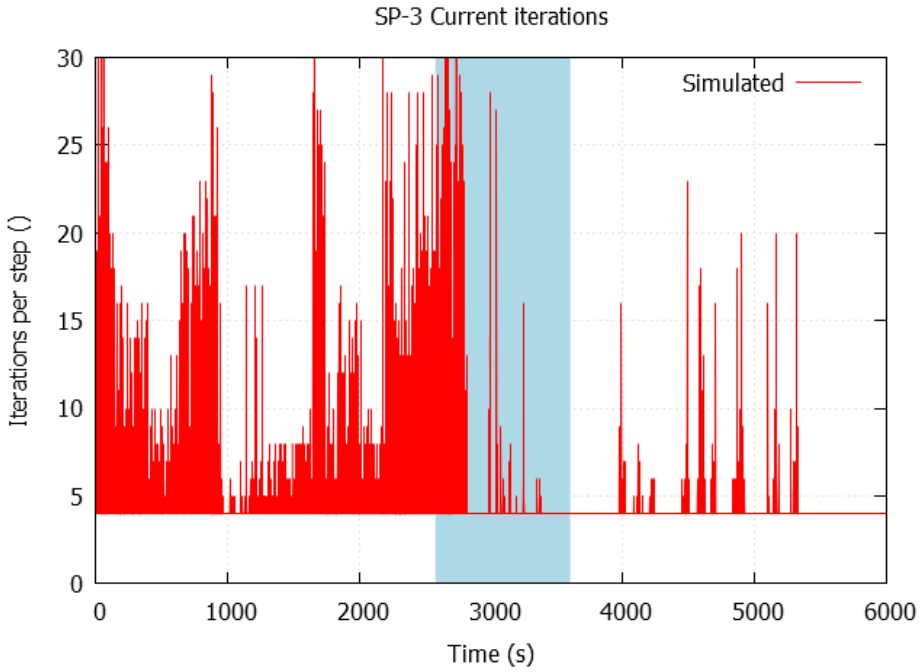

Figure 46. Current iterations during power maneuvering test

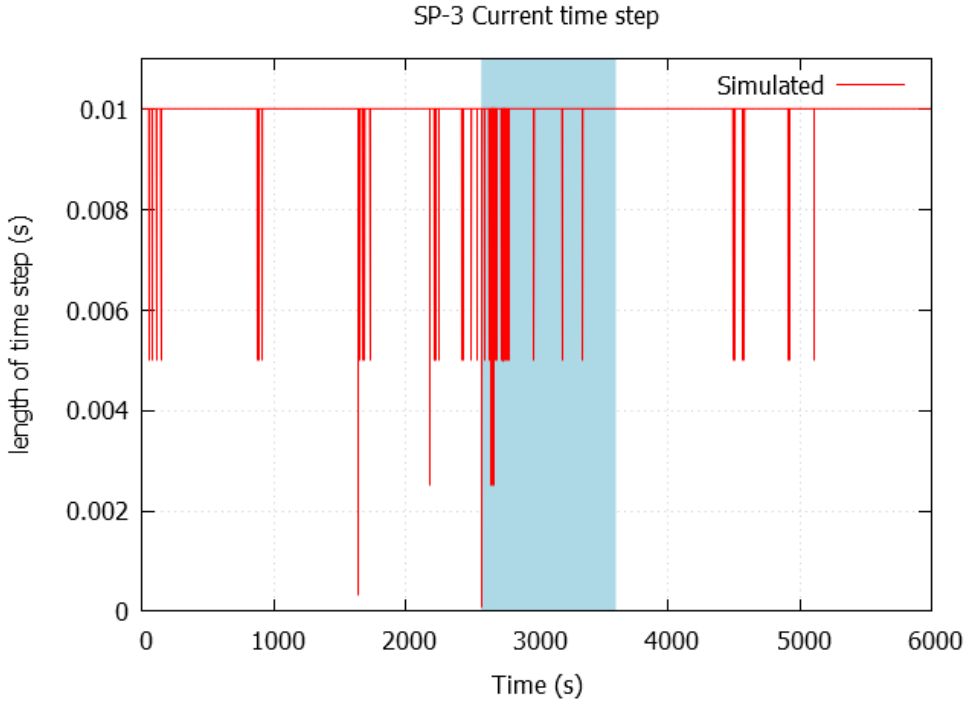

Figure 47. Current time step during power maneuvering test

A more thorough study of the secondary side calculation nodes shows that the evaporation length changes drastically. Before the injection, the evaporation length could be as short as around 10 % of the HCSG's total length, whereas the length is over 75 % after the injection. It seems that nodalization along the evaporation length is insufficient and thus should be fine-tuned in the future. The effect of the rapid transients can also be seen in Figures 46 and 47. The current time step and the number of iterations changes notably after each step. This is expected due to the many changes in the number of flow patterns.

6.3 Sensitivity analysis

A number of sensitivity test runs were issued due to the number of instabilities and deviations presented in section 6.2.3. The test runs are not discussed in depth in the scope of this thesis, but their results are briefly presented.

At the beginning of the simulation a few stability related cases were encountered. Especially when the feed water flow is very small, around 10-15 g/s, which inflicts notable problems with control and stability. For example, a 1 g/s difference in the feed water flow could induce a 10 % deviation to the primary side energy balance. On the other hand, the instabilities could have been induced by the laminar flow regime alone, for which the current correlations are not valid for. In order to test the previous theory, the number of parallel pipes is decreased for the beginning of the simulation, in which case the total feed water flow is not changed, but the secondary flow velocity increases significantly. The outlet steam temperature or primary values are not notably affected. Possible deviations could possibly be evened out by the different flow regime. The decreased number of parallel pipes stabilizes the simulation somewhat, thus supporting the assumption that some of the instabilities are induced by the laminar flow regime and not the small mass flow.

The procedural error at the beginning of the test lead to high super heated steam temperatures in the HCSG outlet, as it was predicted during the pre-test analysis. This complicates the validation of the HCSG code substantially. During the preliminary runs, it was noticed that the steam surpasses 250 °C temperature very early, in some cases as early as 50 % of the HCSG's pipe's length. Furthermore, temperature in the steam outlet was in some cases very close to the downcomer temperature levels. In other words, even large changes to the heat transfer efficiency coefficient had little to no effect on the steam outlet temperature. For example, the heat transfer efficiency coefficient could be lowered from 100 % to 40 % with only a 0.5 °C change to the outlet temperature. Logging suitable heat transfer efficiency coefficients along the superheated section is thus not meaningful, and therefore only the minimum values of heat transfer efficiency were logged. After the injection and the steam outlet adjustment the logged heat transfer, efficiency coefficients are more descriptive, and can be used to validate the used HCSG codes.

Effects of the extra water injection to the primary side downcomer were also examined. First, it was tested what happens if the injection is left out. This resulted in pressure instabilities as the pressurizer liquid water inventory was too small. The second case was a test in which the amount of extra water was overestimated resulting also in pressure instabilities due to a too small vapor inventory. Overall, the extra water could result in some deviations, if the water level is far from the normal operation area, but slight deviations have little to no effect.

Effects of possible primary side modelling errors and uncertainties were briefly examined. A choke was added to the primary side's flow path. Higher pressure loss and lower flow velocity increases the temperature difference over the core significantly. Low flow velocity affects also the HCSG heat transfer forcing the primary side temperatures to rise. As it was estimated in section 5.3, the primary side flow conditions are very sensitive to modelling errors considering primary side pressure losses and dimensioning.

Unnatural stratification encountered in the SP-2 tests was also examined in the power maneuvering tests. The water injection in the SP-3 run did not inflict stratification problems, so a more coarse way was tested. At 30 % of full power the liquid temperature of

three consecutive downcomer nodes changed from 250 °C to 25 °C instantly. The cold water pulse could be seen in the measurement charts (especially in Figure 41), but it had only a very brief effect on the simulation speed and measured values. Furthermore, unnatural stratification did not occur because, unlike in the SP-2, the primary loop was still closed. Although the 1D-modelling approach seems to handle stratification well during power tests, it is, however, not an advised SMR modelling method because unnatural stratification could still occur during the reactor trip. Furthermore, stratification was tested on a 30 % of full power area and with a relatively small water mass, which does not preclude the possibility of unnatural stratification on lower power levels or with larger water injections or temperature changes.

The Apros code's ability to withstand large transients was also briefly examined. As it was mentioned in the previous section 6.2.3, the code managed stepwise power level increases well. Those steps were all 10 % of full power and thus relatively small. Therefore, much larger power increases were examined here. It was decided to increase power level from 10 % to 50 % and from 50 % to 80 %. The code managed both of the cases, but a few changes had to be implemented. Most of the back steps were taken inside the HCSG tubes and the rapid mass flow increases sometimes forced the simulation to diverge. The secondary flow was therefore increased in many small steps like in the case of extra water injection. A more profound study on the Apros console log reveals that the back steps were taken mainly on the HCSG sections under rewetting. Surfaces under rewetting include very complex physical phenomena that have to be simulated carefully. The difficulties arise when a hot tube wall in the area with superheated vapor encounters a cold liquid. The rapid changes in the heat transfer conditions are complex to simulate, and require small simulation time steps and calculation modules. In other words, it could be alleviated with finer nodalization and smaller time steps, which has more to do with modelling and simulation procedures than the code’s calculation capabilities.

Signs of a too coarse nodalization were also examined. Although the nodalization of the primary side seems fine enough, the secondary side could do with some improvements. For example, at the beginning of the HCSG the temperature of the feed water could increase even 20 °C in a single node. The nodalization of the HCSG entrance was fine-tuned, but no difference in the simulation results could be noticed. Although the nodalization seems to have little effect on the steady state values, the nodalization could affect the stability of the calculation.

6.4 Validation status

Overall, the model developed here predicts the experimental results relatively well. A few deviations between the simulated and experimental results were encountered, and therefore further development is proposed. The SP-3 test simulation preliminarily validated Apros as a modelling tool for small scale passive primary circulation in the start-up phase at low power levels. The first version of the HCSG calculation was also tested with relatively promising results.

It should be noted that the steady state behavior and code accuracy was only tested with fixed feed water flow values, so in order to more accurately validate the code different validation cases are needed. First, the precise steady states should be found by lengthening the stabilization time for each value and fine tuning the feed water flow. Second, the stepwise power increments test the solver's capability to react in transients, but typical

start-up procedures could also be continuous. The code is currently tested for large transients, in which the actual transition process is quite short. The current test set validates the stabilization from a transient state, whereas the actual transition is less discussed. Third, the current test case starts from a low power operation, but leaves the cold shutdown area uncovered.

In future, the simulation precision and stability could be improved with a number of modifications. The HCSG outer heat transfer calculation should be developed. As it was noted in section 6.3, development of the inner heat transfer is not meaningful if the outer heat transfer calculation needs development. It also seems that the tested correlations have some difficulties in large transients. This could be alleviated with finer nodalization.

7 Summary

This thesis examines the capability of the Apros software to create dynamic SMR simulation models. The thesis also studies specific NuScale SMR design features and projects them to the Finnish regulatory guides. Both of these tasks are supported by literature surveys executed in the framework of this thesis. In order to investigate Apros' capabilities, a simulation model of a NuScale SMR test facility was constructed and validated against two international standard problem experiments. Furthermore, this thesis presents the simulation characteristics that should be taken into account in future SMR Apros simulations.

The first objective of this thesis is to test the capability of the Apros software to simulate certain phenomena in advanced SMRs. This is executed by developing an existing NuScale SMR test facility model further, and validating it against the published test data. After that, the first version of the VTT developed Helical Coil Steam Generator code is discussed and tested. It is shown that Apros is generally capable of modeling SMRs with certain passive safety features. The simulations conducted in the scope of this thesis reveal a few simulation characteristics that must be taken in account in any future Apros SMR simulations.

The second objective of this thesis is to study NuScale design features and to project them to the Finnish regulatory guides. The study is strongly based on the recent Design Certification Application developed by NuScale and sent to NRC, so a few newly published aspects are briefly discussed. Most of the discussed design features, which are arguably incompatible with the current Finnish regulatory guides, originate mainly from the fact that the YVLs are not prepared for the SMR concept. In the framework of this thesis, some features that require future research and regulative interpretation are found and discussed. However, a lot of the detailed information remains unpublished and the concept is still under development, so further changes are possible.

Although this work supplements SMR related research projects, it does not conclude them. This thesis presents many proposals for future research and development, based on the literature survey and the simulations discussed. The current simulation model would greatly benefit from some future development and could be used to further validate the preliminary version of the HCSG code. It is probable that Apros SMR development could someday lead to a full-scale NPP model. The regulatory SMR study would also benefit from future contribution. Many interesting aspects considering the NuScale design features from regulatory point of view would require in-depth analyses that could not be fitted into this thesis due to their scope or lack of published detailed information. Overall, the SMRs are a relatively sparsely researched field of nuclear engineering and a lot of future research is needed.

8 Bibliography

[1] International Atomic Energy Agency, Advances in SMR Technology Development 2014. Vienna, Austria. 1.9.2014, 2014.

[2] Söderholm, K. *Licensing Model Development for Small Modular Reactors (SMRs) - Focusing on the Finnish Regulatory Framework.* Doctoral Dissertation ed. Lappeenranta: Lappeenranta University of Technology, 20.9.2013, 2013 ISBN 978-952-265-451-9.

[3] International Atomic Energy Agency, *IAEA-TECDOC-1624 Passive Safety Systems and Natural Circulation in Water Cooled Nuclear Power Plants.* Vienna

[4] Schulz, T.L. Westinghouse AP1000 Advanced Passive Plant*. Nuclear Engineering and Design*, 8, 2006, vol. 236, no. 14–16. pp. 1547-1557 ISSN 0029-5493.

[5] International Atomic Energy Agency, *Status Report 106 - NuScale Power Modular and Scalable Reactor (NuScale).* Vienna, Austria. 1.8.2011, 2011.

[6] NuScale Power, LLC. *Passive Safety Systems.* Oregon, United States of America, 2017 Available from: http://www.nuscalepower.com/smr-benefits/safe/reactor-modules.

[7] NuScale Power LLC. *NuScale Standard Plant Design Certification Application Chapter 4 Reactor.* Oregon, United States of America. 12.2016, 2016 ADAMS Public Documents.

[8] Giges, N.S. *Small Modular Reactors Gain Traction.* New York, United States of America: American Society of Mechanical Engineers. 3.2014, 2014.

[9] NuScale Power LLC. *NuScale Standard Plant Design Certification Application Chapter 1 Introduction and General Description of the Plant.* Oregon, United States of America. 12.2016, 2016 ADAMS Public Documents.

[10] Nguyenle, Q. *BWR Drywell Behavior Under Steam Blowdown.* United States: , 1998.

[11] Munson, B.R., Okiishi, T.H., Huebsch, W.W. and Rothmayer, A.P. *Fundamentals of Fluid Dynamics.* 6th ed. United States of America: , 2007 ISBN 978-0470-26284-9.

[12] Ingersoll, D., Colbert, C., Bromm, R. and Houghton, Z. *NuScale Energy Supply for Oil Recovery and Refining Applications.* Oregon, United States of America: NuScale Power, LLC, 1.2014, 2014.

[13] Wuth, J.B. *Comparative Analysis of the Zukauskas Method and Data from the OSU MASLWR Test Facility Steam Generator.* Master's Thesis ed. Oregon, United States of America: Oregon State University, 30.5.2014, 2014.

[14] NuScale Power LLC. *NuScale Standard Plant Design Certification Application Chapter 5 Reactor Coolant System and Connecting Systems.* Oregon, United States of America. 12.2016, 2016 ADAMS Public Documents.

[15] Jo, J.C., Kim, W.S., Choi, C. and Lee, Y.K. Numerical Simulation of Subcooled Flow Boiling Heat Transfer in Helical Tubes*. Journal of Pressure Vessel Technology*, 24.11.2008, 24.11.2008, 2008, vol. 131, no. 1. pp. 011305-011305-9 ISSN 0094-9930.

[16] Chandramouli, P.N. *Fundamentals of Strength of Materials.* PHI Learning Pvt. Ltd., 30.12.2012, 2012 ISBN 8120346726.

[17] Cioncolini, A. et al. *Thermal Hydraulic Analysis of Iris Reactor Coiled Tube Steam Generator.* Tennessee, United States of America ed. Tennessee, United States of America: American Nucl. Society Topical Meeting in Mathematics and Computations, 6-11.4.2003, 2003.

[18] NuScale Power LLC. *NuScale Standard Plant Design Certification Application Chapter 10 Steam and Power Conversion System.* Oregon, United States of America. 14.12.2016, 2016 ADAMS Public Documents.

[19] Jayakumar, J.S. Heat Exchangers - Basics Design Applications J. MITROVIC ed., Rijeka, Croatia: InTech ,9.3.2012, 2012 *Helically Coiled Heat Exchangers*, pp. 311-342 ISBN 978-953-51-0278-6.

[20] United States Nuclear Regulatory Commission, *Typical Pressurized-Water Reactor.* Maryland, United States of America. 15.1.2015, 2015 Available from: https://www.nrc.gov/reactors/pwrs.pdf.

[21] Jerrow, S. *NuScale Design & Operational Overview.* Oregon, United States of America: NuScale Power, LLC. 14.7.2016, 2016.

[22] NuScale Power LLC. *NuScale Standard Plant Design Certification Application Chapter 6 Engineered Safety Features.* Oregon, United States of America. 14.12.2016, 2016 ADAMS Public Documents.

[23] United States Nuclear Regulatory Commission, *State-of-the-Art Reactor Consequence Analyses (SOARCA) Project Sequoyah Integrated Deterministic and Uncertainty Analyses.* J. BARR ed., Maryland, United States of America. 04.06.2016, 2016 ADAMS.

[24] Kotiaho, V.W., Lampinen, M.J. and Seppälä, A. *Termodynamiikan Ja Lämmönsiirto-Opin Taulukoita.* Espoo, Finland: Aalto University School of Engineering, Department of Energy Technology, Applied Thermodynamics, 2011 ISBN 978-952-60-3601-4.

[25] NuScale Power LLC. *NuScale Standard Plant Design Certification Application Chapter 9 Auxiliary Systems Ultimate Heat Sink.* Oregon, United States of America, 14.12.2016, 2016 ADAMS Public Documents.

[26] NuScale Power, LLC. *Seven Layers of Defense.* Oregon, United States of America, 2017 Available from:http://www.nuscalepower.com/smr-benefits/safe/reactor-building-barriers.

[27] NuScale Power LLC. *Triple Crown for Nuclear Plant Safety.* Oregon, United States of America, 2017 Available from: http://www.nuscalepower.com/smr-benefits/safe/triple-crown.

[28] Alarotu, H. *Small Modular Reactors: Specific Safety Features.* Master's Thesis ed. Espoo, Finland: Aalto University, School of Science, 8.2.2013, 2013.

[29] NuScale Power LLC. *NuScale Standard Plant Design Certification Application Chapter 8 Electric Power.* Oregon, United States of America, 14.12.2016, 2016 ADAMS Public Documents.

[30] Reyes, J.N. *Workshop on Technology Assessment of Small and Medium-Sized Reactors (SMRs) for Near Term Deployment* Vienna, Austria: IAEA, 5.9.2011, 2011.

[31] NuScale Power LLC. *NuScale Standard Plant Design Certification Application Chapter 14 Initial Test Program and Inspections, Tests, Analyses, and Acceptance Criteria.* Oregon, United States of America, 14.12.2016, 2016 ADAMS Public Documents.

[32] Sjövall, H. *"Feasibility Studies and Bidding Process* Helsinki/Olkiluoto, Finland ed. , 30.8.2010-3.9.2010, 2010.

[33] *The Constitution of Finland*, 11.6.1999.

[34] Koutaniemi, P. *Ydinenergialainsäädäntö ja -Hallinto.*, 2004.

[35] Radiation and Nuclear Safety Authority (STUK), *YVL B1. Safety Design of a Nuclear Power Plant.* Helsinki, Finland, 15.11.2013, 2013 ISBN 978-952-309-047-7.

[36] European Atomic Energy Community. *Fundamental Safety Principles.* M. ELBARADEI ed., Vienna: International Atomic Energy Agency, 01.11.2006, 2006 ISBN 92-0-110706-4.

[37] NuScale Power LLC. *NuScale Standard Plant Design Certification Application Chapter 21 Multi-Module Design Considerations.* Oregon, United States of America, 14.12.2016, 2016 AD-AMS Public Documents.

[38] Reactor Harmonization Working Group (RHWG), *Safety of New NPP Designs.* Western European Nuclear Regulators' Association (WENRA). 01.03.2013, 2013.

[39] Radiation and Nuclear Safety Authority (STUK), *YVL B6. Containment of a Nuclear Power Plant.* Helsinki, Finland. 15.11.2013, 2013 ISBN 978-952-309-086-6.

[40] Radiation and Nuclear Safety Authority (STUK), *YVL E3. Pressure Vessels and Piping of a Nuclear Facility.* Helsinki, Finland, 15.11.2013, 2013 ISBN 978-952-309-041-5.

[41] Radiation and Nuclear Safety Authority (STUK), *YVL E5. In-Service Inspection of Nuclear Facility Pressure Equipment with Non-Destructive Testing Methods.* Helsinki, Finland, 15.11.2013, 2013 ISBN 978-952-309-148-1.

[42] Radiation and Nuclear Safety Authority (STUK), *YVL B4. Nuclear Fuel and Reactor.* Helsinki, Finland, 15.11.2013, 2013 ISBN 978-952-309-080-4.

[43] International Atomic Energy Agency, *IAEA TECDOC no. 1733: Evaluation of Advanced Thermohydraulic System Codes for Design and Safety Analysis of Integral Type Reactors.* Vienna 1.2.2014, 2013 IAEA Scientific and Technical Publications. ISBN ISBN:978-92-0-100314-0.

[44] VTT Technical Research Centre of Finland Ltd & Fortum Oy, *Apros - Process Simulation Software.* Espoo, Finland, Available from: http://www.apros.fi/en/.

[45] Fortum Nuclear and Thermal Power Division, *Apros Datasheet Thermal Hydraulics Modelling.* Espoo, Finland. 2015.

[46] Hänninen, M. and Ylijoki, J. *The One-Dimensional Separate Two-Phase Flow Model of APROS.* Espoo, Finland: VTT, Valtion teknillinen tutkimuskeskus;, 2008 ISBN 9789513872243.

[47] Viljakainen, O. *Cooling Tower Modelling in Apros Software.* Mater's Thesis ed. School of Engineering: Aalto University, 1.10.2013, 2013.

[48] NuScale Power, LLC. NuScale Test Programs, NIST-1 Integral Testing Facility. Oregon, United States of America, 2017 Available from: http://www.nuscalepower.com/our-technology/test-programs

[49] Mascari, F., et al. Sensitivity Analysis of the MASLWR Helical Coil Steam Generator using TRACE*. Nuclear Engineering and Design*, 4, 2011, vol. 241, no. 4. pp. 1137-1144 ISSN 0029-5493.

[50] Mascari, F., Vella, G., Woods, B.G. and D'auria, F. Analyses of the OSU-MASLWR Experimental Test Facility*. Science and Technology of Nuclear Installations*, 25.10.2011, 2011, vol. 2012.

[51] VTT Technical Research Centre of Finland Ltd & Fortum Oy *Apros 6 Feature Tutorial.* Espoo, Finland. 23.3.2015, 2015.

[52] Eloranta, K. *Apros Simulation of Sp-2 Loss of Feedwater transient ICSP Test using OSU MASLWR Model.* Report ed. Espoo, Finland: , 30.12.2015, 2015.

[53] Tu, J., Yeoh, G.H. and Liu, C. *Computational Fluid Dynamics A Practical Approach.* J. TU, G.H. YEOH and C. LIU eds., Burlington: Butterworth-Heinemann, 2008 ISBN 9780750685634.

[54] Bergma, T.L., Lavine, A.S., Incropera, F.P. and Dewitt, D.P. *Fundamentals of Heat and Mass Transfer.* 6th ed. New York, United States of America: John Wiley & Sons, Inc., 2002 ISBN 978-0470-50197-9.

[55] Seppälä, A. and Lampinen, M.J. *Aineensiirto-Oppi.* Helsinki, Finland: Otatieto, 2004 ISBN 951-672-344-6.

[56] VTT Technical Research Centre of Finland Ltd & Fortum Oy, *Apros Feature Manual.* Espoo, Finland, 2012.

[57] Vierow, K.M. and Schrock, V.E. *Condensation in a Natural Circulation Loop with Noncondensable Gases, 1.* Japan: Japan Society of Multiphase Flow, 1991.

[57] Ito, H. Friction Factors for Turbulent Flow in Curved Pipes*. Journal of Basic Engineering*, 1959, vol. 81. pp. 123-124.

[58] Seban, R.A. and McLaughlin, E.F. *Heat Transfer in Tube Coils with Laminar and Turbulent Flow.* , May 1963, 1963 [viewed 20.2.2017]. Available from: http://www.sciencedirect.com/science/article/pii/0017931063901005 ISBN 0017-9310. DOI http://dx.doi.org/10.1016/0017-9310(63)90100-5.

[59] Mori, Y. and Nakayama, W. Study of Forced Convective Heat Transfer in Curved Pipes (2nd Report, Turbulent Region)*. International Journal of Heat and Mass Transfer*, 11.2.2003, January 1967, 1967, vol. 10, no. 1 [viewed 3.4.2017]. pp. 37-59. Available from: http://www.sciencedirect.com/science/article/pii/0017931067901822 ISSN 0017-9310. DOI http://dx.doi.org/10.1016/0017-9310(67)90182-2.

[60] Owhadi, A., Bell, K.J. and Crain, B. *Forced Convection Boiling Inside Helically-Coiled Tubes.* , December 1968, 1968 Available from: http://www.sciencedirect.com/science/article/pii/0017931068900215 ISBN 0017-9310. DOI http://dx.doi.org/10.1016/0017-9310(68)90021-5.

[61] Thoma, H. *Hochleistungskessel.* Berlin, Germany and New York, United States of America: Springer-Verlag. , 1921.

[62] Reiher, H. *Forschungarbeiten.* 1925.

[63] Zukauskas, A., Makarjavicjus, V. and Slancjauskas, A. *Teplootdaca Puckov Trub V Poperecnom Poteke Zidkosti: (Heat Transfer in Banks of Tubes in Crossflow of Fluid).* Vilnius, Lithuania: Izdatel'stvo Mintis, 1968.

[64] Zhukauskas, A.A. and Ulinskas, R. Heat Transfer in Tube Banks in Crossflow*. Advances in Heat Transfer*, 6.6.2007, 1972, no. 8. pp. 93-160 ISSN 9783540188650.

[65] Kanevets, G.Y. and Politykina, A.A. Heat Transfer in Crossflow Over Bundles of Coiled Heat-Exchange Tubes*. Applied Thermal Sciences*, 1989, no. 2. pp. 38-41.

[66] Austen, D.S. and Soliman, H.M. *Laminar Flow and Heat Transfer in Helically Coiled Tubes with Substantial Pitch.* , April 1988, 1988 Available from: http://www.sciencedirect.com/science/article/pii/0894177788900350 ISBN 0894-1777. DOI http://dx.doi.org/10.1016/0894-1777(88)90035-0.

[67] Ali, M.E. *Experimental Investigation of Natural Convection from Vertical Helical Coiled Tubes.* , March 1994, 1994 Available from: http://www.sciencedirect.com/science/article/pii/0017931094901384 ISBN 0017-9310. DOI http://dx.doi.org/10.1016/0017-9310(94)90138-4.

[68] Ali, M.E. *Laminar Natural Convection from Constant Heat Flux Helical Coiled Tubes.* , July 1998, 1998 Available from: http://www.sciencedirect.com/science/article/pii/S0017931097003220 ISBN 0017-9310. DOI http://dx.doi.org/10.1016/S0017-9310(97)00322-0.

[69] Xin, R.C. and Ebadian, M.A. The Effects of Prandtl Numbers on Local and Average Convective Heat Transfer Characteristics in Helical Pipes. *Journal of Heat Transfer*, 08/01, 1997, vol. 119, no. 3. pp. 467-473 ISSN 0022-1481.

[70] Xin, R.C. and Ebadian, M.A. Natural Convection Heat Transfer from Helicoidal Pipes. *Journal of Thermophysics and Heat Transfer*, 04/01; 2017/04, 1996, vol. 10, no. 2. pp. 297-302 ISSN 0887-8722.

[71] Prabhanjan, D.G., Raghavan, G.S.V. and Rennie, T.J. *Comparison of Heat Transfer Rates between a Straight Tube Heat Exchanger and a Helically Coiled Heat Exchanger.* , February 2002, 2002 Available from: http://www.sciencedirect.com/science/article/pii/S0735193302003093 ISBN 0735-1933. DOI http://dx.doi.org/10.1016/S0735-1933(02)00309-3.

[72] Prabhanjan, D.G., Rennie, T.J. and Vijaya Raghavan, G.S. *Natural Convection Heat Transfer from Helical Coiled Tubes.* , April 2004, 2004 Available from: http://www.sciencedirect.com/science/article/pii/S1290072903001492 ISBN 1290-0729. DOI http://dx.doi.org/10.1016/j.ijthermalsci.2003.08.005.

[73] Klabunde, R.E. *Laminar Flow, Cardiovascular Physiology Concepts.* 06.01.2011, 2011 Available from: http://www.cvphysiology.com/Hemodynamics/H006.

[74] ANSYS Ltd. *ANSYS Fluent, Computational Fluid Dynamics (CFD) Software Tool.* Pennsylvania, United States of America. Available from: http://www.ansys.com/Products/Fluids/ANSYS-Fluent.

[75] White, F.M. *Viscous Fluid Flow.* 3rd ed. McGraw-Hill Education (India) Pvt Limited, 1974 ISBN 9781259002120.

[76] Halliday, D., Resnick, R. and Walker, J. *Fundamentals of Physics Extended, 10th Edition.* Wiley, 2013 ISBN 9781118473818.

[77] Guo, L., Chen, X., Feng, Z. And Bai, B. Transient Convective Heat Transfer in a Helical Coiled Tube with Pulsatile Fully Developed Turbulent Flow. *International Journal of Heat and Mass Transfer*, 17.8.1998, 1.10.1998, 1998, vol. 41, no. 19 [viewed 1.2.2017]. pp. 2867-2875. Available from: http://www.sciencedirect.com/science/article/pii/S0017931098800033 ISSN 0017-9310. DOI http://dx.doi.org/10.1016/S0017-9310(98)80003-3.

[78] Lampinen, M.J. *Lämmönsiirtimien Mitoitus.* Espoo, Finland: Aalto-university, 2005 ISBN 951-22-7557-0.

[79] Hänninen, M., Ylijoki, J. and Kurki, J. *The Constitutive Equations of the Apros Six-Equation Model.* Report ed. Espoo, Finland: VTT Technical Research Centre of Finland Ltd, 23.11.2012, 2012.

[80] VTT Technical Research Centre of Finland Ltd, *Process Component Reference Guide, Cross Heat Exchanger.* Espoo, Finland, 14.12.2015, 2015.

[81] Kokkonen, I. Air/Water Countercurrent Flow Limitation Experiments with Full- Scale Fuel Bundle Structures, IVO Research Report IVO-A-07/89, Helsinki, 1989.

[82] Groeneveld, D.C. and Snoek, C.W., A Comprehensive Examination of Heat Transfer Correlations Suitable for Reactor Safety Analysis, Multiphase Science and Technology, Volume 2, 1986, p. 181-274.

[83] Leskinen, J. "Apros SMR-modelling" in "VTT Research highlights book in Nuclear field", VTT, to be published in 2017

[84] Chen, J.C. Correlation for Boiling Heat Transfer to Saturated Fluids in Convective Flow. *Industrial & Engineering Chemistry Process Design and Development*, 1.5.2002, 07/01, 1966, vol. 5, no. 3. pp. 322-329 ISSN 0196-4305.

[85] Forster, H.K. and Zuber, N. Dynamics of Vapor Bubbles and Boiling Heat Transfer. *American Institute of Chemical Engineers (AIChe) Journal*, 1.12.1955, 1955, vol. 1, no. 4. pp. 531-535.

[86] Lockhart, R.W. and Martinelli, R.C. Proposed Correlation of Data for Isothermal Two-Phase, Two-Component Flow in Pipes. *Chemical Engineering Progress*, 1949, vol. 45, no. 1. pp. 38-48 ISSN 0360-7275.

[87] Chen, W. and Fang, X. A Note on the Chen Correlation of Saturated Flow Boiling Heat Transfer. *International Journal of Refrigeration*, 16.9.2014, 16.9.2014, 2014, vol. 48. pp. 100-104 ISSN 0140-7007.